



*Ministero dell'Istruzione,
dell'Università e della Ricerca*



Unione Europea



Università Degli Studi di Salerno

**Dottorato in Biochimica e Patologia dell'Azione dei Farmaci
IX Ciclo - Nuova Serie
2007 - 2011**

**Trafficking from the Endoplasmic Reticulum to
the Golgi Complex and Gene Expression Profiling
during the Cell Stress**

**Dottorando:
Dott. Giuseppina Amodio**

**Tutor:
Ch. mo Prof. Paolo Remondelli**

**Coordinatore:
Ch.mo Prof. Antonella Leone**

“Considerate la vostra semenza,
fatti non foste a viver come bruti,
ma per seguir virtute e canoscenza”
Dante Alighieri

INDEX

ABSTRACT	pag. 1
RIASSUNTO	pag. 2

Chapter I **Introduction**

Protein Quality Control In and Out of ER	Pag. 3
The exit from ER: Assembly, Organization and Function of the COPII Coat	Pag. 6

Chapter II **Materials and Methods**

Antibodies	Pag. 11
Construction of Plasmids	Pag. 11
Cell Cultures and Drug Treatments	Pag. 11
Immunofluorescence Analysis	Pag. 12
Western Blot Analysis	Pag. 12
Immuno Electron Microscopy Analysis	Pag. 12
Cell Fractionation by Discontinuous Sucrose Gradient	Pag. 13
Cell Transfection and Analysis of TS045G Protein Transport	Pag. 13
Trimerization Assay	Pag. 13
Transfection and FRAP Analysis	Pag. 14
Streptolysin O Assay	Pag. 14
3XFLAG-Sec23a and HA-Ubiquitin Co-Immunoprecipitation	Pag. 15
Identification of Sec23a Ubiquitination Sites	Pag. 15
RNA Extraction and microRNA Microarray	Pag. 15
Northern Blot Analysis	Pag. 16
Bioinformatics Prediction of microRNA Targets	Pag. 16
2D-DIGE Analysis	Pag. 16

Chapter III **ER exit and Trafficking to the Golgi Complex**

Scientific Background, Rationale and Aims	Pag. 19
Results	Pag. 20
Discussion	Pag. 40

Chapter IV **Gene Expression Profiling during ER Stress**

Scientific Background, Rationale and Aims	Pag. 44
Results	Pag. 44
Discussion	Pag. 54

INDEX

CONCLUSIONS AND PERSPECTIVES	pag. 57
ACKNOWLEDGEMENTS	pag. 58
REFERENCES	pag. I-V

ABSTRACT

The *elucidation of the molecular mechanisms regulating the export from the Endoplasmic Reticulum (ER) and the transport to post-ER compartments of secretory proteins* represents the basic aim of the present PhD project.

To ensure that only properly folded proteins exit the ER and locate to their final destination, a quality control system inspects protein folding within the ER. However, several physiological and pathological conditions generate the accumulation of unfolded proteins within the organelle. The ER reacts to this condition, known as ER stress, by turning on the Unfolded Protein Response (UPR), an integrated signal transduction pathway that transforms the unfolding signals into the expression of molecules required to restore protein homeostasis. Notably, the response to the ER stress affects many functions of the secretory pathway and, in particular, the ER-export. Therefore, an essential aim of the present experimental work *was to describe the effect of the ER stress on the molecular events that regulate the exit from ER and the trafficking to the Golgi complex*. Experimental results suggest that the ER stress response attenuates the ER-to-Golgi trafficking by affecting COPII function. This control occurs by targeting Sec16 protein expression and by modifying Sec23a recycling properties on the ER membrane. The results concerning this part are analyzed and discussed in the chapter III.

Since the UPR carries out its function through the regulation of gene expression, we decided to identify new molecular actors of the UPR control by analyzing gene expression profiles in ER stressed cells. In particular, given the increasing importance of microRNAs in the regulation of several signaling transduction pathways, we analyzed the microRNome changes induced by the UPR activation. In parallel, we characterized the proteome signature in the same stress conditions. The results obtained by the study of microRNome and proteome profiles are described in the chapter IV.

RIASSUNTO

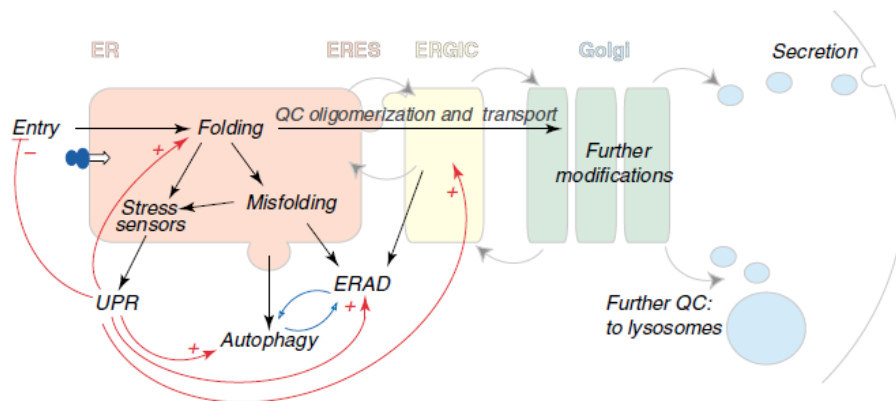
Lo scopo del progetto di dottorato è lo *studio dei meccanismi molecolari che regolano l'uscita dal Reticolo Endoplasmatico (RE) e il trasporto al Golgi delle proteine secretorie*. Un sistema di controllo di qualità opera all'interno del RE per garantire che solo le proteine correttamente conformate possano uscire dal RE e raggiungere la loro destinazione finale. L'alterazione dell'omeostasi proteica, indotta da condizioni fisiologiche o patologiche, determina l'accumulo di proteine non correttamente conformate nel lume del RE generando una condizione di stress. Per reagire a questa situazione, il RE attiva l'Unfolded Protein Response (UPR), un sistema di trasduzione integrato, che trasmette il segnale di unfolding proteico dal RE al nucleo allo scopo di attivare l'espressione di fattori necessari alla ricostituzione dell'omeostasi proteica nel lume del RE. La risposta allo stress del RE coinvolge ogni funzione della via secretoria; in particolare, il controllo dell'uscita dal RE e del trasporto vescicolare potrebbe rappresentare uno strumento fondamentale della risposta adattativa attivata dalla cellula per affrontare la condizione di stress. Pertanto, lo studio delle dinamiche di uscita dal RE e trasporto al Golgi nel corso dello stress del RE rappresentano lo scopo principale di questo lavoro. I risultati ottenuti suggeriscono che lo stress del RE modula il traffico vescicolare dal RE al Golgi attraverso la modulazione dell'assemblaggio del rivestimento proteico COPII. Questo controllo si realizza attraverso la riduzione dei livelli di espressione della proteina Sec16 e la concomitante modulazione delle cinetiche di ricircolo sulla membrana della proteina Sec23a. I risultati relativi a questo aspetto sono analizzati e discussi in dettaglio nel capitolo III.

Poiché la risposta UPR si realizza prevalentemente attraverso il controllo dell'espressione genica, ci siamo proposti anche di identificare nuovi bersagli molecolari dell'UPR attraverso la caratterizzazione dei profili di espressione genica in cellule trattate con taspigargina. In particolare, considerata la crescente importanza dei microRNA nella regolazione della trasduzione del segnale, abbiamo analizzato le modificazioni del microRNoma indotte dall'UPR. Parallelamente, abbiamo caratterizzato le variazioni del proteoma indotte dall'UPR nelle stesse condizioni. I risultati ottenuti dallo studio dei profili di espressione del microRNoma e del proteoma sono descritti in dettaglio nel capitolo IV.

Protein Quality control in and out of ER

The Endoplasmic Reticulum and Quality Control

In eukaryotic cells secreted and resident proteins of the endomembrane system fold into their native conformation within the Endoplasmic Reticulum (ER). The ER is a membrane network of tubules and sheets, whose luminal environment contains molecular chaperones and protein-modification enzymes specialized in protein folding. Folding of secretory proteins must be controlled in the tightest way to ensure proper cell functions. Therefore, within the ER a quality control (QC) system guarantees that only properly folded proteins can reach their final destination in the secretory pathway (Anelli and Sitia, 2008; Ellgaard and Helenius, 2003). The final goals of QC are to recognize, retain and eventually induce to degradation aberrant protein conformers (Fig. 1) even after the transport to the ERGIC (ER Golgi Intermediate Compartment) and the cis-Golgi (Anelli et al., 2007; Qiang et al., 2007). When this control is overwhelmed, protein homeostasis within the secretory pathway is impaired and misfolded proteins accumulate within the ER. This condition is commonly referred as ER stress and, to restore protein homeostasis, the cell activates a coordinated signalling pathway, known as the Unfolded Protein Response (UPR) (Ron and Walter, 2007). The activation of the UPR allows the rapid adaptation of ER-folding capacity to the new cellular requirements. This response is required during the physiological processes, such as cell growth and differentiation, when the flux of proteins entering the ER is higher or during special environmental conditions such as hypoxia, oxidative injury, high-fat diet, hypoglycaemia and viral infection. Dysregulation of UPR contributes to several important human diseases, including diabetes, neurodegeneration and cancer (Kim et al., 2008) (Box 1).



(Anelli and Sitia, 2008)

Fig. 1 *The early secretory pathway.* Secretory proteins enter the ER where they attain their native structure (folding), under strict QC scrutiny. Only properly folded and assembled proteins can reach the Golgi, where they are further modified, to be transported to the extracellular space, to the lysosomes or be inserted in the membrane. Gray arrows indicate the direction of vesicles moving among different compartments; dark arrows indicate the pathways followed by cargoes in the early secretory pathway; red lines show homeostatic control pathways (+ stimulatory, - inhibitory). Misfolded proteins are recognized and eventually destined to degradation by ERAD (ER Associated Degradation) or autophagy (which are likely reciprocally

regulated, as indicated by the blue arrows). Some misfolded soluble ERAD substrates are transported to ERGIC or cis-Golgi before retrotranslocation and degradation. Too high load for the folding machinery or the accumulation of misfolded proteins activate resident ER stress sensors, which elicit the UPR.

Disease	Role of ER stress	Target protein
Alzheimer's disease (AD)	Exact implications of ER stress in AD is unclear (AD brains show increase of protective UPR proteins) AD-associated mutant Presenilin 1 induces ER stress response with suppression of protective UPR signalling Unclear whether ER stress in PD is mainly protective or contributory to disease	Presenilin, PERK-EIF2 α
Parkinson's disease (PD)	Parkin suppresses ER-stress-induced cell death Parkin expression is controlled by ER stress Parkin mutants associated with PD	Parkin, alpha-synuclein and others
Amyotrophic lateral sclerosis	Mutant SOD interferes with ER-assisted degradation machinery and activates ASK1	SOD, ASK1
Polyglutamine disease	Polyglutamine induces the UPR and suppresses proteasomal activity	Huntingtin, SCA, androgen receptor
Prion disease	Brains affected with prions show induction of ER chaperones, implying protective UPR against ER stress	Prion protein
Stroke	Ischaemia induces ER stress in neurons, activates the UPR and finally leads to neuronal apoptosis associated with CHOP induction and ASK1 activation	PERK-EIF2 α , ASK1
Bipolar disease	Medications for treating bipolar disease induce the UPR	XBP1 polymorphisms (controversial)
Heart disease	Induction of ER stress by ischaemia in the heart leads to degeneration of cardiac myocytes Transaortic constriction induces expression of ER stress Myocardial infarction induces the UPR	ASK1
Atherosclerosis	Oxidized lipids and homocysteins induce ER stress in vascular cells, cholesterol in macrophages	IRE1 pathway
Type 1 diabetes	Impaired PERK pathway is responsible for type 1 diabetes (Wolcott-Rallison syndrome)	PERK-EIF2 α
Type 2 diabetes	Obesity (a cause of type 2 diabetes) induces ER stress, leading to insulin resistance	XBP1, JNK
Type 2 diabetes	Fatty acids (palmitate) induce apoptosis of beta cells	CHOP
Cancer	Protective UPR proteins are upregulated in cancer cells subjected to hypoxic environments	GRP78, XBP1, PERK
Autoimmune disease	ER protein overload may contribute to autoantigen production GRP78 can be an autoantigen	GRP78, HLA-B27 and others

Box 1: ER stress related diseases

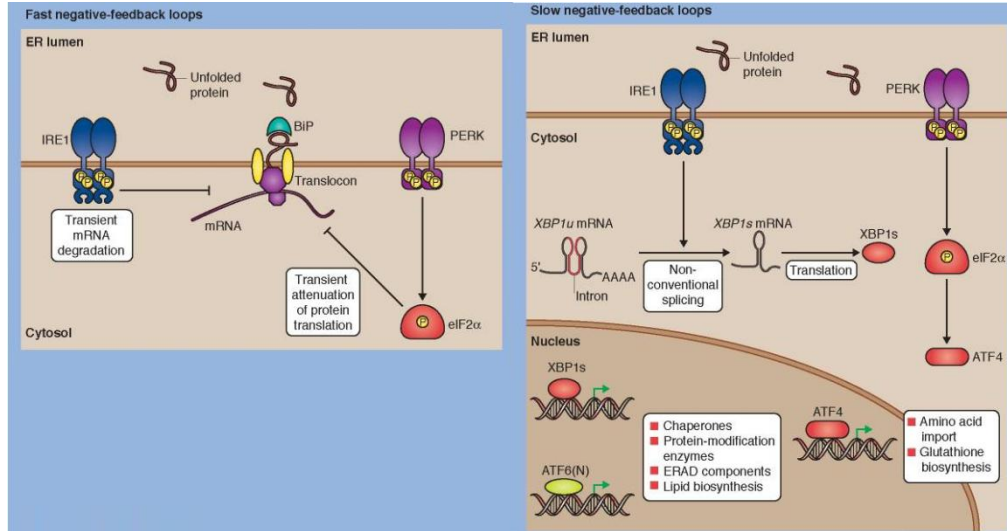
The Unfolded Protein Response

In mammalian cells, the UPR signalling is initiated by three ER-resident transmembrane proteins: PERK, ATF6 and IRE1. The activation of these three proximal detectors is regulated by Bip/Grp78, an ER resident chaperone that under

basal conditions is bound to their luminal domains thus inhibiting their activation. When unfolded proteins accumulate into the ER, Bip dissociates from PERK, ATF6 and IRE1 to preferentially interact with misfolded proteins, thus allowing their activation (Bertolotti et al., 2000). IRE1 is a type-1 transmembrane protein with an N-terminal luminal domain, a cytosolic kinase domain and a cytosolic RNase domain (Wang et al., 1998). After the dissociation of Bip, the monomers of IRE1 oligomerize into dimers or higher structures, causing trans-autophosphorylation of the kinase domains, which in turn activates the RNase catalytic domains. Active IRE1 catalyzes the non-conventional splicing of the XBP1 mRNA, which encodes the XBP1 transcription factor (Yoshida et al., 2001). PERK is also a type-1 transmembrane protein that has a cytosolic kinase domain and an N-terminal luminal domain homologous to that of IRE1. Activated PERK phosphorylates the eukaryotic translation initiation factor 2 α (eIF2 α), which slows down translation initiation (Harding et al., 1999). Concomitantly, translation of the transcription factor ATF4 increases during eIF2 α phosphorylation (Harding et al., 2003) thanks to alternative CAP-independent initiation of translation.

ATF6 is an ER resident type-II transmembrane protein that exists as an oxidized monomer, dimer, and oligomer. After dissociation of Bip, the intra/inter molecular disulfide bonds are reduced and the monomeric ATF6 translocates to the Golgi and becomes a substrate for SP1 and SP2 proteases that liberate the N-terminal cytosolic domain of ATF6 which has transcriptional activity (Haze et al., 1999; Shen et al., 2005). When the proximal UPR sensors are active, they initiate an adaptive response involving several outputs to restore protein-folding homeostasis in the ER (Fig. 2). Two negative feedback loops can be conceptualized: one fast loop that decreases the influx of proteins into the ER, thanks to the PERK-mediated inhibition of eIF2 α , and a slow negative feedback loop that requires de novo mRNA and protein synthesis to increase the folding capacity of the ER through XBP1 and ATF6 transcriptional activity. They increase the transcription rates of genes encoding ER resident chaperones, protein modification enzymes, lipid biosynthetic enzymes and components of the ERAD (ER Associated Degradation) (Yamamoto et al., 2007), to enhance the size of the folding and degradation activities of the ER. In addition, IRE1 is responsible for the rapid degradation of several ER localized mRNAs (Hollien and Weissman, 2006) that, together with PERK-dependent translation attenuation, provides an extended opportunity to fold or degrade the existing unfolded proteins. In particular, the degradation of irreversible unfolded proteins occurs through the ERAD mechanism that involves recognition, retro-translocation in the cytosol of the aberrant proteins and finally degradation by the ubiquitin-proteasomal system (Travers et al., 2000). In addition to ERAD, cells can dispose of protein aggregates difficult to unravel by autophagy. In this process, organelles can be degraded regardless of their size or the folding state of their constituent proteins. Many of the components that mediate autophagy have been identified as UPR target genes (Yorimitsu et al., 2006) and are important for cells to counteract severe ER stress.

The ultimate output of UPR in cells experiencing irremediable ER stress is the commitment to apoptosis. The two apoptotic pathways that are activated by UPR are mediated by CHOP and JNK proteins. CHOP transcription is induced by ATF4 factor and was found to increase the rate of expression of the pro-apoptotic *Bim* during severe ER stress (Puthalakath et al., 2007). In parallel, IRE1 initiates a signalling cascade that results in the activation of JNK that finally activates several pro-apoptotic factors such as *Bid* and *Bim* (Urano et al., 2000).



(Merksamer and Papa, 2010)

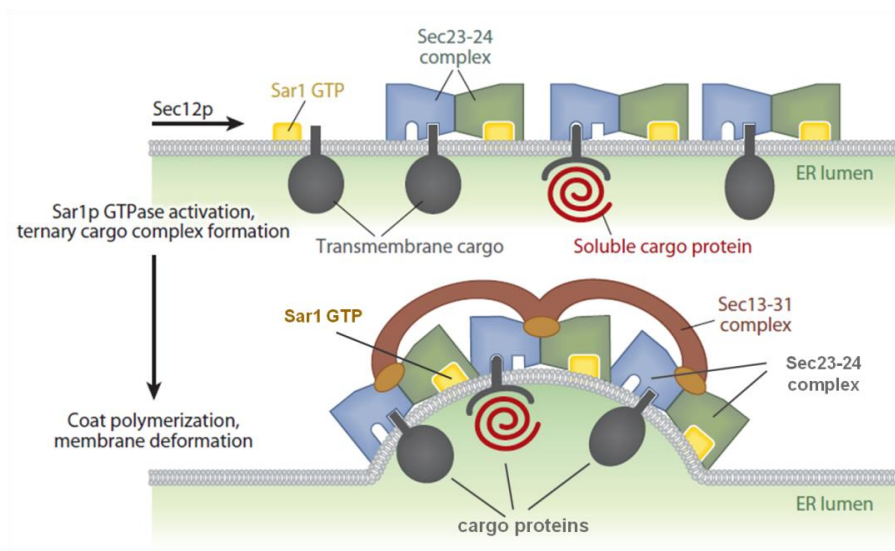
Fig. 2 Adaptive responses of UPR (see text for details)

The exit from ER: assembly, organization and function of the COPII coat

The assembly of the COPII coat

The first membrane trafficking step in the biosynthetic secretory pathway is the export of proteins from the ER, which is mediated by COPII-coated vesicles. COPII is a multiprotein coat consisting of five cytosolic proteins: Sar1, Sec23, Sec24, Sec13 and Sec31 and their isoforms. In particular, the mammalian repertoire consists of: two Sar1 paralogs, Sar1a and Sar1b; two Sec23 paralogs, Sec23a and Sec23b; four Sec24 paralogs, Sec24a, Sec24b, Sec24c, Sec24d; a single Sec13 and two Sec31 paralogs, Sec31a and Sec31b. In cells, Sec23 and Sec24 are found in tight heterodimers, which form the inner COPII coat, whereas Sec13 and Sec31 are found in stable heterotetramers of two subunits of each, which form the outer COPII coat (Barlowe et al., 1994). Biogenesis of COPII vesicles (Fig. 3) is regulated at the most basic level by a GTPase cycle under direction of the small GTPase Sar1. Sar1 is specifically activated on the surface of ER membrane by its guanine nucleotide exchange factor (GEF) Sec12 (Barlowe and Schekman, 1993). Activation of Sar1-GTP exposes an amphipathic α -helix that anchors Sar1-GTP to the ER membrane and initiates membrane curvature (Bielli et al., 2005; Lee et al., 2005). Acting as a membrane bound anchor for the other COPII components, activated Sar1 binds and recruits the heterodimer Sec23-Sec24 through the direct interaction with Sec23 (Bi et al., 2002). This interaction has not only a structural role for the assembling of COPII vesicles but has also a catalytic role since Sec23 is a GTPase activating protein

(GAP) for Sar1-GTP that is necessary to accelerate the GTPase activity of Sar1 (Yoshihisa et al., 1993). Fully GTPase activity is not realized until the complete COPII coat is assembled following the arrival of the Sec31-Sec13 outer coat that stimulates the GTPase activity of Sar1-Sec23 of approximately tenfold (Antonny et al., 2001). The set of proteins consisting of a membrane-bound Sar1 along with a cargo-loaded Sec23-Sec24 dimer has been termed “pre-budding complex”, a complex that is ready for the activity of Sec13-Sec31 to complete the formation of the vesicle. This outer layer of the coat collects pre-budding complexes and shapes the membrane to form a bud enriched in cargo molecules. To accomplish this task, the Sec13-Sec31 complexes polymerize into cuboctahedrons (Fath et al., 2007; Stagg et al., 2006), whereas Sec31 directly interacts with Sec23 and Sar1 (Bi et al., 2007). Once the coat is assembled in its entirety, GTP hydrolysis by Sar1 is maximal and thereby drives immediate coat disassembly (Antonny et al., 2001) leaving a spherical membrane vesicle roughly 60-70 nm in size.



(Dancourt and Barlowe, 2010)

Fig.3 COPII assembly and the Sar1 GTPase cycle

Cargo and not-cargo regulation of COPII function

The coupling of coat formation to cargo packaging is an intrinsic property of the COPII coat. Sec24 is considered to be the primary subunit responsible for binding to membrane cargo proteins at the ER and concentrating them into the forming vesicles (Miller et al., 2002). Many cargo proteins have specific export-signal sequences in their cytoplasmic domains to mark them for COPII transport. Types of COPII signal sequences include di-hydrophobic (e.g. -FF-), diacidic (e.g. -DxE-), C-Terminal hydrophobic and aromatic motifs (Barlowe, 2003; Wendeler et al., 2007). Moreover, cells are endowed with multiple Sec24p isoforms to greatly expand the diversity of export signals that can be recognized by the COPII sorting machinery. Not all proteins

that need to leave the ER contain a signal for the direct binding to Sec24. Some proteins might interact with a transport adaptor and thus be included in the COPII vesicles through an indirect interaction (Baines and Zhang, 2007). Known cargo receptor proteins include ERGIC-53, VIP36 and VIPL. Still other proteins might passively enter COPII vesicles by simple diffusion, a process called bulk-flow (Thor et al., 2009). However, of those cargo proteins tested, several are found in COPII vesicles in concentration higher than a bulk-flow model would suggest, indicating that concentrative sorting by Sec24 might be the rule (Malkus et al., 2002).

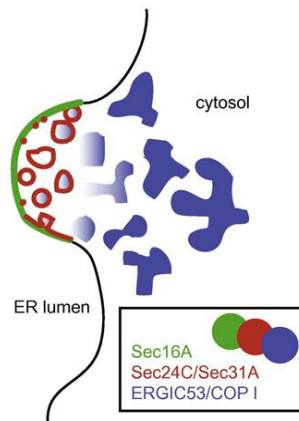
Recent experiments have started to shed some light on how the GTP cycle on Sar1 is modulated to permit cargo loading and vesicles release. The continual presence of Sec12 is able to prolong Sar1-GTP loading onto ER membrane providing a sufficient membrane bound pool of Sar1 and Sec23-24 for cargo concentration to occur (Sato and Nakano, 2005; Tabata et al., 2009). A corollary to the question of cargo loading is how the process of ER export manages to accommodate cargoes of widely disparate sizes. Single particle cryo-EM reconstitution of the spherical cage formed by Sec13-Sec31 revealed a basic architecture capable to create structures of increasing dimensions (Stagg et al., 2006). More recent results indicate that there may be a physical link between COPII coat and high molecular size cargo like pro-collagen filaments: the ER membrane protein TANGO1 interacts with both collagen and COPII coat facilitating collagen capture into COPII vesicles without being itself introduced in the vesicle (Saito et al., 2009).

In addition to cargo regulation of COPII assembling, multiple factors have been identified that impact on COPII function. Such proteins include protein kinases such as PCTAIRE (Palmer et al., 2005), p38 MAP kinase (Wang and Lucocq, 2007), adaptors such as STAM (Rismanchi et al., 2009), and potential regulators of lipid biosynthesis including p125 (Shimoi et al., 2005) and Phosphatidylinositol-4-kinase (Blumental-Perry et al., 2006). The calcium binding protein ALG-2 has also been implicated in COPII assembly (Shibata et al., 2007), potentially providing a point of integration of calcium oscillations and ER export activity. The dynactin subunit p150^{glued} interacts with Sec23 (Watson et al., 2005), providing a direct link and integration with the microtubule cytoskeleton. A potential unifying theme is that many of this proteins including p125, p150^{glued} and PICTAIRE, interact with Sec23-Sec24 component of the coat and so regulates Sar1-GTPase activity. Protein phosphorylation is likely to play a key role, having been shown that Sec31 (Salama et al., 1997) and Sec16 are phosphorylated (Farhan et al., 2010).

Definition and structure of ER exit sites

In mammalian cells, secretory proteins, after their translation at rough ER, enter specific sub-domains of the ER which are devoid of ribosomes and show characteristic COPII positive buds. This domains are called transitional ER (tER) (Orci et al., 1991). The term ER Exit Sites (ERES) originates from light microscopy observations of the localization and dynamics of COPII proteins in cells; but ERES encompass more than just the tER itself and include the post-ER structure characterized by free COPII vesicles and tubular elements prior to fusion with or became the ERGIC (Mironov et al., 2003). Over the past years, many evidences suggested the central role of the peripheral membrane protein Sec16 in the organization of ERES. Sec16 is a 240 KDa peripheral membrane protein that cycles on and off the ER membrane and has a direct interaction with Sec23, Sec24, Sec31

and Sec13 (Bhattacharyya and Glick, 2007; Hughes et al., 2009; Shaywitz et al., 1997; Whittle and Schwartz, 2010). Sec16 facilitates the recruitment of Sec23-24 and Sec13-31 (Supek et al., 2002) acting as scaffold for the assembling of COPII coats. Considerable evidence points show also that cargo can influence the number and the size of ERES providing a means to regulate the COPII vesicle formation when the secretory requirements of the cell change (Aridor et al., 1999; Farhan et al., 2008; Forster et al., 2006); for example following the stimulation of cell growth by growth factors, the control of ERES number is achieved through the ERK2-mediated phosphorylation of Sec16 (Farhan et al., 2010). From this findings a more precise picture of an ERES is developed: they are tER membranes that are defined by the presence of Sec16 (Hughes et al., 2009), the nascent COPII-coated tubule-vesicular-compartment (Zeuschner et al., 2006) and the first post-COPII membranes which are likely to almost immediately become COPI-coated and therefore ERGIC (Appenzeller-Herzog, 2006) (Fig. 4).



(Hughes et al., 2009)

Fig. 4 Schematic model of ERES organization

The COPII proteins in human diseases

In recent years examples of developmental disorders and human diseases caused by mutations in Sar1b, Sec23a, Sec23b and Sec24b have begun to shed light on the reason that the multiple paralogs of COPII proteins have been conserved among higher organisms.

Several different mutations in Sar1b have been associated with two related fat malabsorption diseases: chylomicron retention disease and Anderson disease (Jones et al., 2003). Affected individuals show a lack of chylomicrons in their blood because the mutations in SAR1b prevents their normal secretion from the intestinal epithelial cells. Interestingly, chylomicrons range in size from 75 to 450 nm in diameter while vesicles are only 60–70 nm, so it is possible that Sar1b is specialized to enable the transport of chylomicrons and perhaps of other large cargo molecules such as pro-collagen, even if these issues remain unresolved.

A single missense mutation in Sec23a (F382L) has been found to lead to an autosomal recessive disease called cranio-lenticulo-sutural dysplasia (CLSD) (Boyadjiev et al., 2006). The disease is marked by skeletal defects, cataracts and facial dysmorphism. It was found that the mutation is near the part of Sec23a that

binds and recruits Sec31 (Bi et al., 2007). Failure to recruit Sec31 leads to a large reduction in the packaging of cargo proteins *in vitro*, and is accompanied by swelling of the ER with untransported cargo *in vivo*. Many separate mutations in Sec23b were found in patients with a disease called congenital dyserythropoietic anemia type II (CDAI) (Schwarz et al., 2009). The symptoms of this disease appear to be largely due to defective erythropoiesis; various proteins in the red blood cells show immature glycosylation, indicating transport defects. As with the Sec23a mutation, it seems that the Sec23b mutations only affect a specific tissue. It might be that Sec23a and Sec23b are functionally redundant, and able to largely compensate for one another in unaffected tissues where they are normally both expressed.

Recent reports demonstrate that two distinct premature stop codons in Sec24b lead to major neural tube defects in mice (Merte et al., 2010). Homozygous mutant mice developed craniorachischisis and several other phenotypes indicative of defects within the tissue-organizing planar cell polarity pathway. In this study was revealed that the membrane protein Vangl2 appears to be specifically packaged by Sec24b and that the defective packaging of Vangl2 into COPII vesicles was the cause of the developmental defects. Sec24 is a versatile protein but, in this case, Sec24b appears to have specific binding activity for at least one important cargo protein that cannot be compensated by the presence of other Sec24 paralogs.

Antibodies

The following antibodies were used: mouse monoclonal anti-ERGIC-53 antibody, rabbit polyclonal anti-GM130, rabbit polyclonal anti-Sec31, mouse monoclonal anti-calnexin (Marra et al., 2001); goat polyclonal anti-Sec23, mouse monoclonal anti-GAPDH and anti- γ tubulin, mouse monoclonal (F-7) and rabbit polyclonal (Y-11) anti-HA probe (Santa Cruz Biotechnology); mouse monoclonal anti-FLAG (M2, Sigma-Aldrich); rabbit polyclonal anti-calreticulin and anti-calnexin, mouse monoclonal anti-KDEL (StressGen); rabbit polyclonal anti-Sec16 (KIAA0310, Bethyl Laboratories); rabbit polyclonal anti-Sar1 (Upstate-Millipore); mouse monoclonal anti-GM130 (BD Transduction Laboratories); mouse monoclonal anti-GFP (Molecular Probes); rabbit polyclonal anti-Grp78/BIP (Cell Signaling Technology); mouse monoclonal anti-ALIX (G-10), goat polyclonal anti-PP2A (SET), rabbit polyclonal anti-calumenin (H-40) and PLOD3 mouse polyclonal antibody (B01P) (Abnova); mouse anti-reticulocalbin 2 (RCN2) (Abcam). FITC-, Texas Red- (Jackson Immuno Research Laboratories), TRITC- and CY5- (GE Healthcare) conjugated antibody were used as secondary antibody for indirect immunofluorescence analysis; HRP-conjugated secondary anti-mouse, anti-rabbit and anti-goat IgG (Sigma-Aldrich) were used for immunoblotting analysis.

Construction of plasmids

Human Sec23A cDNA was obtained by One-Step RT-PCR (Invitrogen) performed on HeLa total RNA with the following primers spanning from nucleotide -26 to +2622 of the mRNA sequence (NM_006364): Sec23A forward: 5'-CGC AGA AAT AAG AAT CAA ACT CC-3' and Sec23A reverse: 5'-TAG AGC AAT ATC TGT TGG TTT CC -3'. To create the pEGFP-Sec23a expressing plasmid, the full Sec23A coding sequence (1-767 aa) was consequently obtained by PCR amplification (Roche) with KpnI and XbaI flanked oligonucleotides (forward: 5'-GG GGT ACC **ATG** ACA ACC TAT TTG GAA TTG-3'; reverse: 5'-GC TCT AGA ATT AGC ACT **TCA** AGC AGC-3'; AUG and stop codon are indicated in bold) and inserted in the KpnI-XbaI sites of the pEGFP-C1 vector (Clontech). To obtain the p3xFlag-Sec23a expressing plasmid the full Sec23a coding sequence was amplified by PCR with HindIII and XbaI flanked primers (forward: 5'-CCC AAG CTT **ATG** ACA ACC TAT TTG GAA TTC-3'; reverse: 5'-GC TCT AGA ATT AGC ACT **TCA** AGC AGC-3') and cloned in the HindIII-XbaI sites of the p3xFlag-CMV-7.1 vector (Sigma-Aldrich). The DNA sequences of the obtained constructs were verified by sequencing. The pEGFP-Sec16 expressing plasmid (Watson et al., 2006) was kindly provided by Dr. David Stephens (University of Bristol, UK). The pHA-Ubiquitin vector was previously described (Mauro et al., 2006).

Cell cultures and drugs treatments

Human hepatoma Huh7 cells, mouse embryonic fibroblast MEF wt and IRE1 α knock-out were grown in DMEM 10% FCS supplemented with 4.5 g/l D-glucose, 1 mM Na-pyruvate, 2 mM L-glutamine, at 37°C, in a humidified atmosphere with 5% CO₂. When indicated, actively growing cells were incubated either with 1 mg/ml of the NO donor DETA NONOate (2,2-[hydroxynitrosohydrazino bis-ethanamine] (Calbiochem), 300 nM thapsigargin (TG, Sigma-Aldrich), 2 mM dithiothreitol (DTT), 10 μ M MG132 (Sigma-Aldrich), 50 μ M BAPTA-AM, 2 μ M Ionomycin (Calbiochem) or 10 μ g/ml Cycloheximide (CHX; Sigma-Aldrich). Brefeldin A (BFA) (Sigma-Aldrich) was used at a final concentration of 5 μ g/ml.

Immunofluorescence analysis

Huh7 or MEF cells seeded on glass cover slips were washed, fixed 10 min in PBS-4% paraformaldehyde and incubated 30 min in PBS containing 0.5% BSA, 0.005% saponin and 50 mM NH₄Cl at room temperature. Cells were then labelled with the appropriate primary antibody and with fluorophore-conjugated secondary antibodies. Cover slips were mounted with the Prolong AntiFade kit (Molecular Probes, Invitrogen). For ERGIC-53 staining, cells were fixed with PBS-3.7% formaldehyde for 30 min at room temperature and made permeable with 0.1% Triton X-100 in PBS. Images were collected as specified using either an Axiophot microscope (Carl Zeiss MicroImaging) equipped with a Photometrics Sensys camera controlled by IP lab spectrum software or a laser scanning confocal microscope (Zeiss LSM 510 or Leica TCS SP5 II) equipped with a plan Apo 63X, NA 1.4 oil immersion objective lens.

The quantification of mean fluorescence intensities after VSV ts045G transport assay was performed as previously described (Nichols et al., 2001). In particular, fluorescence intensity was measured in areas of equal size in the ER or in the Golgi complex in a single z-plane through the cell volume (from a range of 1–3 μ m starting from the top of the cell) and normalised for the average area of the ER and the Golgi complex measured in the selected regions of interest. The sum of the ER or Golgi apparatus amounts was regarded as total fluorescence. The COPII coats labelled with Sec 31 or the ER-exit sites labelled with Sec 16 were measured by counting the fluorescent spots in two in-focus z-planes by using Image J software. The degree of co-localization of the two fluorescence signals was quantified either by using the LSM 510 or by Image J software. The number of co-localized pixels was normalized for the total of pixels of the fluorophore in the image.

Western Blot analysis

Huh7 cells were lysed in B-Buffer (10 mM Tris-HCl pH 7.4, 150 mM NaCl, 1 mM EDTA pH 8.0), containing 1% Triton, on ice, for 20 min and cleared by centrifugation at 12.000 x g for 15 min to remove debris. In order to validate the differential expression of mass spectrometry-identified proteins, Huh7 cells were lysed in RIPA buffer. Protein concentration of the supernatant was measured according to Bradford method (Bio-Rad). Proteins were separated on 10-12% polyacrylamide gels by SDS-PAGE and then blotted on Protran nitro-cellulose membranes (Schleicher&Schuell Bioscience GmbH, Dassel, Germany). Filters were blocked with PBS containing 10% non-fat dry milk and 0.1% Tween-20, overnight, and then incubated for 2-12 h with the optimal dilution of the primary antibody. Anti-rabbit or anti-mouse IgG horseradish peroxidase conjugated were used as secondary antibodies; bands were visualised by autoradiography of ECL reaction (Amersham International, Amersham, UK). γ -tubulin or GAPDH were used to normalise for equal amounts of proteins separated on the gels and to calculate the relative induction ratios. Quantitative analyses were performed on protein samples giving signals in the linear range of the ECL assay. Densitometry of auto-radiographs was performed by the Image J program; values obtained were the mean \pm SD of three independent experiments. Statistical analysis was performed using the Student t-test (n=6-9).

Immuno Electron Microscopy analysis

For cryo-sectioning, Huh7 cells were fixed with 2% paraformaldehyde and 0.2% glutaraldehyde in PBS for 2 h at room temperature, washed with PBS containing 20 mM glycine, scraped off the dish, centrifuged and embedded in PBS-12% gelatin.

Small blocks of embedded cells were incubated overnight with 2.3 M sucrose at 4°C, mounted on aluminium pins and frozen in liquid nitrogen. 60 nm ultrathin cryosections were cut at -120°C, using a cryo-ultramicrotome (Leica-Ultracut EM FCS), and picked up with 1% methylcellulose in 1.15 M sucrose. Cryosections were then incubated with primary antibodies and revealed with protein A gold.

Cell fractionation analysis by discontinuous sucrose gradient

Huh7 cells ($7-10 \times 10^7$) were homogenised by 10 strokes in a Wheaton glass homogeniser in a buffer containing HEPES/KOH pH 7.3 20 mM, sucrose 120 mM. Post Nuclear Supernatant (PNS) was obtained by centrifugation at 500 x g for 5 min in a micro centrifuge and loaded on the top of a discontinuous sucrose gradient (15, 20, 25, 30, 35, 40, 45, % w/v) made up in the same buffer. The gradient was spun in a SW 50.1 rotor for 1 h at 43000 rpm in a Beckman ultracentrifuge and 13 fractions were collected from the bottom of the tube with a peristaltic pump. Fractions were TCA precipitated and proteins were separated by SDS-PAGE, transferred to ECL membranes and subjected to Western blot analysis. Densitometry of autoradiographs was performed by the NIH image program and values obtained are representative of three independent experiments.

Cell transfection and analysis of ts045G protein transport

Actively growing Huh7 cells were transfected with 2 µg of the expression vector encoding a GFP variant of the temperature sensitive mutant ts045 of the VSV G protein (ts45G) (Presley et al., 1997) by using Fugene 6.0 according to the manufacturer instruction (Roche). After 4 h cells were incubated 16 h at 39°C to obtain complete retention of the chimeric protein within the ER. Cells were moved to the permissive temperature (32°C) and the protein progression through the secretory pathway has been evaluated at 15 min at 32° by fluorescence analysis. In the ER stress experiments cells were pre-incubated for 5 min with 300 nM TG prior to shift the cells at 32°C.

Trimerization Assay

Actively growing Huh7 cells were transfected with the expression vector encoding the ts045G protein. 4 h after transfection, cells were incubated at 39°C for 16 h and then moved to the permissive temperature of 32°C for 4 min in presence or not of 300 nM TG. After the temperature-shift cells were transferred on ice and incubated for 30 min in ice-cold MNT Buffer at pH 5.8 containing 20 mM MES, 30 mM Tris-HCl, 100 mM NaCl and 1% Triton X-100 (Doms et al., 1987). Lysates were collected by scraping, sheared through a 26-g needle and separated from nuclei by centrifugation. The glucose gradient (40-20%) was made at 4° in MNT buffer containing 0.1% Triton X-100 at pH 5.8 and layered into a centrifuge tube. The lysate was added to an equal volume of 6% part of gradient, loaded on the gradient and ultracentrifuged at 45000 RPM (SW50 rotor, Beckman) for 16 h at 4°C. Fifteen fractions of 300 µl were harvested from the top of the gradient (Meunier et al., 2002). The pellet formed to the bottom of the tubes was solubilised in the gel loading buffer by incubation at 37°C for 1 h with shaking. Proteins in each fraction were TCA-precipitated, separated by SDS-PAGE, transferred to ECL-membranes and revealed with rabbit polyclonal anti-GFP antibody. Densitometry of autoradiographs was performed by the NIH image program. Values obtained are representative of three independent experiments.

Transfection and FRAP analysis

Huh7 cells were grown on live cell dishes (MatTek, Ashland, MA) and transfected with 2 µg of GFP-Sec16 or GFP-Sec23a plasmid by using Fugene 6 (Roche). 24 h after transfection, the cells were imaged as previously described (Hughes et al., 2009) at 37°C with the Zeiss LSM 510 META scanning confocal microscope enclosed in a heated box in DMEM, supplemented with 30 mM HEPES, pH 7.4 and 10% FCS. For quantitative FRAP measurements a 63x 1.4 NA Plan-Apochromat objective was used. The bleaching was performed on individual Sec16 or Sec23 positive spots with five iterations of the 488 laser at 100% AOTF power. Their post-bleaching images were collected for 90 seconds with a scan rate of 1 frame every 1 second and twofold line averaging. Fluorescence recovery in the bleached region during the time series was quantified using Zeiss LSM 510 FRAP Wizard and exported for analysis to Microsoft excel. Recycling kinetics were obtained by curve fitting to a one phase exponential $f(t) = A \times (1 - e^{-kt}) + B$, where, A is the mobile fraction, B is the fluorescence directly after photobleaching (%), and k is the rate of fluorescence recovery from which $t_{1/2}$ is determined [$t_{1/2} = \ln(2)/k$]. Statistical significance was determined using standard deviation and the Student's unpaired t-test.

Streptolysin O assay

The Streptolysin O (SLO) toxin was preactivated for 5 min at 37°C in SLO buffer (SB) containing 20 mM Hepes-KOH pH 7.2, 110 mM KOAc, 2 mM Mg(OAc)₂, 1mM DTT and SLO at a final concentration of 0,8 U/ml. Huh7 cells were seeded on glass coverslips, washed twice with SB and incubated 10 min on ice with the SB containing active SLO to allow the binding of the toxin to the cell membrane. Cells were washed twice at 4°C with Transport Buffer (TB) containing 25 mM HEPES KOH, 2.5 mM Mg(OAc)₂, 110 mM KOAc, 5 mM EGTA, 1.8 mM CaCl₂. To complete pore formation cells were incubated for 15 min at 37°C. When indicated, TB was supplemented with an ATP regeneration system containing 100 mM ATP, 500 mM Phosphocreatine, 1000 U/ml Creatine phosphokinase (Sigma-Aldrich) or TB supplemented with the same buffer containing a non-hydrolysable form of GTP (GTPγs; Sigma-Aldrich). For the immunofluorescence analysis of SLO-treated cells, cells were fixed 10 min in PBS-4% paraformaldehyde, incubated 30 min in PBS containing 0.5% BSA and 50 mM NH₄Cl without saponin and then stained for GM130 in order to label only SLO permeabilized cells. After GM130 staining, cells were permeabilized with PBS-Saponin 1% and then stained for the specific primary antibody (Sec 31 or Sec 16). Images were collected as previously described by LSM 510 confocal microscopy. The fluorescence intensity of Sec 31 or Sec 16 was measured in the region of interest of SLO-permeabilized cells; this value was normalized for the fluorescence intensity obtained by the Golgi structural protein GM130 measured in a equal area of the cell. For MEF cells, the SLO assay was performed as for Huh7 cells except that SLO concentration in SB was 0,4 U/ml, the time of incubation on ice with SLO was 6 min and the incubation at 37°C necessary for pore formation was performed for 20 min. In the Western Blotting analysis of SLO-permeabilized cells, the cytosolic fraction of proteins recovered after cell permeabilization in the TBs was subjected to TCA-precipitation; instead the membrane retained fraction of proteins was obtained after lysis of the adherent cells. Then, the cytosolic and membrane fractions (referred as *Out* and *In* respectively) were subjected to SDS-PAGE and immunoblotting with the specific antibodies. GAPDH protein was monitored as marker of cytosolic proteins and used to normalize for the rate of SLO-permeabilization. After densitometry of auto-radiographs, the percent of the protein released in the cytosol was calculated as

the percent of sum of *In* and *Out* mean values and then normalized for the corresponded *Out* fold of GAPDH release in the cytosol.

3xFlag-Sec23a and HA-Ubiquitin Co-Immunoprecipitation

10 cm dish-cultured HuH7 cells were co-transfected with 4 µg of either the p3xFlag-Sec23a or the p3XFlag empty vector plus 4 µg of the pcDNA3/HA-Ubiquitin expression vector. At 48 hours, cells were pre-treated for 2 h with 10 µM MG132 to inhibit proteasomal activity and then either co-stimulated or not with 300 nM TG for the indicated time before to be harvested in B buffer 1% Triton X-100 complemented by protease inhibitor mix (Roche). Equal amounts of cell extracts were immunoprecipitated by the anti-HA mouse antibody and the co-immunoprecipitated 3xFlag-Sec23a revealed after SDS-PAGE by the anti-Flag monoclonal antibody.

Identification of the Sec23a ubiquitination sites

Actively growing Huh7 cells were transfected with 8 µg of 3X-FLAG-Sec23a and 48 h after transfection were lysed in B-Buffer 1% Triton. Lysates were immunoprecipitated by the anti-FLAG resin (Sigma-Aldrich), subjected to SDS-PAGE and revealed by comassie colloidal staining. The gel band strongly enriched by FLAG modified beads was cut out and subjected to *in situ* protein digestion as described in Shevchenko protocol. Briefly, gel slices were reduced and alkylated using 1,4-dithiothreitol (10 mM) and iodoacetamide (54 mM) respectively, then washed and rehydrated in trypsin solution (10 ng/µl) on ice for 1h. After the addition of 30 µl ammonium bicarbonate (10 mM, pH 7.5), samples were digested overnight at 37 °C. The supernatants were collected and peptides were extracted by the gel slices using 100% CH₃CN. Finally, the supernatant was collected and both were combined. All peptides sample were dried out and dissolved in 10% FA before mass spectrometry analysis. 5 µl of the obtained peptide mixture were injected onto a nano Acquity LC system (Waters Corp. Manchester, United Kingdom). The peptides were separated using a 1.7 µm BEH C-18 column (Waters Corp. Manchester, United Kingdom) at a flow rate of 400 nl/min. Peptide elution was achieved with a linear gradient from 15 to 50% (solution A: 95% H₂O, 5% CH₃CN, 0.1% FA; solution B: 95% ACN, 5% H₂O, 0.1% FA) in 55 min. MS and MS/MS data were acquired using a Q-TOF Premier mass spectrometer (Waters Corp., Micromass, Manchester, United Kingdom). Five most intense doubly and triply charged peptide-ions were automatically chosen by the MassLynx software and fragmented. After mass spectrometric measurements, data were automatically processed by ProteinLynx software to generate peak lists for protein identifications. Database searches were carried out with MASCOT server. The SwissProt database (release 2010_11 of 02 Nov 10, 522019 sequences, 184241293 residues) was searched, allowing 2 missed cleavages, carbamidomethyl (C) as fixed modification o and oxidation (M) and phosphorylation (ST) as variable modifications. The peptide tolerance was set to 80 ppm and the MS/MS tolerance to 0.8 Da.

RNA extraction and microRNA Microarray

10 cm dishes of actively growing Huh7 cells were treated 8h with 300 nM TG, then total RNA was extracted from control and TG cells using TRIZOL reagent (Invitrogen) according to supplier's protocol. Three samples of control (A1, A2, A3) and TG-treated (B1, B2, B3) RNA were analyzed by LC Sciences (www.lcsciences.com) for microRNA microarray. The service provided RNA quality control, microRNA

enrichment and labelling according to the colour reversal strategy, microRNA detection through the hybridization to a μ Paraflo[®] microfluidics chip and finally data extraction and analysis. The microarray was performed in triplicate on three chips: on the first chip sample A1 is labeled with Cy3 and sample B1 with Cy5, on the second chip sample A2 is labeled with Cy5 and B2 with Cy3, on the third chip A3 is labeled with Cy3 and B3 with Cy5. 640 Human microRNAs were analyzed according to the Sanger miRBase release 11.0. The microarray images were carefully scanned and analysed through background subtraction, normalization and p-value calculation to produce a list of statistically-differentially expressed transcripts.

Northern Blot analysis

Northern blot analysis was carried out on 25 μ g of total RNA. All RNA samples were dissolved in loading buffer (0.05% bromophenol blue, 0.05% cyanol, 5% Ficoll type 400, 80% formamide and 7M Urea), boiled for 5 min at 95°C and fractionated on a denaturing 15% polyacrylamide gel containing 8 M urea for 90 min at 150 V. Then the RNA was transferred onto Nylon membranes (Hybond N+, Amersham/GE Healthcare) by capillary method. The membrane was prehybridized in 0.5% SDS, 5x SSC, 5x Denhardt's solution, and 20 μ g/mL sheared, denatured, salmon sperm DNA at 42°C for 2h. We used miRCURY[™] LNA probes (Locked Detection Probes, purchased from Exiqon: www.exiqon.com) for detection of miR 29-b1* and miR 663. For radiolabeling of the miRCURY[™] probes, 10 pmol of probe was combined with one μ l of γ ³²P-ATP and T4 polynucleotide kinase according to standard protocol. The labelled and denatured probes were added to membrane in the prehybridization buffer and the hybridization was carried out overnight at 42°C. After hybridization the membranes were washed at low stringency in 2x SSC, 1% SDS at 42°C twice for five minutes and exposed by autoradiography. The signals were quantified by Image-J software analysis.

Bioinformatics prediction of microRNA targets

The search of microRNA targets was performed through the comparative assessment of three targets prediction programs: Miranda (www.microrna.org), TargetScan (www.targetscan.org) and PicTar (www.pictar.org). The three lists of the putative targets were matched by MatchMiner program (www.discover.nci.nih.gov/matchminer/index.jsp) to obtain a final list of overlapping putative targets. The ontological analysis of the matched targets was performed by using the Functional Annotation Tool of DAVID (Database for Annotation, Visualization and Integrated Discovery).

2D-DIGE analysis.

Huh7 cells were lysed in B-Buffer containing 1% Triton as previously described. Samples obtained from lysis of three different preparations of control and TG-treated Huh7 cells were precipitated in acetone/methanol (8:1, v:v), for 16 h, at -20 °C, and recovered by centrifugation at 16,000 x g for 30 min, at 4 °C. Proteins were solubilized in 7 M urea, 2 M thiourea, 4% CHAPS, 30 mM Tris-HCl. Protein concentration was determined using the Bradford method (Bio-Rad Laboratories, Hercules, CA). Before labelling, the pH of the samples was adjusted to a value of 8.5. Each labelling reaction was performed with 50 μ g of the protein extracts, in a 10 μ l volume, in the presence of 400 pmol of Cy2-, Cy3- or Cy5-dyes (GE Healthcare, Little

Chalfont, Buckinghamshire, UK). A dye-swapping strategy was used; thus two Huh7 control lysates were labelled with Cy3, while the third was labelled with Cy5. In a complementary manner, two TG-treated Huh7 lysates were labelled with Cy5, and the third was labelled with Cy3. Three mixtures of the six samples (50 µg each) were labelled with Cy2 dye, as the internal standard required by the 2D-DIGE protocol. The labelling reactions were performed in the dark for 30 min, at 0 °C, and were stopped by addition of 1 mM lysine. Sample mixtures, including appropriate Cy3- and Cy5-labeled pairs and a Cy2-labeled control, were generated and supplemented with 1% IPG buffer, pH 3-10 NL (GE Healthcare, Little Chalfont, Buckinghamshire, UK), 1.4% DeStreak reagent (GE Healthcare, Little Chalfont, Buckinghamshire, UK) and 0.2% DTT (w/v) to a final volume of 450 µl in 7 M urea, 2 M thiourea, and 4% CHAPS. The mixtures (150 µg of total protein content) were used for passive hydration of immobilized pH gradient IPG gel strips (24 cm, pH 3-10 NL) for 16 h, at 20 °C, in the dark. Isoelectric focusing (IEF) was carried out with a IPGphor II apparatus (GE Healthcare, Little Chalfont, Buckinghamshire, UK) up to 75,000 V/h, at 20 °C (current limit set to 50 µA per strip). The strips were equilibrated in 6 M urea, 2% SDS, 20% glycerol, and 0.375 M Tris-HCl (pH 8.8), for 15 min, in the dark, in the presence of 0.5% (w:v) DTT, and then in the presence of 4.5% (w:v) iodacetamide in the same buffer, for additional 15 min. Equilibrated IPG strips were transferred onto 12% polyacrilamide gels, within low-fluorescence glass plates (ETTAN-DALT 6 system, GE Healthcare, Little Chalfont, Buckinghamshire, UK). The second-dimension SDS-PAGE was performed using a Peltier-cooled DALT II electrophoresis unit (GE Healthcare, Little Chalfont, Buckinghamshire, UK) at 1.5 W/gel, for 16 h. Gels were scanned with a Typhoon 9400 variable mode imager (GE Healthcare, Little Chalfont, Buckinghamshire, UK) using appropriate excitation/emission wavelengths for Cy2 (488/520 nm), Cy3 (532/580 nm), and Cy5 (633/670 nm). Images were captured in the Image-Quant software (GE Healthcare, Little Chalfont, Buckinghamshire, UK) and analyzed using the DeCyder 6.0 software (GE Healthcare, Little Chalfont, Buckinghamshire, UK). A DeCyder differential in-gel-analysis (DIA) module was used for spot detection and pairwise comparison of each sample (Cy3 and Cy5) to the Cy2 mixed standard present in each gel. The DeCyder biological variation analysis (BVA) module was then used to simultaneously match all of the protein-spot maps from the gels, and to calculate average abundance ratios and statistical parameters across triplicate samples (Student's t-test).

For preparative protein separations, 600 µg of unlabeled protein samples from control and TG-treated Huh7 cell lysates were used to hydrate passively two 24 cm strips for first dimension pH 3-10 NL IPG strips (GE Healthcare, Little Chalfont, Buckinghamshire, UK). The first and second dimension runs were carried out as previously described for the analytical separations. After 2-DE, gels were fixed and stained with SyproRuby fluorescent staining (Invitrogen, Carlsbad, CA). After spot matching with the master gel from the analytical step in the BVA module of DeCyder software, a pick list was generated for spot picking by a robotic picker (Ettan spot picker, GE Healthcare, Little Chalfont, Buckinghamshire, UK).

For protein identification, picked gel spots were minced and washed with water. Proteins were reduced, S-alkylated, and *in-gel* digested with trypsin, as previously reported (Caratu et al., 2007). Digest samples were desalted and concentrated on microC18 ZipTips (Millipore Corp., Bedford, MA) using acetonitrile as eluent before MALDI-TOF-MS analysis. Peptide mixtures were loaded on the MALDI target together with α -cyano-4-hydroxycinnamic acid as matrix, by using the dried droplet technique, and analyzed in a Voyager-DE PRO mass spectrometer (Applied

Biosystems, Inc., Foster City, CA). Spectra were acquired in reflectron mode; internal mass calibration was performed with peptides derived from trypsin autoproteolysis. The MASCOT software package was used to identify unambiguously spots from the SwissProt human sequence database by peptide mass fingerprint experiments (Perkins et al., 1999). Candidates with MASCOT scores > 62 (corresponding to $p < 0.05$ for a significant identification) were further evaluated by comparison with molecular mass and pI experimental values obtained from 2-DE. The occurrence of protein mixtures was excluded by sequential searches for additional protein components using unmatched peptide masses. Protein identification was confirmed by performing PSD fragment ion spectral analysis of the most abundant mass signal within each MALDI-TOF-MS spectrum.

Scientific background, rationale and aims

The exit from ER and the vesicular transport of newly synthesized proteins is indispensable to ensure the physiological level of secretion for hormones, neurotransmitters and proteins of the extracellular matrix. Noteworthy, dysfunctions of the molecular components of the export and transport machinery strongly impairs the proper organization and function of cellular organelles and the maintenance of cell polarity (Boyadjiev et al., 2006; Jones et al., 2003; Merte et al., 2010; Schwarz et al., 2009). Given its central function, it is conceivable that the exit from the ER could be carefully monitored by the quality control system and be one of the target of the UPR (Farhan et al., 2008; Sato et al., 2002; Travers et al., 2000). Indeed, several proteins involved in the vesicular transport between the ER and the Golgi complex are under the UPR control. In previous works, we and others demonstrated that the cargo receptor proteins ERGIC-53, MCFD2 and VIP36 are regulated by UPR (Nyfeler et al., 2003; Renna et al., 2007; Spatuzza et al., 2004).

Given these considerations, we analyzed the molecular mechanisms controlling the export and the transport of secretory proteins from the ER to the cis-Golgi in the contest of ER stress. The experimental system is composed of Huh7 human hepatoma cells, in which the ER stress is induced by thapsigargin (TG), dithiothreitol (DTT), nitric oxide (NO) or MG132.

In this contest, we first investigated the effect of ER stress on the morphology and the activity of the secretory pathway at the ER–Golgi boundary. In particular we explored the effect of the ER Stress on the maintenance of the architecture of ERGIC and cis-Golgi by analyzing the distribution of ERGIC-53 and GM130. Moreover, we studied the rate of ER-to-Golgi transport by the use of the temperature sensitive mutant of the G protein of the Vesicular Stomatitis Virus fused to GFP (VSV G ts045). Since the anterograde transport from the ER is mediated by COPII coated vesicles, we analyzed the effect of the ER stress on COPII vesicles assembling at ER Exit Sites. We found that ER Stress rapidly targets the formation of the COPII vesicles. These results prompted us to identify the molecular components of COPII which are sensitive to ER Stress. To this aim, we analyzed the protein expression levels, the distribution and the kinetics of binding to ER membrane of Sec16a, Sec23a and Sec31 that represent respectively the scaffold, the inner and the outer layer of COPII coats. We found that ER Stress changes COPII coats assembling by affecting Sec16 expression and the Sec23a binding to ER Exit Sites.

Results

ER stress modifies the subcellular localization of ERGIC-53 and GM130 proteins

To analyze the effect of ER stress on post-ER compartments we examined the effect of thapsigargin (TG) and nitric oxide (NO) exposure on the intracellular localisation of ERGIC-53 and GM130 that are respectively markers of ERGIC (ER Golgi Intermediate Compartment) and *cis*-Golgi. The cargo receptor ERGIC-53 recycles between the ERGIC and the ER to export from the ER a group of N-glycoproteins (Anelli et al., 2007; Appenzeller et al., 1999; Nyfeler et al., 2008). GM130 is a member of the family of coiled-coil golgins, (Linstedt and Hauri, 1993) and continuously cycles between the ERGIC and the *cis*-Golgi compartments (Barr et al., 1998). Confocal microscopy showed that in the control cells (Fig. 1: C panels) endogenous ERGIC-53 protein was visible in spots dispersed throughout the cytoplasm and concentrated in the perinuclear region of the cell. In non-stressed cells, a portion of ERGIC-53 colocalizes with the *cis*-Golgi protein GM130 in the perinuclear area (Fig. 1: C panels, merged picture and insert). In response to the ER stress induced by either 300 nM TG or 1 mg/ml of the NO donor DETA NONOate for 2 h, both proteins were present in spots more dispersed throughout the cytoplasm (Fig. 1: TG and NO panels) indicating that the subcellular organisation of the ERGIC and *cis*-Golgi underwent significant changes during the ER stress response. In addition, endogenous ERGIC-53 and GM130 segregated in different membrane structures upon stress induced either by TG or NO (Fig. 1: NO and TG panels, merged pictures and inserts). These observations were confirmed by immunoelectron microscopical analysis, (Fig. 2) which revealed that in the ER stressed cells ERGIC-53 and GM130 proteins located in distinct vesicles. Furthermore, in all the sections prepared from ER stressed cells, the Golgi stacks were no longer visible indicating that, similarly to the ERGIC, the ultrastructural organisation of the Golgi complex was severely compromised by either the TG or the NO treatment (Figure 2: B and C panels, respectively).

ERGIC-53 and GM130 localise in lighter density vesicles upon ER stress

To further describe the effect of ER stress on post ER structures of the secretory pathway we analysed by sucrose gradient the sedimentation profile of ERGIC-53 and GM130. To this end, the postnuclear supernatant fraction of uninduced or ER stress induced cells was loaded on a sucrose discontinuous gradient (Spatuzza et al., 2004). In the thirteen fractions obtained, ERGIC-53 and GM130 were revealed by Western Blotting (WB). WB analysis showed that in normal conditions ERGIC-53 was enriched in fractions 5-7 and GM130 in fractions 3-7 (Fig. 3). 2 h incubation with 300 nM TG or 1 mg/ml of the NO donor DETA NONOate changed the distribution of ERGIC-53 to fractions 5-10 and of GM130 to 3-13 (Fig. 3) suggesting that ER stress induced the shift of both proteins to lighter density vesicles. We also analyzed the sedimentation profile of calreticulin and found that its distribution was clearly not influenced by ER stress (Fig. 3) indicating that the distribution within the ER of calreticulin was not affected by ER stress. Since ERGIC-53 and GM130 are both mobile proteins, these results could suggest that ER stress alters the dynamic of their recycling in the retrograde and/or anterograde direction and/or the structure of ERGIC and *cis*-Golgi derived vesicles.

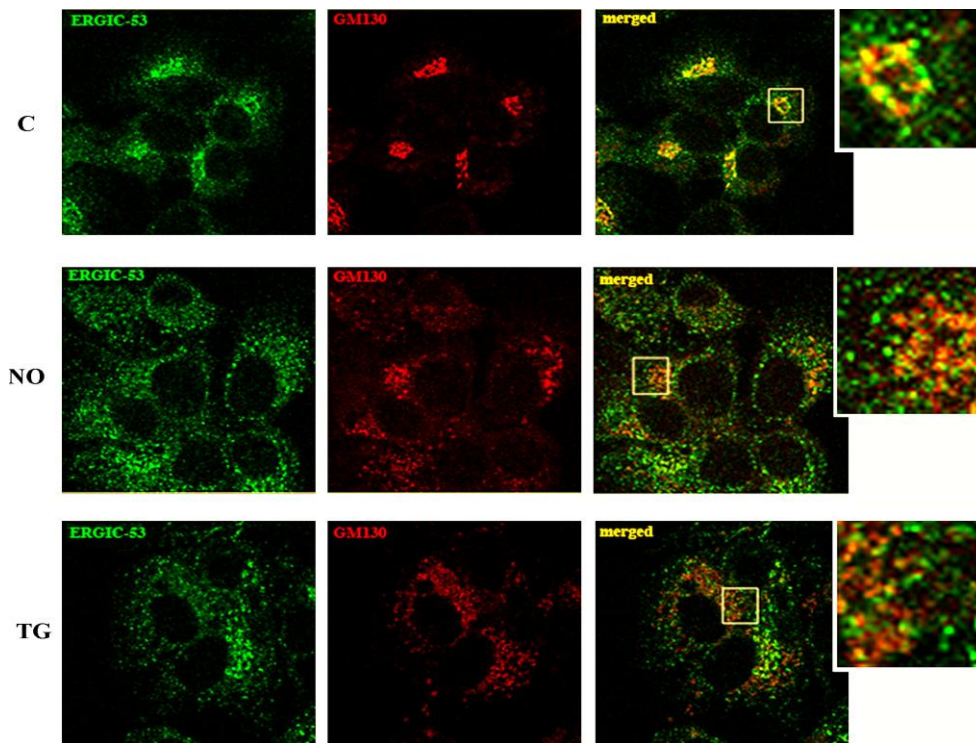


Fig. 1 Effect of ER stress on the distribution of protein markers of the early secretory pathway. Huh7 cells seeded on glass coverslips were either left untreated (C) or subjected to ER stress for 2 h with 300 nM thapsigargin (TG) or 1 mg/ml detanonoate (NO) fixed and processed for immunofluorescence analysis with the anti-ERGIC-53 and GM130 antibodies. Confocal analysis was then performed as detailed in the materials and methods section.

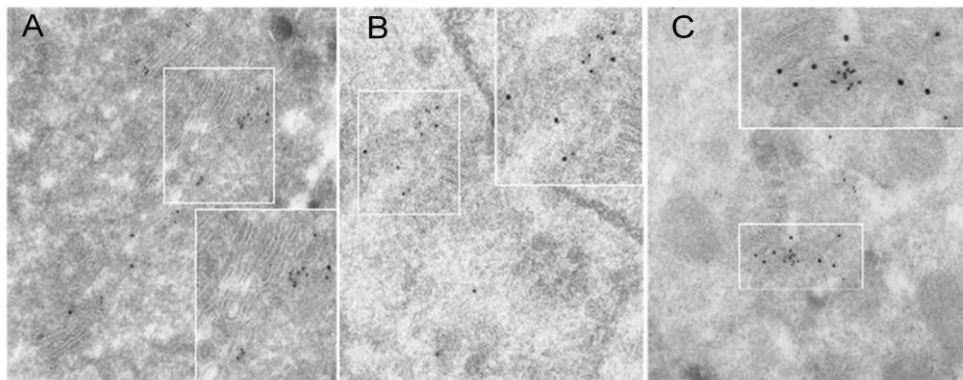


Fig. 2 Ultrastructural analysis of the effect of the ER stress induced by thapsigargin (TG) and detanonoate (NO) on the ERGIC and the Golgi complex. Golgi and peri-Golgi areas of control (A) or 2 h TG- (B) or nitric oxide-treated (C) Huh7 cells display immunostaining for anti-ERGIC-53 (10 nm) and anti-GM130 antibody (15 nm). The two antigens do not co-localize in the same vesicles. Insets display enlarged views of the Golgi complex included in the boxed areas. The morphology of the Golgi complex is modified in response to ER stress and appears fragmented (e.g., compare A vs. B and C). Bar: A = 321 nm; A inset = 284 nm; B = 367 nm; B inset = 249 nm; C = 367 nm; C inset = 194 nm

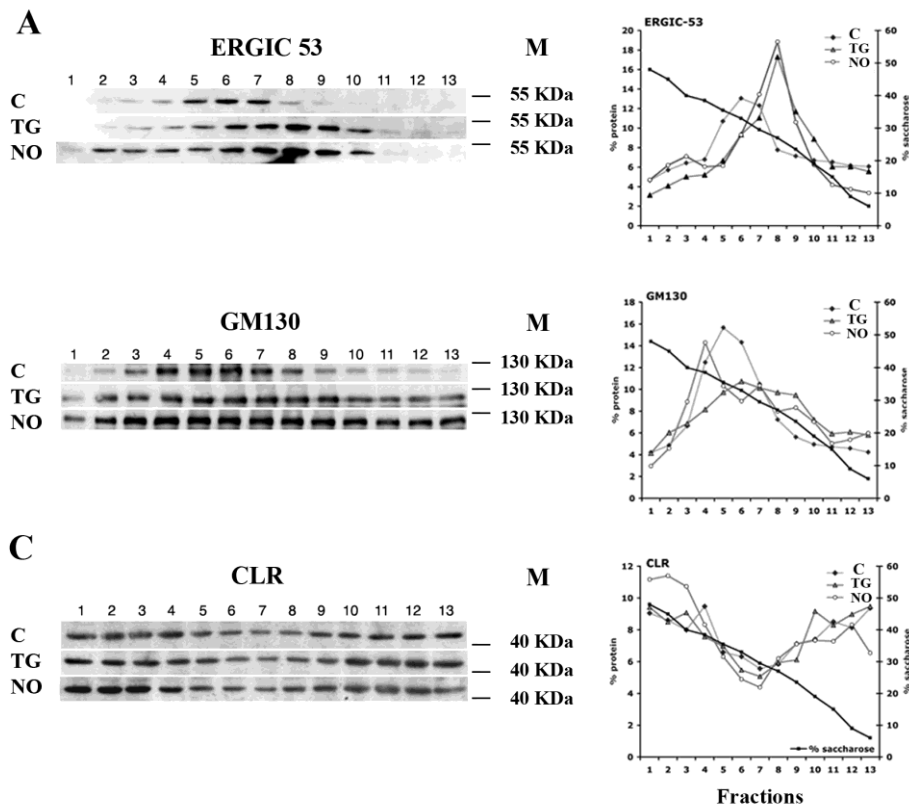


Fig. 3 Cell fractionation analysis of the intracellular distribution of ERGIC-53, GM130 and CLR in response to ER stress. (A-C) Control or ER stress-induced Huh7 cells were homogenised by a Wheaton cell cracker and the post nuclear supernatant fraction loaded on the top of a discontinuous sucrose gradient (Erra et al., 1999; Spatuzza et al., 2004). After ultracentrifugation, 13 fractions were collected, TCA-precipitated and analysed by immunoblotting with the indicated antibodies. The graphs on the right side of the panels report the relative distribution of the proteins along the gradient. Values obtained are representative of three independent experiments.

ER stress impairs the reconstitution of ERGIC and cis-Golgi after Brefeldin A (BFA) treatment

To test whether ER stress could interfere with the formation of the ERGIC and of the *cis*-Golgi complex we performed BFA wash-out experiments. BFA treatment induces breakdown of the Golgi complex, redistribution of Golgi proteins into the ER and accumulation within the ER of newly synthesized proteins (Klausner et al., 1992). As expected, either ERGIC-53 or GM130 relocalised to peripheral structures (Figure 4, 1 h BFA), known as the ERGIC remnants, which are close to the ERES (Ward et al., 2001). Upon removal of BFA, both ERGIC-53 and GM130 progressively gained their ERGIC and *cis*-Golgi pattern respectively, reaching the optimal recovery at 60 min (Figure 4: wash out, upper panel). Interestingly, when BFA wash out was performed in the presence of 300 nM TG for the times indicated, ERGIC-53 and GM130 were unable to recover the original intracellular pattern (Figure 4: wash out, lower panel). This result indicates that ER stress interferes with the reconstitution after BFA of both ERGIC and Golgi complex. This suggests that the vesicular transport from the ER to the Golgi complex might be altered by ER stress preventing the proper delivery of proteins required for the maintenance of the architecture of post-ER compartment or for the process of membranes homotypic fusion.

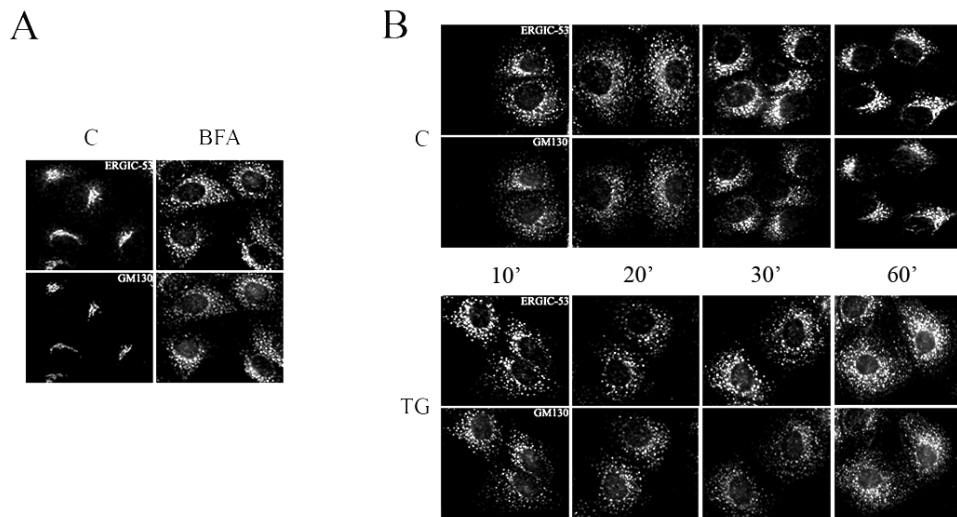


Fig. 4 Time course analysis of ERGIC-53 and GM130 localisation during BFA wash-out. (A) Huh7 seeded on glass coverslips were untreated (C) or treated for 1 h with 5 μ g/ml of Brefeldin A (BFA). (B) Following BFA treatment, the cells were washed-out and incubated in the presence (TG) or in the absence (C) of 300 nM TG for the times indicated, and then processed for the immunofluorescence analysis with anti-ERGIC-53 or anti-GM130 antibodies.

ER stress rapidly delays the anterograde transport of the VSV G ts045G reporter glycoprotein

To test whether ER stress could interfere with the rate of the ER to Golgi transport, we analyzed the effect of ER stress on the rate of cargo glycoproteins transport from the ER to the Golgi complex, using the ts045 conditional mutant of the VSV G protein fused to the reporter protein GFP (ts045G) as reporter for transmembrane-type proteins. This viral secretory protein is unable to correctly fold when expressed at non-permissive temperature (39°C) and is therefore trapped in the ER by quality control system. Upon shifting the temperature to 32°C, the protein rapidly folds and moves toward Golgi compartment until the reaching of plasma membrane (Presley et al., 1997). The ts045G protein was used in transient transfections to compare the rate of transport to the Golgi apparatus in normal and ER stressed cells (Fig. 5). The cells transfected with the fusion protein were maintained at 39°C for 16 h to induce ts045G unfolding and retention within the ER (Fig. 5A; ts045G green panel). Upon shifting to 32°C, ts045G rapidly moved forward the secretory pathway to reach the Golgi complex within 10 min (Fig. 5B, green panel). Fluorescence quantification showed that $67,4 \pm 12,5\%$ of total ts045G reached the Golgi area while the remaining $32,6 \pm 12,5\%$ was retained within the ER (Fig. 5B and 6). Instead, when the shift to 32°C was performed in the presence of 300 nM TG for 15 min the amount of ts045G protein in the Golgi area drastically declined ($36,4 \pm 4,2\%$, Fig. 5C and Fig. 6), indicating that the induction of ER stress rapidly reduces the transport of the reporter protein from the ER to the Golgi complex. In all the experimental conditions either the membrane network of the ER, revealed by an anti-KDEL antibody, which stains ER resident proteins bearing KDEL retention signal (i.e. GRP78/BiP) (Fig. 5A; KDEL panel), or the *cis*-Golgi, stained by the anti-GM130 antibody (Fig. 5A; GM130 blue panel), appeared unmodified, suggesting that the ER stress did not alter the ER and the Golgi complex organization. One of the possible hypothesis for the impairment of the ER to Golgi transport could be the reduction of the amount of protein competent for the export from ER. It's known in literature that trimerization is a prerequisite for the ER to Golgi transport of the ts045 variant of the VSV G protein (Doms et al., 1987), so to understand whether the reduced transport to the Golgi complex was due to a defective oligomerization of the reporter protein induced by the ER stress, we performed velocity gradient analyses to evaluate the rate of oligomerization of the ts045G protein (Fig. 7) (Meunier et al., 2002). Results showed no significant decrease in the amount of total ts045G reporter recovered from the cell extracts obtained from the uninduced and the induced cells, indicating that in our experimental condition there was no decrease of the reporter protein due to induced ER stress dependant degradation. More interestingly, the velocity gradient analysis showed that the cells shifted for 4 min to the permissive temperature (32°C) showed the same rate of conversion to the trimeric form of the reporter ts045G protein either in the presence or in the absence of 300 nM TG. This finding indicated that incubation with TG did not alter the oligomerization of the reporter protein, thus suggesting that the reduced rate of transport was not due to a rapid decrease of the amount of the cargo protein competent for the export step.

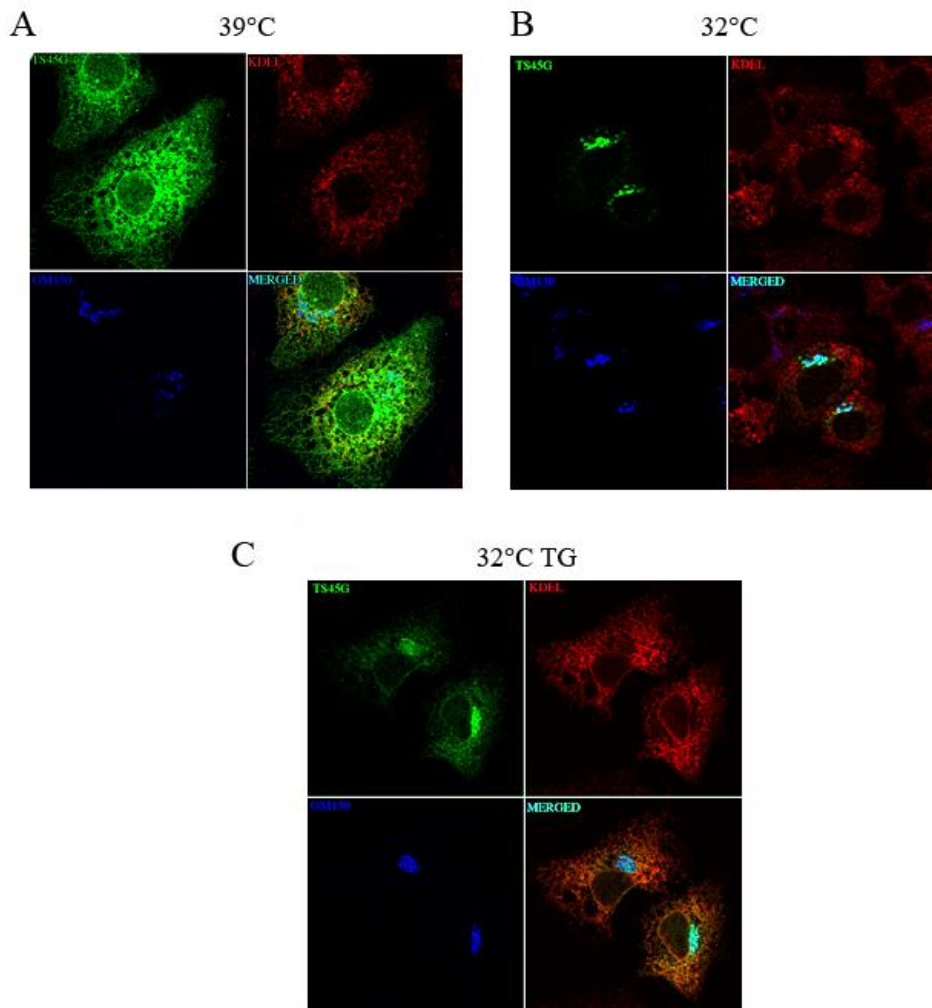


Fig. 5 Effect of ER stress on the anterograde transport of VSV ts045G glycoprotein. (A) Huh7 seeded on glass coverslips were transiently transfected with the ts045G expression vector and kept at the non permissive temperature (39°C) from 12 to 24 h post-transfection. (B) and (C) Cells transfected as in (A) were shifted at the permissive temperature (32°C) for 10 min in the absence (B) or in the presence (C) of 300 nM TG and then fixed, stained with the anti-KDEL (KDEL), the anti-GM130 (GM130) and the anti-GFP (ts45G) antibodies and subjected to confocal immunofluorescence analysis. TG was added at 39°C 5 min before the shift to 32°C only to the cells shown in C.

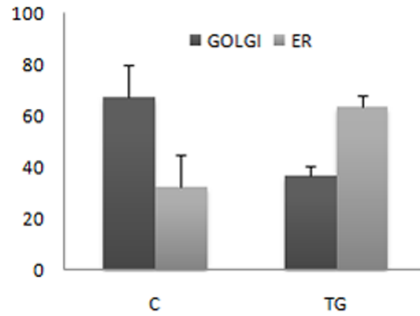


Fig. 6 Quantitative analysis of the effect of ER stress on the ER-to-Golgi transport of VSV-G *ts045G* glycoprotein. Diagrams represent the quantification of the mean intensity of the *ts045G* fluorescence in the Golgi or in the ER area obtained by using a laser scanning microscope (LSM 510; Carl Zeiss MicroImaging, Inc.). Fluorescence intensities were measured on selected regions corresponding to the ER or to the Golgi complex area of untreated (C) or TG treated cells in a single z-plane through the cell volume (from a range of 1–3 μ m starting from the top of the cell). 100% was considered the sum of ER plus Golgi area fluorescence. Results represent the mean of three experiments performed in triplicate.

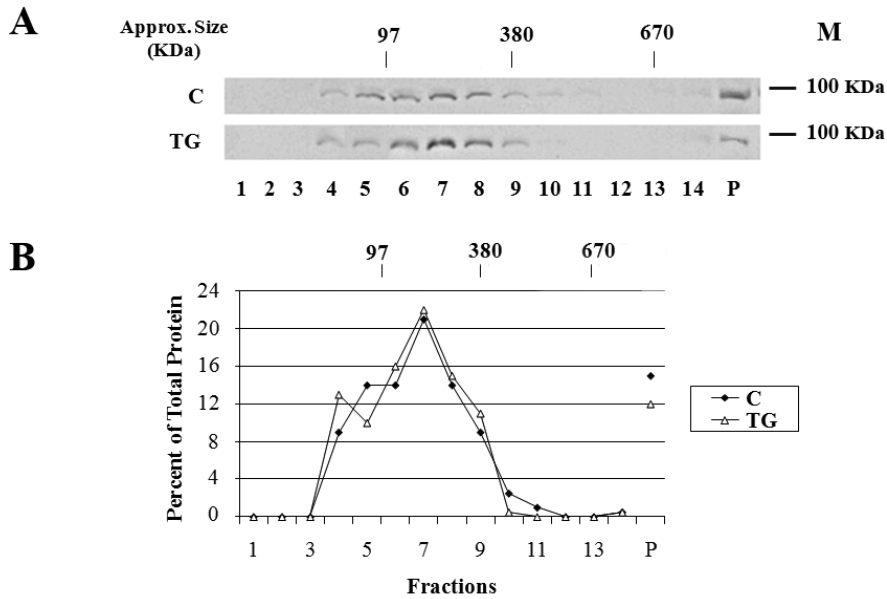


Fig. 7 Velocity gradient centrifugation to determine the trimerization rate of the *ts045G* protein. Protein extracts were prepared from Huh7 cells transiently transfected with the *ts045G* expression vector. Lysates were ran through 20-40% glycerol gradients. Fractions of 300 μ l were collected from the top (fraction 1) to the bottom (fraction 14) of the gradients. Proteins were precipitated with TCA and detected by western blotting using anti-GFP antibody. The position of the molecular mass markers is indicated.

ER stress rapidly reduces the number of COPII-coated transport vesicles assembling on ER membranes

A possible explanation to the rapid decrease in the transport of the reporter protein in the presence of ER stress could be the impairment of the ER-export machinery. To test this hypothesis, we took advantage of the temperature block at 10°C, that allows the assembly of the COPII coated vesicular carriers at the ERES but prevents their fission, thus allowing a better evaluation of these transport complexes (Mezzacasa and Helenius, 2002; Ronchi et al., 2008). Thus, the temperature shift experiment shown in Fig. 5 B and C was repeated but lowering the temperature to 10°C for 1 hour, and the cells incubated with anti-Sec31 antibody to stain the assembling COPII-coated transport vesicles. As shown in Fig. 8, a drastic reduction of the number of Sec31 labelled puncta was induced by the presence of 300 nM TG, while the overall distribution of both ts045G and Sec31 labelling did not appear changed. Interestingly, the spots labelled by Sec31 colocalized with ts045G at a similar extent in the presence as well as in the absence of 300 nM TG (about 70%), a finding more compatible with a decreased number of assembling COPII-coated transport vesicles than with a decreased interaction between VSV-G and COPII proteins. To explore this view, we measured with the Image J software the number of Sec31 labelled spots in the different experimental conditions used, simply assuming that each individual spot would represent one COPII assembling transport vesicle. The results of this quantitative analysis, summarized in Fig. 9, together with representative images, show that 300 nM TG induce almost a 50% decrease in the number of Sec31 spots at either 32, 37 or 39°C, indicating that the effect previously seen at 10°C was not peculiarly due to low temperature. Most importantly, the effect is displayed already after 5 min incubation at 39°C, suggesting that it represents an important and quick route by which ER stress exerts its function. Intriguingly, the maximum effect was detected by the combination of prolonged incubation with TG (1 h) and low temperature (10°C), suggesting that TG overwhelms the stabilization effect of low temperature. In addition, these results were confirmed when anti-Sec23 antibody were used to follow another component of the COPII coat, although the lower quality of the fluorescence signal did not allowed a quantitative analyses (data not shown). Finally, the distribution of ER resident protein calnexin changed only slightly, suggesting the ER-stress did not grossly alter the structure of the ER in all conditions tested (Fig. 9B).

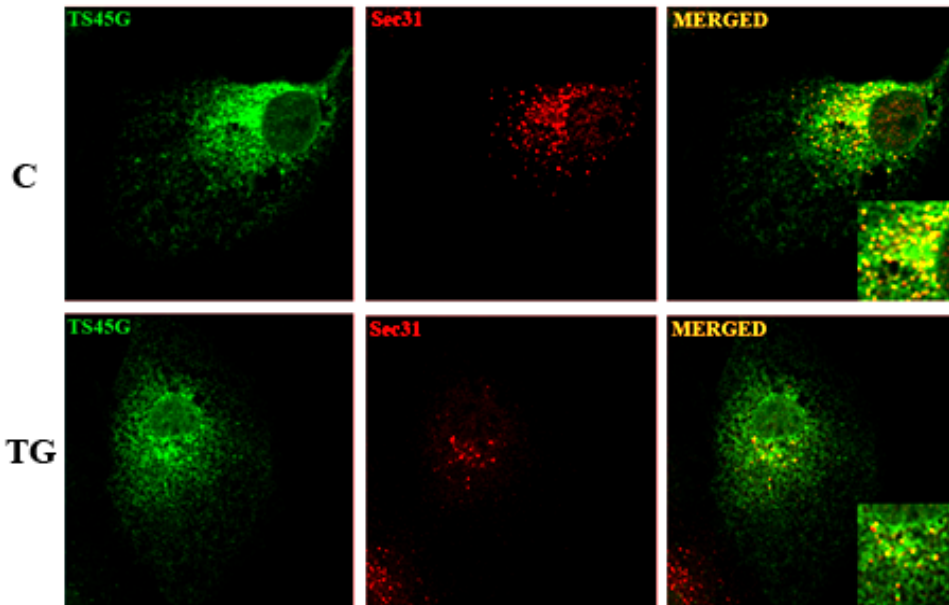


Fig. 8. Effect of ER stress on the COPII coated transport vesicles. Huh7 seeded on glass coverslips were transfected with the VSV G ts045G expression vector, incubated at 39°C for 24 h and shifted to 10°C for 1 h in the absence or in the presence of 300 nM TG. TG was added at 39°C 5 min before the temperature shift. After fixation, the cells were stained with the GFP and anti-Sec31 antibody.

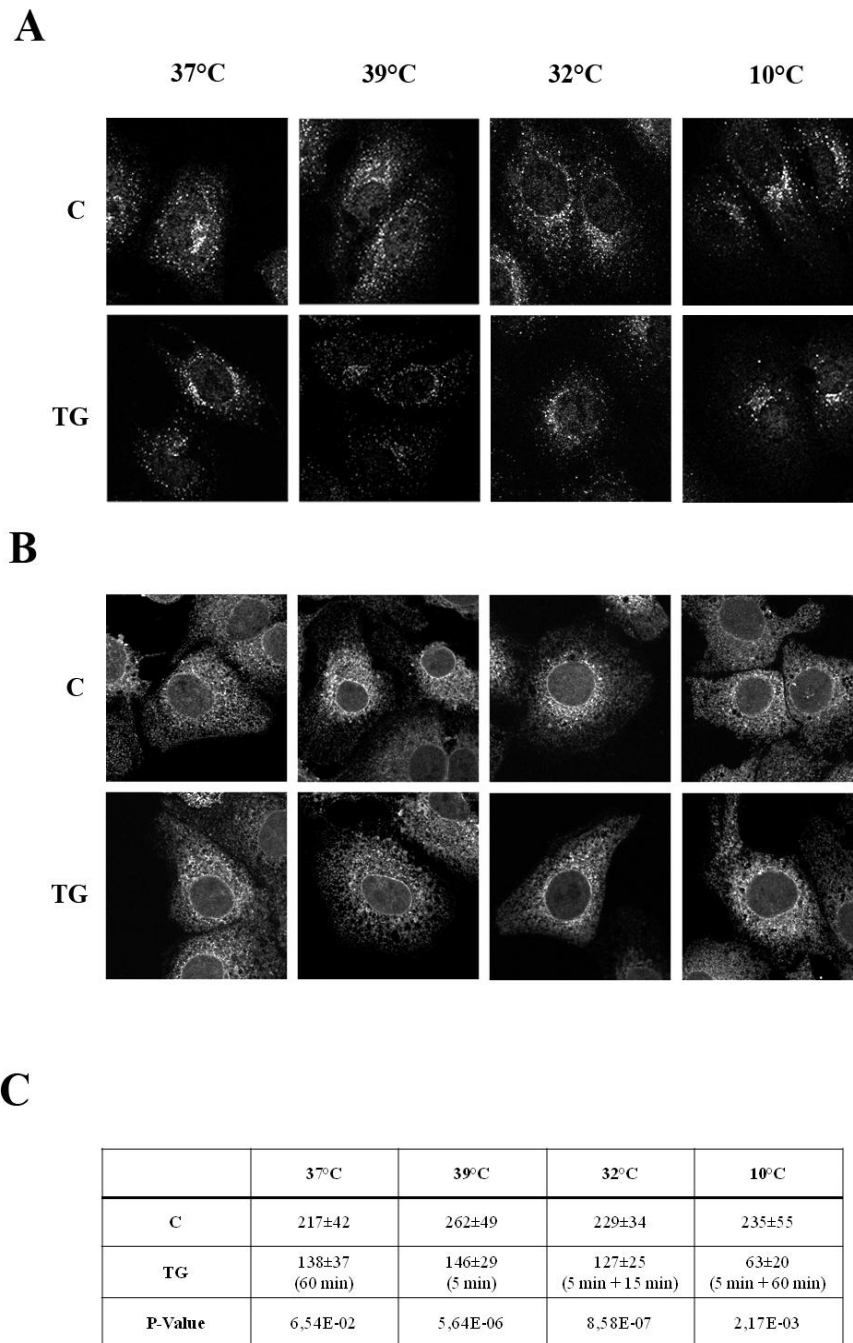


Fig. 9. Quantitative evaluation of the effect of ER stress on the assembling of the COPII coats at different temperatures. (A) Untransfected Huh7 cells kept at 37°C (37°C)

were either untreated (panels C) or incubated with 300 nM TG for 1 h (panels TG); VSV G ts045G transfected cells (39, 32 and 10 °C panels), were processed as in Figs. 5 and 6; TG was added to the cells kept at 39 °C 5 min before fixation. All cells were fixed and processed for immunofluorescence analysis with the anti-Sec31 antibody. (B) Immunofluorescence analysis with anti-calnexin antibody of Huh7 treated as in A. (C) Average number of Sec31 positive spots counted in cells processed as in panel A. Quantitative analysis was performed by the ImageJ software. For each condition, a minimum of 50 different cells were counted.

TG treatment modifies the distribution of Sec16 at the ER Exit Sites

Formation of the COPII coat occurs at ER Exit Sites (ERES) (Tang et al., 2005), where the Sec16 protein is localized to initiate the assembling of COPII complex (Watson et al., 2006) Thus, to test whether the reduction of COPII observed in the TG induced cells was the consequence of changes in the localization of Sec16 at the ER membrane, we studied the distribution in the Huh7 cells of the endogenous Sec16 protein at the steady state and following different times of TG exposure by indirect immunofluorescence. Our results (Fig. 10) showed that in control cells Sec16 is localized in punctuate structures disseminated all through the cytoplasm with an average number of 537 spots/cell. This number represents the amount of potential ERES present at the steady state in the Huh7 cells. In agreement with previous report (Hughes et al., 2009), the spots labelled by Sec31 colocalized only partially with the Sec16 puncta (30%). Instead, in the TG induced cells quantitative analysis showed that the number of Sec 16 spots as well as Sec31s, declined consistently. Meanwhile, the Sec31 colabelled with Sec16 at the same extent as in the control cells suggesting that TG could influence the formation of COPII by targeting Sec16.

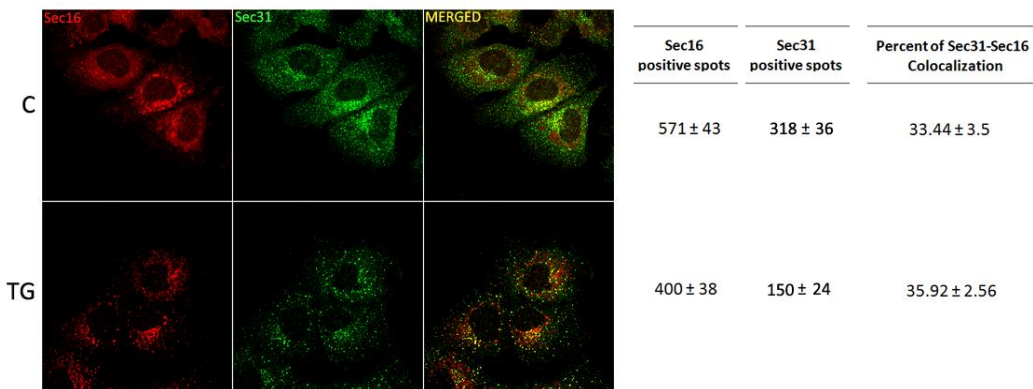


Fig.10 Analysis of Sec16 localization and expression during TG treatment in Huh7 cells. Huh7 cells seeded on glass coverslips were either untreated (C) or incubated with 300 nM TG for 2 h, fixed and processed for immunofluorescence analysis with the anti-Sec16 (sec16) and anti-Sec31 (Sec31) antibodies. Images were acquired by Leica confocal microscope. Colocalization measurements were performed on a minimum of 50 different cells by Leica software.

ER Stress down-regulates the Sec16 protein expression

To establish whether the reduction of the number of Sec16 spots in response to TG treatment was the effect of defective expression of Sec16 or of one or more components of the COPII coat, we analysed by WB the level of the endogenous Sec16 protein in the normal or in the TG induced cells (Fig. 11). The response of Sec16 to TG was compared to that displayed by the other components of the COPII coat Sar1, Sec23a and Sec31. Densitometry analysis of WB showed that the amount of the Sec16 protein was reduced (70%) by the 2 h of TG treatment. Instead, the amount of Sec31, Sec23a and Sar1 proteins was slightly reduced in the TG treated cells. TG efficiently induces general inhibition of translation by the activation of the PERK dependant eIF2 α phosphorylation (Harding et al., 1999). Therefore, this event could severely reduce the level of those proteins having short half-life. Therefore, to verify whether the reduced level of Sec16 was the effect of the general attenuation of protein synthesis, the amount of Sec16 was measured by densitometry of WBs performed on cells treated with cycloheximide (CHX) for different times. Results showed that CHX inhibited Sec16 expression only partially and at similar extent to Sec31, Sar1 and Sec23A suggesting that the decreased amount of the Sec16 protein was only in part due to the TG dependent inhibition of the mRNA translation.

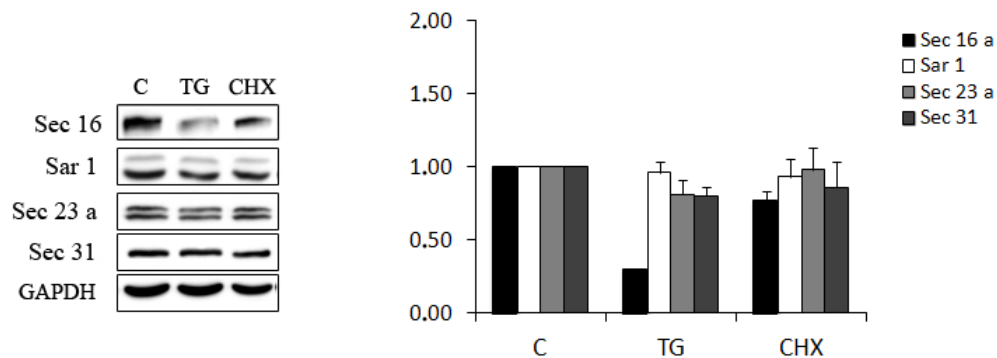


Fig. 11 Western blotting analysis of COPII proteins level in TG-treated Huh7 cells. Huh7 cells exposed to 300 nM thapsigargin for 2 h or control cells (C) were lysed in B-Buffer Triton 1%; protein extracts (30 μ g) were subjected to western blotting for the indicated proteins. One out of three separate experiments is shown. The histogram shows the relative normalized abundance of Sec 31, Sec23a and Sar1 in Huh7 cells calculated from densitometry of immunoblots using GAPDH as internal standard (n = 3 independent replicates/each Ab reaction).

ER Stress doesn't modify the dynamic of association of Sec16 to ERES

We next asked whether TG could affect the amount of Sec16 bound on the ER membrane *in vivo*. Thus, to measure the amount of Sec16 retained on ER membranes in the course of TG treatment we made use of the immunofluorescence analysis of cells perforated by the SLO toxin. SLO is a toxin that upon binding to cholesterol enriched plasma membrane polymerizes to form pores larger than 10 nm. In this condition cytosolic proteins of perforated cells can be washed out and the amount of proteins retained at the intracellular membranes can be measured by

immunofluorescence (Fig 13). By the use of the SLO assay, we found that permeabilization with SLO toxin left about the 50 % of Sec16 on ER membranes in control cells but 2 h of TG treatment didn't modify the level of Sec16 retention (Fig.14 A, B). Indeed, the comparison between the steady state samples of control and TG treated cells (Fig. 14 C) reveals that in TG-cells only the 60 % of Sec16-related fluorescence is detectable compared to control cells. This data is in agreement with the down-regulation of Sec16 protein expression and suggests that the recycling kinetic of Sec16 at ERES is not modified by ER Stress. To test this hypothesis we performed the Fluorescence Recovery After Photobleaching (FRAP) on Huh7 cells transiently transfected with a GFP-Sec16 expressing vector (Fig. 14 D). We found that the rate of recycling of Sec16 in control cells is 7 ± 1.9 and that 2 h of TG treatment doesn't modify significantly this value (7.5 ± 1.7) suggesting that ER stress does not impair Sec16 association to ERES.

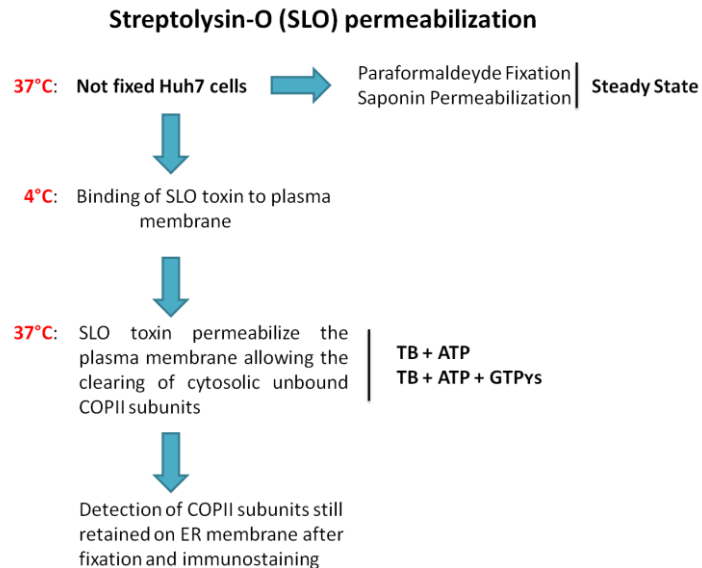


Fig. 13 *Scheme of Streptolysin-O permeabilization.* At 4°C SLO toxin binds the cholesterol of plasma membrane on unfixed cells; after shifting the temperature to 37°C, SLO becomes active and perforates the membrane allowing the clearing of the cytosol in the presence of specific buffers (TB+ATP;TB+ATP+GTP γ s). The detection of COPII proteins still associated to ERES is performed by immunofluorescence or Western Blotting. The value of proteins retention on ER membrane is compared to that of Steady State cells that are fixed and permeabilized by the saponin detergent.

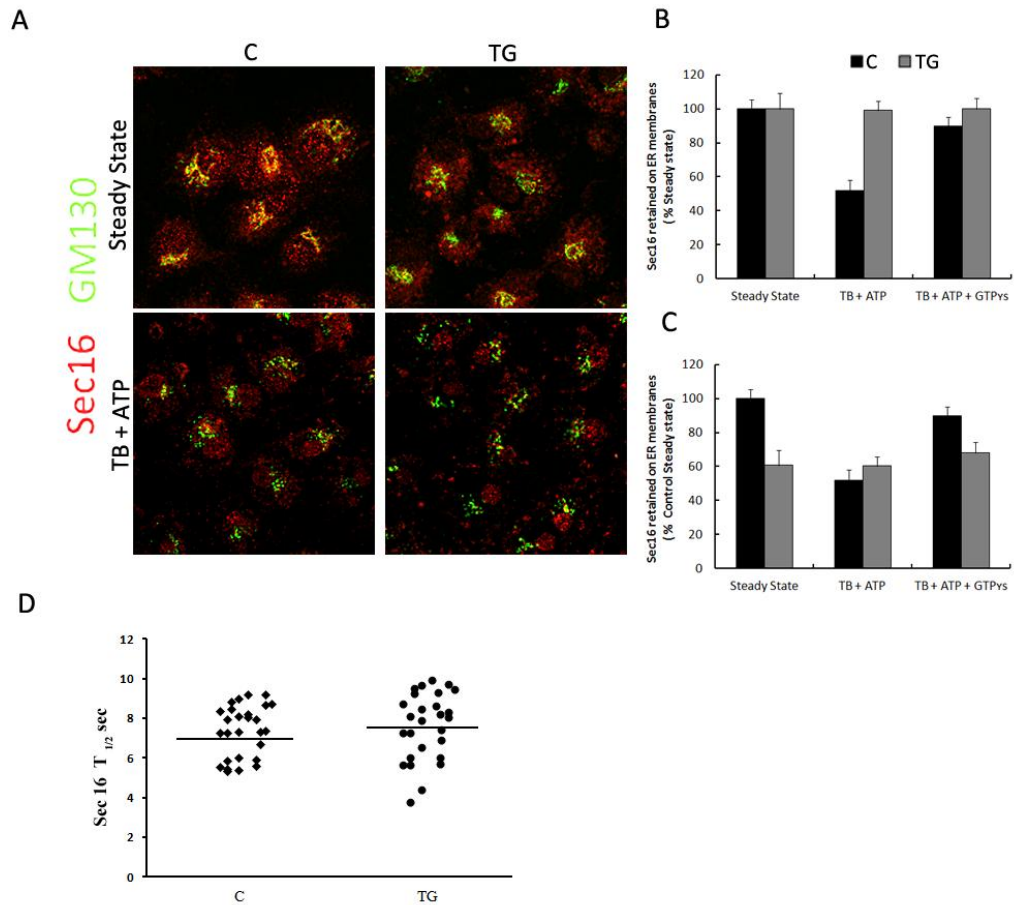


Fig. 14 Analysis of the association of Sec16 to the ER membrane. (A) Huh7 control (C) cells or cells treated 2 h with 300 nM TG were permeabilized with 0,8 U/ml of SLO 15 min at 37°C in presence of TB+ATP or TB+ATP+GTPys. Steady State cells were only permeabilized with PBS - saponin 1%; all the coverslips were fixed and stained for Sec16 and GM130. GM130 is used as marker of SLO-permeabilization. Panels show Sec16 and GM130 staining for Steady State and TB+ATP conditions. (B;C) The histograms show the percent of Sec16 retained on the ER membrane and normalized for GM130 mean intensity of fluorescence. The value of Sec16 retention measured in control and TG-treated cells for Steady State samples (B) or only in control Steady State cells (C) is set to 100%. For each condition, a minimum of 50 different cells were counted. (D) Huh7 cells were transfected with 2 µg of GFP-Sec16 expressing vector, 24 h after transfection were treated (TG) or not (C) with 300 nM TG for 2 h and subjected to FRAP analysis. TG was maintained also during FRAP experiment. Individual T_{1/2} value are plotted. Horizontal bar indicates the mean of T_{1/2} values of at least 25 individual Sec16 positive spots of 10 different cells.

The IRE1 knock-out reduces the binding of Sec31 and Sec16 to ER membranes

Few data present in literature (Sato et al., 2002) suggest the involvement of IRE1 alpha in the control of vesicles budding from ER. Therefore, we analyzed the distribution of the COPII marker Sec31 and of the ERES marker Sec16 in wild type MEF and in MEF knock-out for the IRE1 transducer. The immunofluorescence staining of Sec31 and Sec16 (Fig. 15 A) reveals for both Sec31 and Sec16 a significant reduced number of spots and a more dispersed distribution in the cytosol for knock-out MEF compared with WT cells. Given this preliminary data, we conducted a SLO assay to measure the level of Sec31 and Sec16 association to ER membranes in MEF cells. We found that already at steady state both Sec31 and Sec16 are less associated to ER in IRE1 $-/-$ MEF compared to WT (Fig. 15 B). After SLO permeabilization (TB+ATP condition) the amount of Sec31 retained on ER membranes is still reduced for MEF WT and knock-out while the amount of retained Sec16 is reduced in WT MEF but doesn't change in Knock-out cells. The latter result is consistent with the level of Sec16 retention observed in TG-treated HUH7 cells after SLO permeabilization (TB+ATP condition: Fig. 14 B, C). It's interesting that the reduced association to ER is relevant in Knock-out cells only at steady state condition and not after SLO permeabilization both for Sec31 and Sec16. This could suggest that even if Sec31 and Sec16 are halved in Knock-out cell, they are stably associated at ERES. In conclusion, the data shown demonstrate that the UPR, through the IRE1 pathway, regulates the formation of COPII-coated transport intermediates although we can't exclude the simultaneous participation of other pathways activated by UPR.

ER Stress alters the dynamic association of Sec23a and Sec31 to ERES

We next asked whether the ER Stress could affect the binding of Sec23a and Sec31a to ERES. Therefore, to measure the amount of Sec23a and Sec31 retained on the ER membrane during ER Stress we performed the SLO-toxin permeabilization of Huh7 cells untreated or treated 2 h with TG. The amount of Sec23a retained on ER was revealed by Western Blotting. Figure 16 A shows that the TG-treated cells retained on ER membrane only the 57 % of Sec23a (panel A, *In fraction*) compared to 89% of the control cells. To confirm the reduced association of Sec23a to ER membrane during the ER Stress we performed the Fluorescence Recovery After Photo-bleaching (FRAP) experiment on Huh7 cells transiently transfected with a GFP-Sec23a expressing vector. We found that the recycling rate of sec23a-GFP was 5.48 ± 1.1 in control cells (Fig. 16 B) and 4.33 ± 0.92 in the TG-treated cells. This reduction, although small, is statistically significant (p-value: 0.015) and indicates a more rapid spreading of Sec23a-GFP at ERES. This data indicates that, conversely to Sec16 protein, Sec23a is less associated to ER membrane and its recycling kinetic is faster than control cells but isn't down-regulated by ER Stress (Fig. 11). We also analyzed the residual association of Sec31 to ERES by immunofluorescence of SLO-permeabilized cells. Interestingly, as shown in Figure 17, TG reduces of about 50 % the level of Sec31 association to ER membranes. Moreover, in order to evaluate whether the altered association of Sec31 was actually related to ER-stress condition, we performed the SLO assay in Huh7 cells treated with either dithiothreitol (DTT), which induces ER stress by interfering with disulphide bonds stability and/or formation, or MG132, which induces ER stress by acting as an inhibitor of the proteasomal degradation pathway. The results demonstrate that not only TG but also MG132 and DTT significantly reduce the binding of Sec31 to ER membrane.

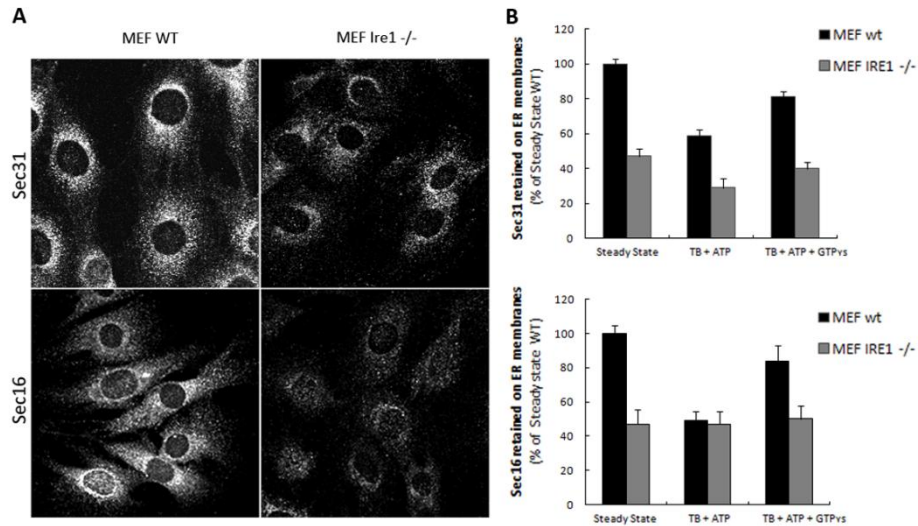


Fig. 15 Immunofluorescence analysis of Sec31 and Sec16 association to ER membranes in MEF wt and IRE1 knock-out cells. (A) MEF wt and IRE1 knock-out cells seeded on glass coverslips were fixed and processed for immunofluorescence analysis with anti-Sec31 and anti-Sec16 antibodies. (B) Histograms showing the percent of retention on ER of Sec31 and Sec16 measured by SLO assay in MEF wt and knock-out cells. Steady State cells (imaged in A) were permeabilized with PBS - saponin 1%. TB+ATP or TB+ATP+GTP γ s samples were permeabilized with 0,4 U/ml of SLO 20 min at 37°C; all the coverslips were fixed and stained for Sec31 and GM130 or Sec16 and GM130. GM130 is used as marker of SLO-permeabilization. The histograms show the percent of retention on ER membrane of Sec31 and Sec16 normalized for the correspondent GM130 mean intensity of fluorescence. For each condition, a minimum of 50 different cells were counted.

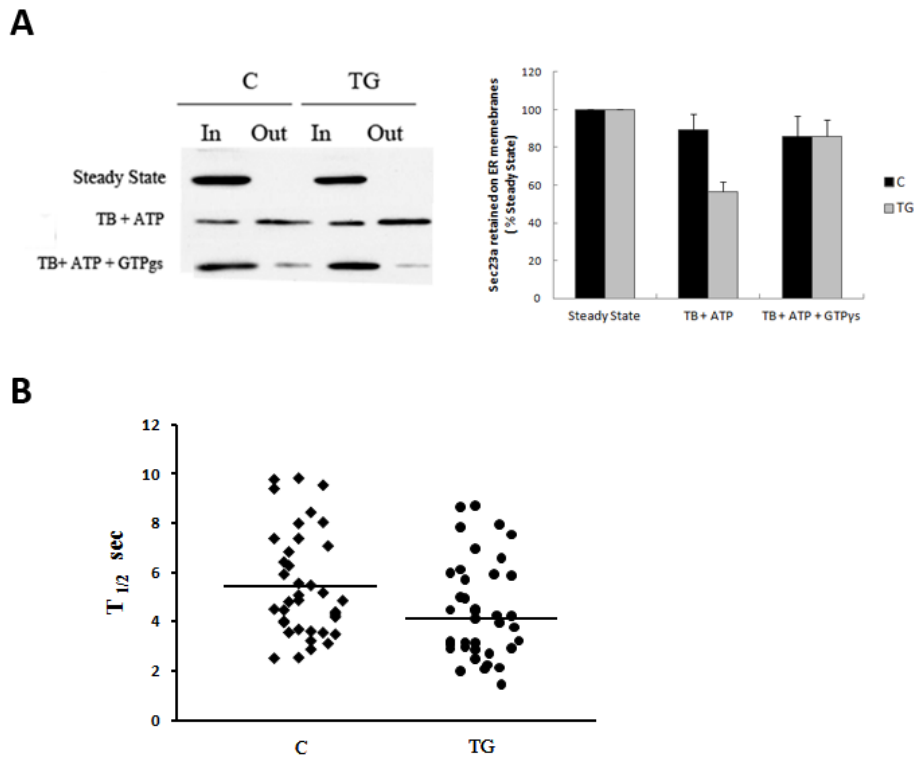


Fig. 16 Dynamics of the Sec23a association to the ERES. (A) Huh7 cells treated 2 h with 300 nM TG or not treated (C) were incubated with 0,8 U/ml of SLO. After linking of SLO to plasma membrane, cells were maintained on ice (Steady State) or permeabilized for 15 min at 37°C in presence of TB+ATP or TB+ATP+GTP γ s. The membrane retained fraction of proteins (In) and the cytosolic fraction (Out) of Steady State or permeabilized cells were recovered and analysed by SDS-PAGE. The blots were probed with goat polyclonal anti-Sec23a antibody. One out of three separate experiments is shown. The histograms show the percent of retention on ER membrane, calculated as described in the methods section. (n = 3 independent replicates/each Ab reaction). (B) Huh7 cells were transfected with 2 μ g of Sec23a-GFP expressing vector, 24 h after transfection were treated (TG) or not (C) with 300 nM TG for 2 h and subjected to FRAP analysis. TG was maintained also during FRAP experiment. Individual T_{1/2} value are plotted. Horizontal bar indicates the mean of T_{1/2} values of at least 35 individual Sec23 positive spots of 15 different cells.

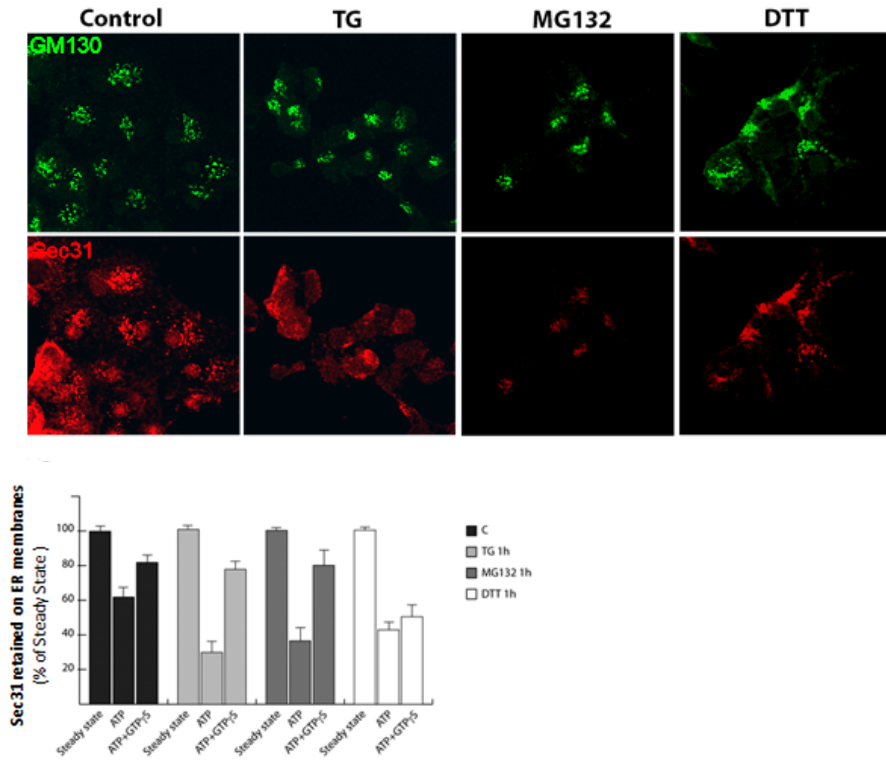


Fig. 17 Immunofluorescence detection of the residual association of Sec31 to ER-membranes in SLO permeabilized Huh7 cells. Huh7 control (C) cells or cells treated 2 h with 300 nM TG, 2 mM DTT or 10 μ g/ml MG132 were permeabilized with 0,8 U/ml of SLO 15 min at 37°C in presence of TB+ATP or TB+ATP+GTP γ s. Steady State cells were only permeabilized with PBS - saponin 1%; all the coverslips were fixed and stained for Sec31 and GM130. In the top panels are shown the membrane retained fraction of Sec31 and GM130 for TB+ATP condition. GM130 is used as marker of SLO-permeabilization. The histogram shows the percent of Sec31 retained at the ER membrane and normalized for GM130 mean intensity of fluorescence as described in the methods section. For each condition, a minimum of 50 different cells were counted.

TG treatment reduces Sec23a ubiquitination

Ubiquitination is a reversible post-translational modification of proteins that is involved in many cellular processes including cell division, differentiation, signal transduction, protein trafficking, and quality control (Mukhopadhyay and Riezman, 2007). It has been reported that in budding yeast Sec23 undergoes to ubiquitination/de-ubiquitination and that this balance is essential for the proper activity of the secretory pathway (Cohen et al., 2003). We therefore decided to analyze Sec23 ubiquitination in Huh7 cells during ER Stress. To this end, Huh7 cells were transiently co-

transfected with the 3xFLAG-Sec23a and HA-Ubiquitin coding vectors and then subjected to a 2 h pre-treatment with 10 μ M MG132 followed or not by 4 h incubation with TG. The ubiquitinated form of the exogenous Sec23a protein was purified by anti-HA immunoprecipitation and revealed by anti-FLAG immunoblotting. As shown in Fig.18, FLAG antibody revealed a band of about 90 Kda indicating that Sec23a undergoes to ubiquitination. Moreover, since we didn't find any bands at higher molecular weight, we reasoned that Sec23a was mono-ubiquitinated rather than poly-ubiquitinated. Interestingly, the mono-ubiquitinated form of Sec23a was enriched after MG132 treatment and reduced of about 40% after TG treatment indicating that TG interferes with the ubiquitination of Sec23a. Since it's known that mono-ubiquitination doesn't support degradation but is involved in membrane trafficking, DNA repair, gene transcription and DNA replication (Chen and Sun, 2009), it would be interesting to investigate if ER Stress exerts its control on ER to Golgi trafficking by regulating Sec23a ubiquitination.

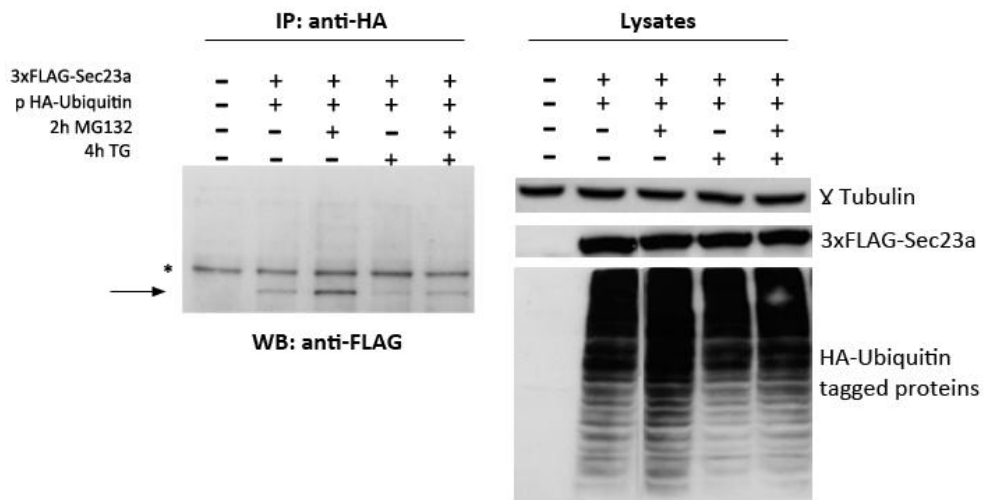


Fig. 18 TG reduces the ubiquitination of Sec23a. HuH7 cells were co-transfected with 4 μ g of the pHA-Ubiquitin expression vector plus 4 μ g of the 3xFLAG-Sec23 vector, as indicated. 48 h after transfection, cells were pre-incubated for 2 h with 10 μ M MG132 and then treated or not with TG for the time indicated. Cell lysates were immunoprecipitated by a mouse monoclonal anti-HA antibody in order to selectively pull down the ubiquitinated proteins and then the 3xFLAG-Sec23a was revealed by a mouse monoclonal anti-FLAG antibody. Total lysates were checked by W. Blot as control of the input samples. The asterisk indicates a not specific band.

Sec23a is ubiquitinated on the CYS 432 and CYS 449 of the β -barrel domain

To identify the site/s of Sec23a ubiquitination, we used a mass spectrometry approach. This method has been used to identify ubiquitination sites, based on the fact that trypsin proteolysis of an ubiquitinated protein produces a signature peptide. This signature peptide is characterized by a Gly-Gly remnant from the C-terminus of the ubiquitin attached to the lysine residues of the substrate and can be identified by a mass shift in the modified residue or peptide (Kirkpatrick et al., 2005; Peng et al., 2003) (Fig. 19 A). Thus, we over-expressed 3X-FLAG-Sec23a in Huh7 cells by

CHAPTER III

ER Exit and Trafficking to the Golgi Complex

transient transfection. Following that, the exogenous protein was purified from the total protein extract by affinity chromatography with anti-FLAG agarose resin and subjected to SDS-PAGE. The proteins were revealed by comassie staining (Fig. 19 B) and the 3X-FLAG-Sec23a specific band was extracted from the gel, subjected to trypsin digestion and the resulting peptides analyzed by mass spectrometry. As shown in Fig 19 C and D we found two peptides modified by Gly-Gly remnants bound to cysteine residues. The ubiquitinated cysteines were at position 432 and 449 and are localized in the second β -Barrel domain of Sec23a protein (Fig. 19 E). Interestingly, the β -Barrel domain is involved in the binding of Sec23a to the ER membrane (Bi et al., 2002; Lederkremer et al., 2001) suggesting that the ubiquitination of this domain on cys 432 and 449 could affect the ability of Sec23a to bind to ERES during COPII coat assembling.

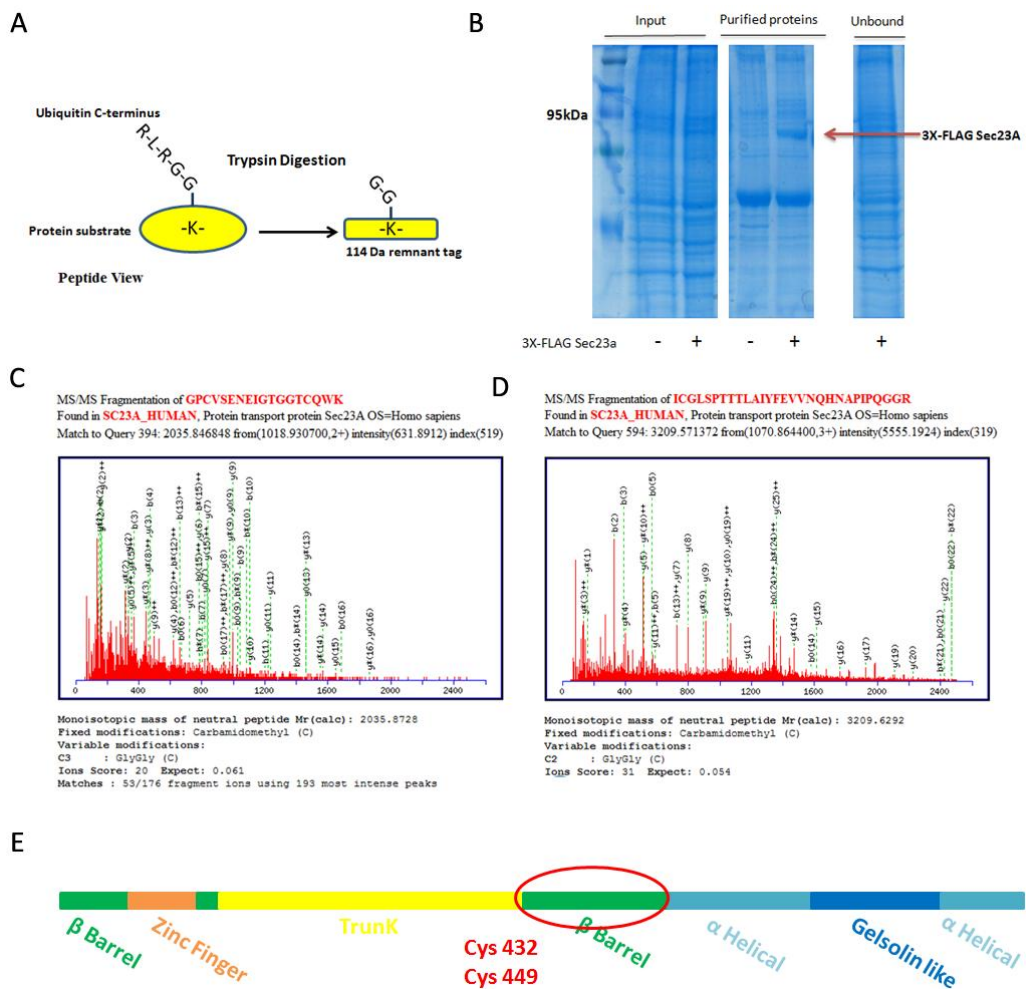


Fig. 19 Sec23a is ubiquitinated on cys432 and cys449. (A) Schematic representation of the Gly-Gly remnant left on ubiquitinated residues after trypsin digestion of the C-terminus of

the linked ubiquitin (B) Huh7 cells were transfected with 8 µg of 3X-FLAG-Sec23a and 48 h after transfection were lysed in B-Buffer 1% Triton. Lysates were immunoprecipitated by the anti-FLAG resin, subjected to SDS-PAGE and revealed by comassie staining (purified proteins). The total extracts (input) and the supernatant of the resin (unbound) are also showed. (C;D) Output view of the software used for the search of the Gly-Gly modified peptides of Sec23a. The sequence and the MS/MS fragmentation peaks of the peptides containing the Gly-Gly-Cys 432 (C) and Gly-Gly-Cys 449 (D) are shown. (E) Schematic representation of the structural domains of Sec23a. The position of Cys 432 and Cys 449 are indicated in red.

Discussion

The results presented describe three main effects of the ER stress on the early segment of the secretory pathway: alterations in the architecture of the ERGIC and of the Golgi complex, lower rate of ER to Golgi transport and apparent reduced number of assembling COPII-coated transport vesicles. These effects could be independent and concomitant phenomena. But, it is more likely that the first two are at least in part the result of the third one. Indeed, a rapid and drastic decrease of assembling COPII-coated transport vesicles would explain the lower rate of anterograde transport from the ER to the Golgi, which in turn impairs the homeostasis of the ER, the ERGIC and the Golgi complex. The alteration of the architecture of ERGIC and Golgi complex is clearly shown by the immunofluorescence and cell fractionation analysis of the distribution of ERGIC-53 and GM130. ERGIC-53 recycles continuously between the ER and the ERGIC, and GM130 between the ERGIC and the *cis*-Golgi. The normal distribution of both proteins is certainly due to a dynamic equilibrium between anterograde and retrograde trafficking. Upon ER stress activation, both proteins move from the perinuclear region to the periphery of the cell, suggesting that the vesicular trafficking at the ER Golgi boundary is altered for a defective transport either in the anterograde or in the retrograde, or in both directions. In addition, both markers are present in different vesicular structures that have a lighter sedimentation density on sucrose gradient, suggesting that the ER stress could also directly alter the structure of ERGIC and *cis*-Golgi. Finally, the EM analysis shows that 2 hours after stress activation the Golgi ribbon and most cisternae stacks are not detectable, while the ER is almost unaffected (a finding supported by the immunofluorescence analysis).

Our evidences confirm that the cell lowers the amount of anterograde transport by reducing ER export. It is well documented that the mutant VSV-G glycoprotein made by the ts-045 strain accumulates in the ER at the non-permissive temperature of 39 °C in a misfolded status. Upon lowering the temperature to 32 °C the VSV G protein is promptly changed to the folded and oligomerized status, which is competent for ER export. By immunofluorescence microscopy, the first VSV-G molecules are detectable in the Golgi complex already 3-5 min after the temperature shift (Presley et al., 1997). Thus, our finding that only 5 min incubation with TG at 39 °C followed by 15 min at 32 °C in the continuous presence of TG are sufficient to lower to 50% the amount of VSV-G that reaches the Golgi complex suggest that it is very unlikely that the decrease in transport could be due to some pleiotropic effect caused by the stress. The shutting off of protein synthesis has to be excluded because the great majority of the VSV-G involved has been synthesized before TG addiction. In addition, the exposure of Huh7 cells to TG requires longer time (15-30 min) to activate the PERK dependent phosphorylation of eIF2α (Franceschelli et al., 2011). The first and simplest explanation for the decreased exit from the ER of the reporter protein might

be that the ER stress, induced by TG, very rapidly affects the folding and the oligomerization of the ts045G protein, thus decreasing the total amount of protein competent for ER export. The finding that the oligomerization profile of ts045G protein shown by velocity sucrose gradient analysis is almost identical in the control and in the ER stressed cells strongly argues against this hypothesis and also excludes that the lower amount of the ts045G protein found in the Golgi area could be due to decreased amount of reporter protein as a result of ER stress enhanced protein degradation (ERAD). On this line, we also observed by immunofluorescence microscopy an ER stress-dependent deficient reconstitution of both ERGIC and Golgi complex after BFA treatment. Also this finding could be the consequence of an insufficient ER export of factors required to re-establish the architecture of post-ER compartments, although we cannot exclude that the combination of BFA and TG effects could selectively impair the function of some protein(s) crucial for the ERGIC and the Golgi architecture. The ER stress-dependent decrease in ER export of the cargo protein ts045G, in the apparent absence of an effect on its folding/oligomerization, prompted us to investigate if the assembly of COPII coats was altered by ER stress. A simple way to follow these processes in the live cell is to use immunofluorescence microscopy with antibody directed against component of the Sec23p/24p or the Sec13p/Sec31p complexes. The assembling COPII-coats are visualized as small fluorescent puncta, each probably representing several budding figures at the ERES. Using this procedure, we observed a strong reduction of the number of Sec31 (and Sec23) fluorescent puncta, in parallel to the decrease ER export, in all experimental conditions. Most importantly, untransfected cells incubated with TG for 5 min at 39 °C showed almost the same reduction, indicating that the result was not due to cargo loading in the ER or to a direct effect of the drug onto VSV-G protein. On this line, also the finding that the same percentage of Sec31 puncta was co-labelled by the VSV-G reporter in control as well as ER stressed cells suggests that the target of ER stress is the formation of COPII coats, not the cargo-COPII interaction.

Following the conclusions of these results new questions promptly arise: what step in COPII assembly is impaired by ER stress? Is there a single target among COPII proteins? What molecular mechanism is implied? To address these questions we decided to investigate the effect of ER Stress on COPII vesicles formation/stability at key steps of the coat assembling: 1) the recruitment of the COPII proteins on ERES that is achieved by Sec16 protein 2) the polymerization of the inner coat and the activation of Sar1 GTPase activity, both mediated by Sec23a 3) the assembling of the outer coat, indispensable for membrane curvature and vesicle fission through the analysis of Sec31. Our results describe three main effects of ER Stress on the COPII coat assembling: significant down-regulation of the Sec16 protein, reduced permanence of Sec23a and Sec31 on ER membrane during coat formation, deubiquitination of Sec23a. The down-regulation of Sec16 protein is clearly showed by immunofluorescence and western blotting while we didn't observe any impairment in the dynamics of binding of Sec16 to ERES nor after SLO-permeabilization, neither during FRAP experiment. This finding is not surprising considering that mammalian Sec16 cycles between a membrane-bound (ERES) pool and a cytosolic pool with a slow rate and dynamics compared to the other COPII proteins and that the membrane bound form is stably associated to ERES (Watson et al., 2006). The reduced expression of Sec16 is not explained by the shutting off of protein synthesis since the treatment with CHX is not able to down-regulate Sec16 as TG does, but is most

likely due to an enhanced degradation of the protein. Recent publications have shown that Sec16 is target of ERK2 MAP kinase and that Sec16 phosphorylation positively regulates its binding to ER membrane and the number of ERES (Farhan et al., 2010), on the contrary the kinase ERK7 leads to a post-translational modification in the C-terminus of Sec16 eliciting the consequent disassembly of ERES (Zacharogianni et al., 2011). In agreement with these findings, we hypothesize that the down-expression of Sec16 could be due to a post-translational modification induced by ER Stress. On this line we found that the amount of Sec16, together with Sec31, are significantly reduced in MEF knock-out for the UPR transducer IRE1 alpha indicating that IRE1 alpha is involved in the trafficking from the ER to the Golgi complex. It's known that the IRE1 pathway of UPR is required for the adaptation of ERES to the cargo load from ER (Farhan et al., 2008); thus it would be interesting to test if the putative modification of Sec16 is linked to the activation of IRE1 during the UPR.

Together with the down-regulation of Sec16 protein, our evidences indicates that ER Stress reduces the amount of Sec23a associated to the ER membrane and accelerates its recycling rate at ERES. This finding could be explained by two hypothesis: the faster recycling of Sec23a is necessary to compensate for an overload of proteins exiting from the ER; or the faster recycling causes a reduced permanence at ERES which is insufficient to ensure the proper assembling of COPII vesicles. The latter hypothesis is most likely true since it is consistent with the reduced anterograde transport of VSVG glycoprotein and with the reduced number of COPII vesicles. Noteworthy, Sec23a functions as GTPase activating protein for Sar1 and its shorter permanence at ERES would be responsible for the impairment of COPII vesicles formation observed during ER Stress. Another remarkably result of our work is that Sec23a is physiologically mono-ubiquitinated on cysteines 432 and 449 and that upon ER Stress these cysteines are presumably de-ubiquitinated. It has been reported that in budding yeast Sec23 undergoes to ubiquitination/de-ubiquitination cycles and that this balance is essential for the proper activity of the secretory pathway (Cohen et al., 2003), thus the first question is: does the mono-ubiquitination of Sec23a target it to the degradation by the proteasome? Our preliminary results indicates that the accumulation of the ubiquitinated Sec23a after MG132 treatment is associated to an higher number of COPII vesicles compared to the cells in which the ubiquitination of Sec23a is reduced by TG treatment (not shown). This finding suggests that the ubiquitination of Sec23a is not the signature for its degradation but is required for the activation of specific signaling pathway/s. This hypothesis is confirmed by accumulating evidences showing that mono-ubiquitination doesn't support degradation but is involved in membrane trafficking, DNA repair, gene transcription and DNA replication (Chen and Sun, 2009). Moreover, even more interesting is that the residues ubiquitinated are not lysine but both cysteines residues. Cysteine ubiquitination occurs through a thio-esterification and emerging evidences have demonstrated its implication in cell physiology. For instance, in yeast and mammals mono-ubiquitination of the peroxisome import receptor Pex5p on a conserved cysteine is required for its release from the peroxisome membrane to recycle for another round of import (Okumoto et al., 2011). Interestingly, cysteines 432 and 449 are both localized in the β -barrel domain of Sec23a that is known to be required for the binding of Sec23 to the membrane phospholipids (Bi et al., 2002; Lederkremer et al., 2001). Finally, these observations strongly suggest that ER Stress could regulate Sec23a binding to the ER membrane by modulating its ubiquitination.

In conclusion, our results clearly indicate that ER Stress influences the COPII coat assembling by targeting both Sec16 and Sec23a proteins: Sec16 is controlled through its down regulation, which does not alter the binding to ER membrane. Instead, Sec23a is controlled on the ability to bind to ERES without affecting its intracellular level. How and if this is modulated by Sec16 post-translational modification and/or by the mono-ubiquitination of Sec23a has yet to be elucidated. In our model (Fig. 20) these effects could be independent or concomitant phenomena and could be directly or indirectly related to the activation of the UPR transducer IRE1 alpha. Certainly the reduction of the ER export through the impairment of COPII vesicles formation would represent another defence to cope with ER Stress by avoiding to fill up the post-ER compartments with misfolded proteins that could be more efficiently either be refolded in the ER or destined to degradation through the ERAD.

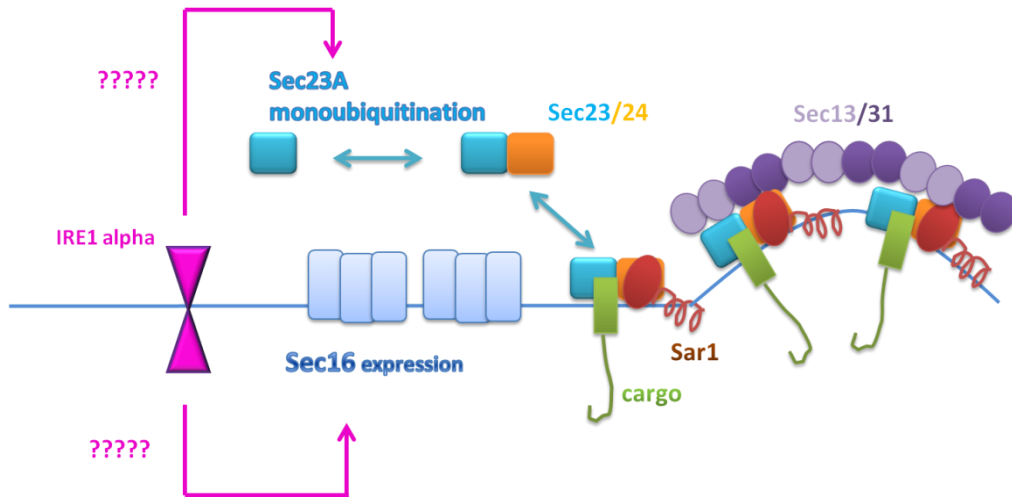


Fig. 20 Schematic model of the ER stress-dependent modulation of COPII assembling. See text for details.

Scientific background, rationale and aims

The UPR regulates gene expression in response to the ER Stress. Regulation of gene expression by the UPR allows the cell to tolerate folding stress and to assist in correction of the unfolded proteins accumulated within the ER. In order to identify new molecules controlled by the UPR, we analyzed the gene expression profiles of TG-treated Huh7 cells by the parallel evaluation of microRNome and proteome changes. In the past decade, microRNAs have been uncovered as key regulators of gene expression at the post-transcriptional level by binding complementary regions of transcripts to gain repression of translation or to activate RNA degradation (Berezikov, 2011). Currently, accumulating evidences demonstrate an interconnection between microRNA regulatory network and signal transduction pathways. Therefore, we asked whether microRNA could be involved in the regulation of gene expression in response to ER stress. To this aim, we performed a microRNA microarray on TG-treated cells and found twenty-four differentially expressed microRNA. We identified miR 663 and miR 29b-1* as the most significantly induced miRs. Interestingly, the ontological analysis of the predicted targets of miR 663 and miR 29b-1* revealed that about the 25 % of their putative targets exert a function within the secretory pathway. On the other hand, the proteomic analysis performed by the use of 2D-DIGE and mass spectrometry revealed differential expression for a number of proteins that function within the secretory pathway. Interestingly, we demonstrated that one of these proteins, PLOD3, is significantly down-regulated during ER Stress and revealed that it is at high score one of the predicted target of the UPR-induced miR 663.

Results

Hsa-miR 29b-1* and hsa-miR 663 are up-regulated during TG treatment

In order to identify miRs regulated by UPR, we performed a large-scale screening on total RNA extracted by Huh7 cells either untreated or treated 8 h with 300 nM TG. In particular, three control samples and three TG-treated samples were analyzed by MicroRNA microarray (LC Sciences). Among the 640 miRs tested, in TG-treated cells we found 24 differentially expressed miRs (Box 1; Fig. 1). To validate microarray results, we analysed by Northern Blots the expression level of the identified miRs that had a fold change greater than 1.5 and a basal level of expression higher than 100. Thus, we measured the expression of hsa-miR 29b-1*, hsa-miR 92a-1*, hsa-miR 663, hsa-miR 23a*, hsa-miR 513a-3p, hsa-miR 22*. The results obtained by Northern Blotting showed the increased expression of miRs 29b-1* and 663 already after one hour of TG treatment (not shown) with maximum induction after 8 h of TG treatment (Fig. 2). We didn't manage to obtain any signal for miR 92a-1*, miR 23a*, miR 513a-3p and miR 22*.

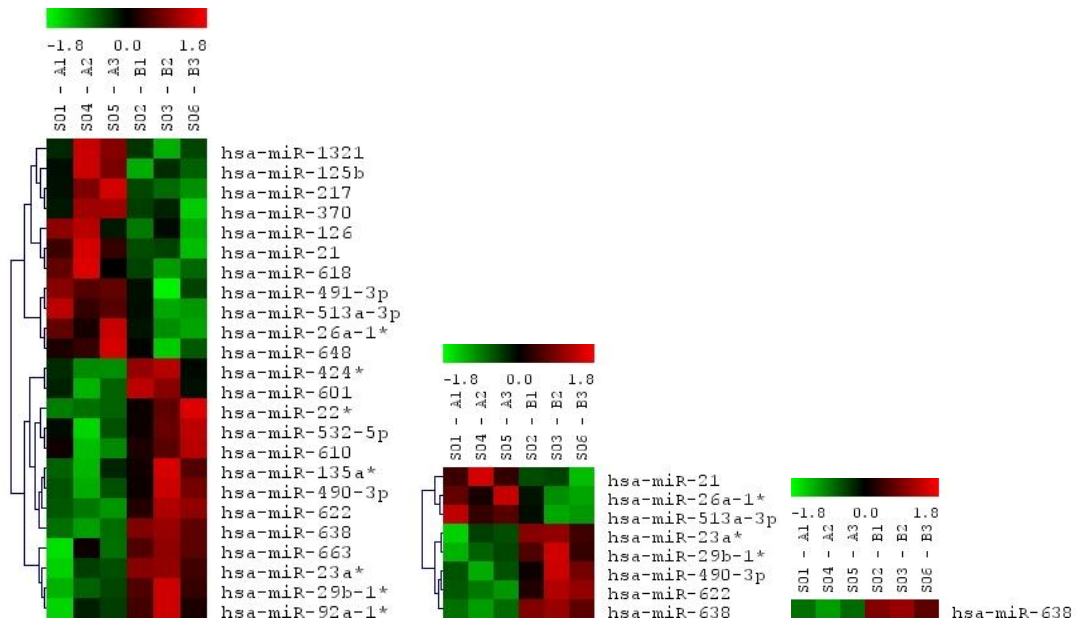


Fig. 1 *Statistic test and clustering analysis of differentially expressed miRs.* Regions of chip images for differentially expressed miRs, grouped by p-value (p-value < 0.10, p-value < 0.05, p-value < 0.01 from left to right). A and B refers to control and TG treated samples respectively.

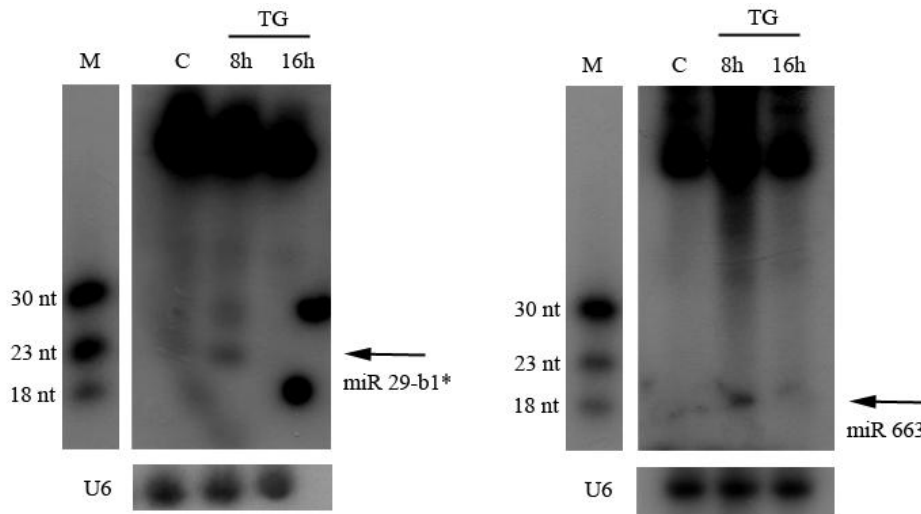


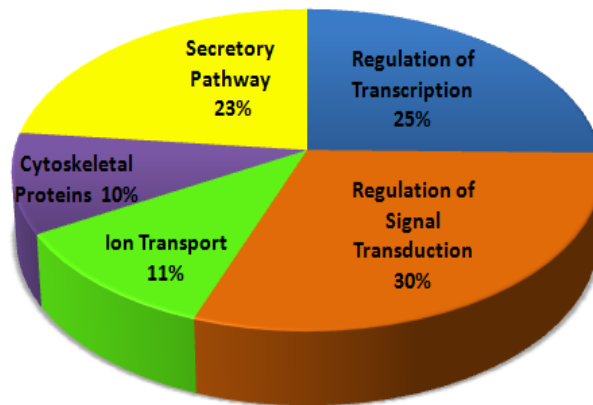
Fig. 2 *Northern Blotting of miR 29-b1* and miR 663.* Total RNA samples extracted by control or TG-treated Huh7 cells for the indicated times were subjected to Northern Blot analysis by using miRCURY™ LNA probes specific for miR 29-b1* and miR 663. U6 snRNA was used for normalization. miR 29-b1* and miR 663 specific bands and the radioactive base pairs marker are indicated. Ibridization with LNA probes reveals also the precursor transcripts running as high molecular weight species.

microRNA		C	TG	
	p-value	Mean	Mean	Fold
hsa-miR-638	1.65E-03	3,132	4,374	1.397
hsa-miR-29b-1*	2.76E-02	403	883	2.191
hsa-miR-21	4.18E-02	31,133	28,547	-1.091
hsa-miR-125b	6.56E-02	1,276	1,080	-1.181
hsa-miR-92a-1*	8.12E-02	290	453	1.562
hsa-miR-126	8.58E-02	930	763	-1.219
hsa-miR-663	9.80E-02	1,070	1,782	1.665
hsa-miR-23a*	2.12E-02	144	262	1.819
hsa-miR-622	3.53E-02	46	65	1.413
hsa-miR-490-3p	3.77E-02	25	31	1.240
hsa-miR-513a-3p	4.07E-02	29	11	-2.636
hsa-miR-26a-1*	4.90E-02	52	40	-1.300
hsa-miR-424*	5.03E-02	129	189	1.465
hsa-miR-135a*	6.08E-02	48	60	1.250
hsa-miR-22*	6.69E-02	212	346	1.632
hsa-miR-601	6.86E-02	109	143	1.312
hsa-miR-610	7.72E-02	31	45	1.452
hsa-miR-532-5p	7.82E-02	78	95	1.218
hsa-miR-618	8.78E-02	39	30	-1.300
hsa-miR-370	9.08E-02	65	41	-1.585
hsa-miR-491-3p	9.16E-02	41	26	-1.577
hsa-miR-217	9.23E-02	43	27	-1.593
hsa-miR-648	9.30E-02	41	32	-1.281
hsa-miR-1321	9.48E-02	73	60	-1.217

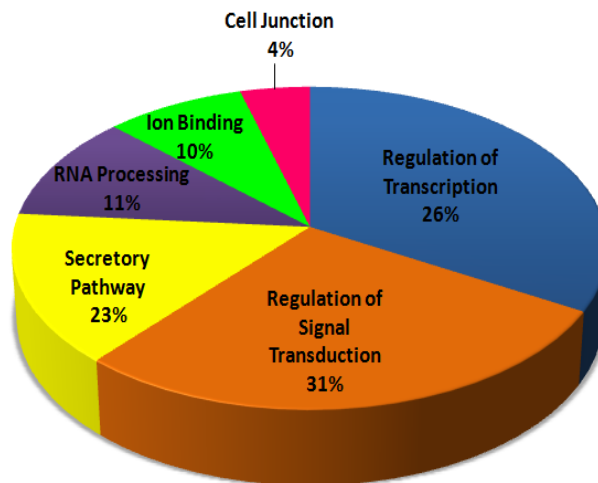
Box 1 Differentially expressed miRs in control and TG treated samples.

Functional clustering of miR 29b-1* and miR 663 putative targets

In order to predict the biological function of miR 29b-1* and 663 during the TG-induced activation of UPR, we performed an “in silico” analysis to find putative targets of miR 29b-1* and 663. The search was performed through the comparative assessment of three prediction software: Miranda (www.microrna.org), TargetScan (www.targetscan.org) and PicTar (www.pictar.org). The three lists of the putative targets were then matched by the MatchMiner program (www.discover.nci.nih.gov/matchminer/index.jsp) to obtain a final list of putative targets that have been predicted by all the three programs. Of the about two thousands targets predicted by each program we found 262 common targets for miR 663 and 211 common targets for miR29b-1*. The final list of common targets was subjected to ontological analysis by the Functional Annotation Tool of DAVID (Database for Anotation, Visualization and Integrated Discovery) in order to cluster them in functional common classes. We found five functional classes for miR 663 (Box 2) and six different cluster for miR 29b-1* (Box 3). Interestingly for both miR 663 and miR 29b-1*, about the 30% of the putative targets are involved in the control of signal transduction pathways while the 20% are regulators of transcription. However, the most striking result obtained by the ontological analysis is that about the 26% and the 14% of the predicted targets of miR 663 and 29b-1* respectively, are specifically related to the secretory pathway function. In more details, for miR 663, we can identify different groups of proteins related to protein synthesis and folding (PLOC3, PDIA2), to the vesicle mediated transport (SLC32A1, AKAP3, RAB5C, DENND1A, UNC13D, FAM125A), to the secretory proteins degradation (USP11, DPP9, PCSK1N, KLK15, PRSS22, and USP5) or to the glycoprotein metabolic process (CD37, MGAT4B, ST3GAL2, ABO). For miR 29b-1* the number of the putative targets related to the secretory pathway is significantly less represented; however we can identify proteins involved in the ubiquitin-linked proteolysis (USP28, KIAA0317, USP4, UBE2J1) or in the protein sorting and transport (IER3IP1, EXOC7, IPO5, ERP44, GORASP2, SH3BP4). In conclusion, the ontological analysis conducted for both miR 663 and 29b-1* is certainly a preliminary indication of their putative involvement in the control of gene expression during the ER stress. Obviously, further experiments need to be done to validate in vitro the results of the “in silico” targets prediction and to explain the biological scope of the TG-dependent upregulation of miR 663 and 29b-1*.



Box 2 *Functional annotation of miR 663 putative targets.* The putative targets of miR 663 were predicted by three different programs. The matching targets were subjected to ontological analysis by DAVID software. For each cluster the percent of enrichment is indicated.



Box 3 *Functional annotation of miR 29b-1* putative targets.* The putative targets of miR 29b-1* were predicted by three different programs. The matching targets were subjected to ontological analysis by DAVID software. For each cluster the percent of enrichment is indicated.

Differentially expressed proteins in TG-treated human hepatocytes.

In parallel with the characterization of microRNome changes during ER stress, we investigated the effect of ER Stress also on protein expression in Huh7 cells; to this end a differential expression proteomic analysis based on the 2D-DIGE approach was used. Three biological replicates of control and TG-treated Huh7 cells were generated for protein extraction and fluorescence labelling with Cy-dyes. Figure 3A shows a merged image of the representative gel (master gel), used to match the 2-D profiles obtained from three sample pairs. Analysis of the images according to the DeCyder bioinformatics software (see Materials and Methods section for details) allowed us to detect about 1,100 matched protein spots within the three gels. Thirty-one spots (circled in Figure 3B) appeared to be deregulated following quantitative and statistical analysis, under parameters defined as relative expression ratio in TG-treated versus control Huh7 cells; +1.25 for spots up-regulated (4 in number) and -1.25 for spots down-regulated (27 in number), with a P value < 0.05 (data not shown). These spots were matched with the corresponding ones from the preparative gels stained with fluorescent stain SyproRuby (yellow circles in Figure 3C); the latter were, indeed, individually excised from preparative gels and further subjected to MS analysis for protein identification. Table I summarizes their relative expression ratios in TG-treated versus control Huh7 cells as well as the mass spectrometry data for the corresponding 20 identified proteins. A multiple identification occurred for spot 531, which showed the concomitant presence of the protein products of *PLOD3* and *PDCD6IP* gene encoding for procollagen-lysine, 2-oxoglutarate 5-dioxygenase 3 (PLOD3) and ALG2-interacting protein X (ALIX), respectively.

Protein name	SwissProt code	GENE name	Theor. pl	Theor. Mr	Mascot score	Peptides	Sequence coverage (%)	Ratio TG-treated vs. control cells	P value
Procollagen-lysine, 2-oxoglutarate 5-dioxygenase 3	O60568	<i>PLOD3</i>	5.64	82383	87	9	16	-1.42	0.047
ALG2-interacting protein X, programmed cell death 6-interacting protein	B4DHD2	<i>PDCD6IP</i>	6.14	95891	70	8	15		
78 kDa glucose-regulated protein	P11021	<i>HSPA5</i>	5.01	70478	148	13	25	+1.37	0.05
Sec1 family domain-containing protein 1	Q8WVM8	<i>SCFD1</i>	5.90	72248	65	7	13	-1.45	0.0086
Mortalin, stress-70 protein mitochondrial	P38646	<i>HSPA9</i>	5.44	68759	70	7	12	-1.44	0.011
Copine-1	Q99829	<i>CPNE1</i>	5.52	59058	74	8	18	-1.3	0.0069
Tubulin beta chain	P07437	<i>TUBB</i>	4.78	49670	126	13	23	-1.41	0.044
Alpha-1-antitrypsin	P01009	<i>SERPINA1</i>	5.37	44324	116	12	36	+1.78	0.0065
Keratin, type II cytoskeletal 8	P05787	<i>KRT8</i>	5.52	53573	191	17	44	-1.68	0.020
Reticulocalbin-2	Q14257	<i>RCN2</i>	4.19	34527	84	6	26	-1.51	0.013
Keratin, type II cytoskeletal 8	P05787	<i>KRT8</i>	5.52	53573	88	14	34	-1.49	0.036
Keratin, type II cytoskeletal 6A	P02538	<i>KRT6A</i>	8.14	59913	75	9	16	-1.57	0.028
Calumenin	O43852	<i>CALU</i>	4.46	34961	115	10	29	-1.45	0.021
Creatine kinase B-type	P12277	<i>CKB</i>	5.35	42513	88	8	26	-1.25	0.05
Protein SET	Q01105	<i>SET</i>	4.23	33357	91	9	31	-1.77	0.05
COP9 signalosome complex subunit 4	Q9BT78	<i>COPS4</i>	5.57	46137	129	13	46	-1.42	0.031
Eukaryotic translation initiation factor 3 subunit I	Q13347	<i>EIF3I</i>	5.38	36501	71	9	29	-1.26	0.05
Nascent polypeptide-associated complex subunit α	Q13765	<i>NACA</i>	4.52	23383	125	6	27	-1.57	0.0045
14-3-3 protein epsilon	P62258	<i>YWHAE</i>	4.63	29173	124	10	42	-1.26	0.025
Thioredoxin domain-containing protein 9	O14530	<i>TXNDC9</i>	5.61	26534	87	6	39	-1.3	0.0068

Table 1 Differentially expressed proteins in TG-treated Huh7 cells as revealed by 2D-DIGE analysis

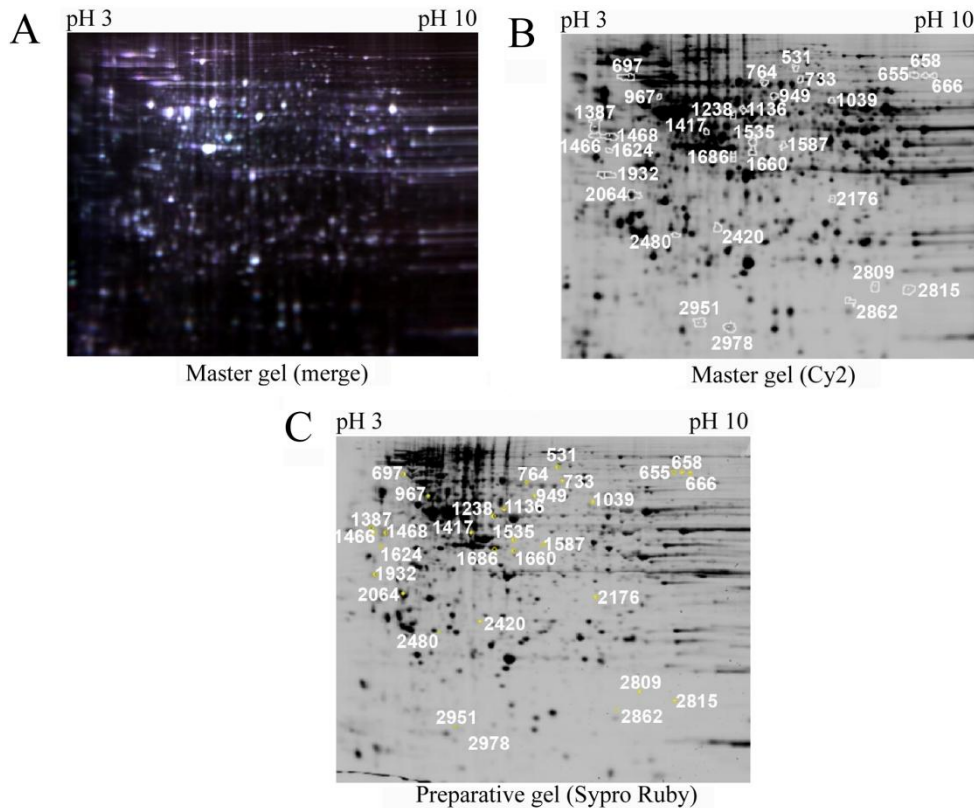


Fig. 3 2-DE map of differentially expressed proteins in TG-treated Huh7 cells. The Figure shows the master gel (panels A and B) and the preparative gel (panel C). In panel A, the master gel is shown as the overlay of the three cy-dyes used to label protein lysates. In panel B, the relevant deregulated spots (31 in number) are surrounded by a white border and numbered; matched spots within the preparative gel (panel C) are highlighted by a yellow circle, which also indicates the picking surface for the robotic spot picker. The representative image reported in panel B shows to the Cy2-labelled proteins on the scanned master gel; protein spots in panel C were stained with Sypro Ruby fluorescent staining.

Validation of 2D-DIGE results by western blot analysis of proteins differentially expressed in TG-induced cells.

Biochemical validation of the proteomic results was performed by western blotting analysis of six out of the 20 identified proteins; such proteins were selected, according to their potential relevance in the cell response to ER Stress (Figure 4). Thus, we first examined the accumulation of GRP78, the major marker of the ER stress, shown as one of the up-regulated proteins in the 2-DE analysis (Table 1). Grp78, also referred to as Bip, is a major ER chaperone with anti-apoptotic properties, which plays a key role in the control of the UPR activation through the binding-release of the transmembrane ER stress sensors (IRE1, PERK, and ATF6). As we would have expected, and consistently with our 2-DE data, treatment of Huh7 cells with TG induced an increase of the Grp78/Bip protein level compared to the control cells (Figure 4A). Next, we examined the quantitative levels of calumenin

(CAL) e reticulocalbin 2 (RCN2), two ER resident and functionally related Ca^{2+} binding proteins²⁰ (Figure 4; panels B and C). Our experiments showed that calumenin was slightly down-regulated by TG either at 4 h or at 8 h of drug treatment, while RCN2 level decreased with time in the TG-treated cells, showing a higher reduction rate at 8 h (Figure 4, panels B and C). Similarly, we examined the expression level of SET (Figure 4D), a multifunctional protein with prosurvival properties.²¹ Western blot and densitometry analyses revealed that SET is appreciably down-regulated in the TG-treated cells; such effect was particularly evident at 8 h of TG-treatment (Figure 4D). Finally, we tested the expression of ALIX and of the PLOD3 protein, which were co-identified in spot 531 (Table I). Quite intriguingly, western blotting analysis showed an up-regulation of the ALIX protein in TG-treated cells (Figure 4E) and a down-regulation of PLOD3 (Figure 4F), which would explain the 2-DE measurement, where both proteins comigrated within the gel. To determine whether the downregulation was due to the TG-dependent inhibition of translation induced by eIF2a phosphorylation, Huh7 cells were treated with the inhibitor of protein synthesis cycloheximide (CHX) and the expression of the selected downregulated proteins was examined. As shown in Figure 5, no one of the proteins was down-regulated by cycloheximide treatment, even after four hours inhibition of protein translation demonstrating that the effect of TG on protein expression is not due to eIF2a phosphorylation.

The validations obtained by western blotting analysis were indeed quite consistent with 2D-DIGE data, with the exception of calumenin, which resulted down-regulated to a more limited extent by immunoblot analysis. Taken together, these experiments highlighted the up-regulation of GRP78 and ALIX, as well as the down-regulation of reticulocalbin 2, SET and PLOD3 in response to TG.

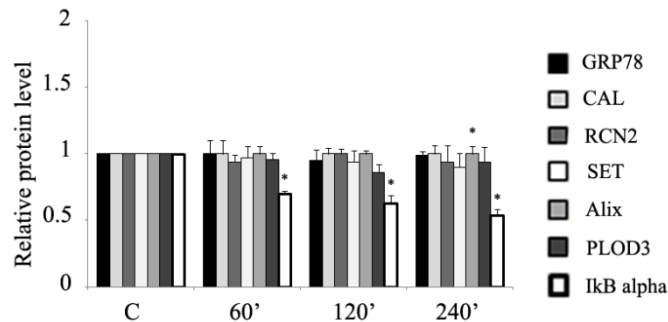


Fig. 5 *Grp78, CAL, RCN2, SET, ALIX and PLOD3 expression levels in cycloheximide-treated cells.* Western blotting analysis of cell extracts obtained from Huh7 cells exposed to 10 $\mu\text{g}/\text{ml}$ CHX for the indicated times or control (C). Protein extracts (10-15 μg) were used to obtain signals in the linear range of the ECL assay. The blots were probed with antibodies against the indicated proteins. Histogram shows the relative normalized abundance of Grp78, CAL, RCN2, SET, ALIX, PLOD3 and IKB- α in Huh7 cells calculated from densitometry of immunoblots using GAPDH as internal standard ($n = 3$ independent replicates/each Ab reaction). IKB- α was used as positive control of CHX-inhibition of protein synthesis.

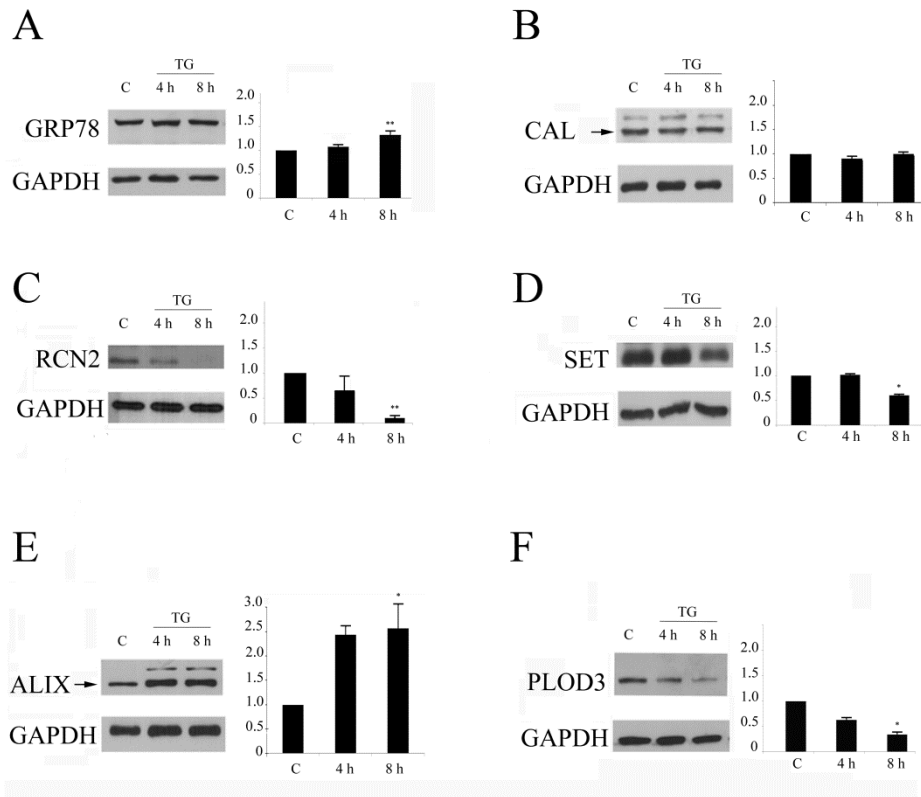


Fig. 4 *Grp78*, *CAL*, *RCN2*, *SET*, *ALIX* and *PLOD3* expression levels in TG-treated cells. Western blotting analysis of cell extracts obtained from Huh7 cells exposed to 300 nM thapsigargin for the indicated times or control (C). Protein extracts (10-15 μ g) were used to obtain signals in the linear range of the ECL assay. The blots were probed with antibodies against the indicated proteins. One out of three separate experiments is shown. Histograms show the relative normalized abundance of Grp78 (panel A), CAL (panel B), RCN2 (panel C), SET (panel D), ALIX (panel E) and PLOD3 (panel F) in Huh7 cells calculated from densitometry of immunoblots using GAPDH as internal standard (n = 3 independent replicates/each Ab reaction).

Effects of ER stress induced by dithiothreitol or MG132 on calumenin, reticulocalbin 2, SET, ALIX and PLOD3 expression levels.

In order to evaluate whether the altered expression of the deregulated proteins was actually related to ER-stress condition, we analyzed their accumulation in Huh7 cells treated with either dithiothreitol (DTT), which induces ER stress by interfering with disulphide bonds stability and/or formation, or MG132, which induces ER stress by acting as an inhibitor of the proteasomal degradation pathway. As expected, our results showed that the amount of Grp78 protein increased in MG132-treated cells and, particularly, in those treated with DTT for 8 h (Figure 6A).

Differently from what observed for the TG-induced ER stress condition, the immunoblots showed slightly increased calumenin levels in Huh7 cells treated with

MG132 (Figure 6B), while even higher levels of this protein were revealed following 4 to 8-hour treatment in DTT-treated cells. Similarly, and in clear contrast with the results from 2D-DIGE (Table 1) and western blotting in TG-treated cells (Figure 4C), reticulocalbin 2 was slightly up-regulated in MG132- and, to a higher extent, in DTT-treated cells (Figure 6C).

As far as SET expression is concerned, and similarly to the occurrence of its observed down-regulation in TG-treated cells, its levels were clearly decreased in the MG132-treated cells, after 8 h from stimulation. On the other hand, SET levels were rather stable in DTT-treated cells (Figure 6D). Finally, as already observed in TG-treated cells, also in MG132- and DTT-treated Huh7 hepatocytes, the ALIX protein accumulated to levels higher than those observed in control cells, both at 4 and 8 h after treatment (Figure 6E); PLOD3 showed decreased levels in the MG132-treated cells after 8 h, while in the DTT-treated cells, normal amounts were detected following DTT exposure (Figure 6F).

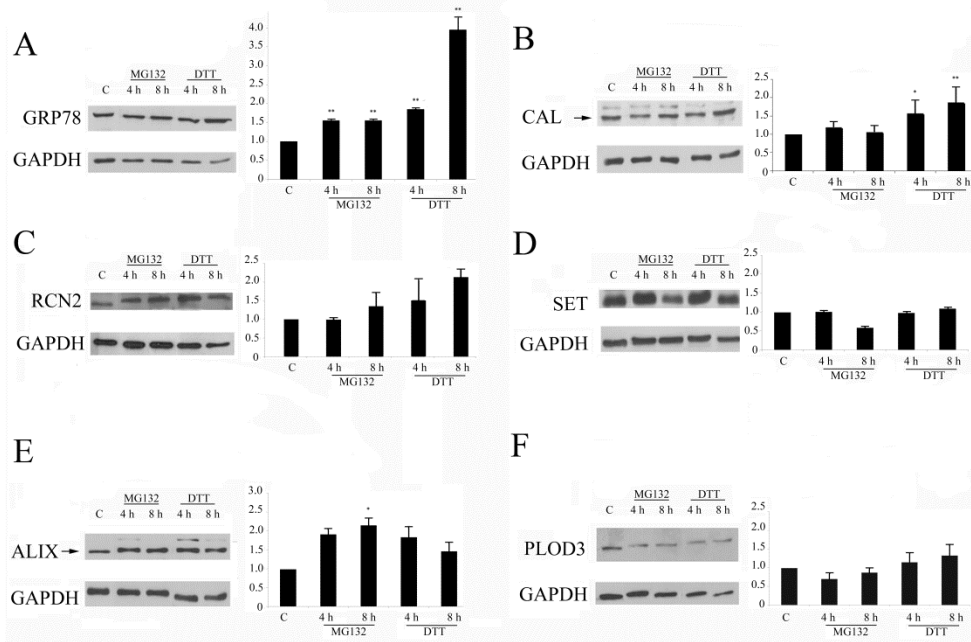


Fig. 6 *Grp78*, *CAL*, *RCN2*, *SET*, *ALIX* and *PLOD3* expression levels in MG132- and DTT-treated cells. Western blotting analysis of cell extracts obtained from Huh7 cells exposed to 2 mM dithiothreitol (DTT) or 10 μ M MG132 for the indicated times or control (C). Protein extracts (10-15 μ g) were used to obtain signals in the linear range of the ECL assay. The blots were probed with antibodies against the indicated proteins. One out of three separate experiments is shown. Histograms show the relative normalized abundance of Grp78 (panel A), CAL (panel B), RCN2 (panel C), SET (panel D), ALIX (panel E) and PLOD3 (panel F) in Huh7 cells calculated from densitometry of immunoblots using GAPDH as internal standard ($n = 3$ independent replicates/each Ab reaction).

Discussion

The microarray analysis shown in the first part of this chapter describes the microRNA expression pattern generated by the induction of ER stress. Little is known about the correlation between the UPR and specific microRNA (Bartoszewski et al., 2011; Yang et al., 2011a). Interestingly, by microarray analysis we identified 24 miRs differentially expressed after TG treatment. Among them, six were further examined by northern blotting, which validates the results for miR 663 and miR 29b-1*. Recent publications show that miR-663 may possess a tumor suppressor activity (Jian et al., 2011; Ni et al., 2011; Yang et al., 2011c) and could be involved in the inflammatory response of endothelial cells (Ni et al., 2011). Instead, the biological function of miR 29b-1* is not reported in literature. During typical microRNA biogenesis, one strand of an approximately 22 nt RNA duplex is preferentially selected for entry into a silencing complex, whereas the other strand, known as the passenger strand or microRNA* strand, is degraded. Recently, some microRNA* sequences were reported as functional guide microRNAs with abundant expression (Yang et al., 2011b). Noteworthy, three of the miRs selected for validation (miR 92a

1*, miR 23a*, miR 22*), together with miR29b-1*, are passenger or microRNA*. Therefore, it's quite striking that we found the up-regulation of the passenger microRNA* without the concomitant induction of its correspondent mature microRNA, suggesting that UPR could be specifically involved in this phenomena. The ontological analysis conducted on miR 663 and miR 29b-1* putative targets shows that the most representative functional cluster are the regulation of transcription and the regulation of signal transduction suggesting that both miR 663 and 29b-1* are potentially able to inhibit the expression of several transcription factors thus altering the pathways in which these factors are involved. About the 30 % and 14 % of the putative targets of miR 663 and 29b-1* are clustered in the secretory pathway group. This is well in agreement with the physiological scope of the UPR. Moreover, included in the secretory pathway cluster are proteins involved in the vesicle mediated transport and protein sorting (SLC32A1, AKAP3, RAB5C, DENND1A, UNC13D, FAM125A, IER3IP1, EXOC7, IPO5, ERP44, GORASP2, SH3BP4) suggesting that microRNA could be involved in the impairment of protein trafficking observed during the ER Stress. Among the putative targets of miR 663 we found the PLOD3 or LH3 protein an ER-resident enzyme involved in biosynthesis of the highly glycosylated type IV and VI collagens, whose deficiency is associated with a number of known collagen disorders (Salo et al., 2008). Surprisingly, by proteomic analysis, we also found lower amounts of PLOD3 (spot 531), suggesting that the up-regulation of miR 663 observed during ER stress could be responsible for the down-regulation of the LH3 protein during TG treatment. Moreover, the proteomic analysis shows that the most striking effect is the down-regulation of protein expression and, in particular, of proteins that have a function within the secretory pathways. We have demonstrated that this down-regulation is not due to the inhibition of protein synthesis observed during UPR activation, therefore, it's very interesting to investigate if the expression of these proteins could be regulated by microRNA.

In agreement with the down-regulatory effect of ER Stress, the proteomic analysis described in the second part of this chapter reports that important factors involved in regulatory steps of protein synthesis are down-regulated. In particular, we found reduced expression of the translation factor eIF3 (spot 1848), a protein that retains key regulatory functions, including the regulation of translation reinitiation on polycistronic mRNAs and the kinase-dependent control of protein synthesis (Hinnebusch, 2006). Reduced levels were also observed for nascent polypeptide-associated complex (NAC) (spot 1932), a cytosolic protein that stabilizes nascent polypeptide emerging from ribosomes and whose expression is related to ER stress (Hotokezaka et al., 2009). Interestingly, we also found lower levels of the COP9 signalosome (CSN) (spot 1660), a protein factor that controls the ubiquitin-proteasome-mediated protein degradation in a number of cellular and developmental processes (Wei et al., 2008). Proteomic profiling of TG-induced cells showed decreased levels for a number of ER resident proteins. Calumenin (spot 1468) and reticulocalbin 2 (spot 1387), for example, are two EF-hand proteins belonging to the CREC family of Ca^{2+} -binding proteins (Honore and Vorum, 2000). Interestingly, CAL is functionally associated with the release/uptake of Ca^{2+} by interacting either with ryanodine receptors (RyRs), the intracellular calcium channels mediator of calcium-induced calcium release (CICR) in animal cells, or with SERCA2 transporters. Therefore, changes in the expression of calumenin are consistent with the perturbation of Ca^{2+} cycling induced in the TG-treated cells. Instead, the decreased levels observed for RCN2 could be explained by the effect of Ca^{2+} depletion within ER on the stability of the protein, which is a six EF-hand protein and requires Ca^{2+} for its

binding to target proteins in the ER. Our results suggest that down-regulation of RCN2 and CAL is most likely calcium dependent. This conclusion is supported by the observation that either MG132 or DTT, which induce ER stress through different mechanisms, are able to effectively up-regulate CAL and RCN2 protein levels.

The results reported in the chapter III revealed that ER Stress impairs ER to Golgi transport within the early secretory pathway and alters the morphology of post-ER compartments. In agreement with these findings, 2-DE data reported in this study revealed reduced level of proteins involved in membrane-trafficking events, such as copine 1 (spot 949), a member of the copine family of Ca²⁺-dependent, phospholipid-binding proteins (Tomsig and Creutz, 2002), and Sec1 family domain-containing protein 1 (spot 733), which is involved in fusion events during vesicular trafficking (Halachmi and Lev, 1996). According to the role of UPR in the control of cell survival, we show that TG induces down-regulation of the prosurvival factors mortalin (spot 1848) and SET (spot 1624). Mortalin, also known as hsp70/PBP74/Grp75, is a molecular chaperone that resides in multiple cell compartments, including mitochondria, ER, plasma membrane, transport vesicles and cytosol, and performs various functions related to cell survival, control of proliferation and stress response (Wadhwa et al., 2002). Interestingly, the SET protein was found down-regulated upon TG treatment and also in the ER stressed cells exposed to MG132. SET retains dual functions, namely as histone chaperone and phosphatase (PP2A) inhibitor (Gamble and Fisher, 2007). Thus, its down-regulation, as observed in ER stress cells, may enhance apoptosis caused by the re-activation of PP2A phosphatase (Samanta et al., 2009).

Among identified proteins, we observed only three up-regulated proteins: ER chaperone Grp78 (spot 697), serine proteinase inhibitor alpha-1-antitrypsin (SERPINA1) (spot 1136) and ALIX (spot 531). Quantitative expression of Grp78 is not surprising, given its central role in the ER stress response. Similarly, SERPINA1 accumulates in TG-treated cells in the same way to what shown in ER-stressed cells after incubation with tunicamycin (Nadanaka et al., 2004). Intriguingly, the spot leading to ALIX identification (spot 531) was also containing PLOD3, and it appeared to be a down-regulated spot in TG-treated cells. However, western blotting analysis demonstrated that ALIX is actually up-regulated after TG treatment, as well as in ER-stressed cells resulting from MG132 or DTT treatment. These results are in perfect agreement with previous reports, which link ALIX expression and its calcium-dependent interaction with the proapoptotic factor ALG2 in TG-induced apoptosis (Strappazon et al., 2010). Besides its proapoptotic properties, ALIX retains important functions in several processes including endocytosis, endosomal sorting, virus budding, cytokinesis and vesicle budding events at the ER exit sites (Odorizzi, 2006). In conclusion, this study has provided a representative picture of the changes observed in hepatoma cells proteome and microRNome as result of the treatment of cells with TG, a powerful inductor of ER Stress. Strikingly, the tandem analysis of microRNA and protein expression allows to identify some attractive coincidence and new players of the UPR signalling pathway, not least the microRNAs. Obviously, further experiments need to be done in order to identify miR 663 and 29b-1* targets among the predicted ones and to clarify their role during UPR activation. Moreover, further comparative proteomic and microarray analyses with additional UPR modulators may contribute to a detailed characterization of the different stress-responsive pathways activated in each case.

CONCLUSIONS AND PERSPECTIVES

The results shown suggest that the modulation of ER exit is an essential device to cope with the changes of protein homeostasis in the secretory factory. As emerged by this work, this modulation leads to one main effect: the reduction of COPII vesicles assembling at ER Exit Sites that causes the impairment of the anterograde transport of secretory proteins. In particular, two essential components of the ER exit machinery, namely Sec16 and Sec23a, play a role in this regulatory step. Therefore, decreased ER export takes an important part in the quality control, by avoiding the exit of proteins that need to be more efficiently either refolded in the ER or destined to degradation through the ERAD. Thus, our work introduces another step in the control of protein homeostasis: not just ER associated folding (ERAF) and ERAD but also the ER export. Certainly, future work will be aimed to underscore some unsolved aspects of COPII assembling. In particular we want:

- clarify the mechanism responsible for Sec16 down-expression
- investigate the role of MAPK pathway in the mechanism of COPII formation
- elucidate the biological function of the Sec23a mono-ubiquitination
- confirm the involvement of IRE1 alpha in the ER export of secretory proteins

In line with the major purpose of this work, the analysis of gene expression profiling discussed in the second part confirms that the activity of the secretory pathway is influenced by gene expression affecting the proteome and MicroRNome profiles. Certainly, how these changes are related to the quality control machinery and to the object of this study requires further investigations.

Finally, we think that the new insights in the mechanism of ER export and COPII coat formation could give important contribution to the understanding of the molecular basis of the COPII diseases.

ACKNOWLEDGEMENTS

I would like to express my sincere gratitude to:

Prof. Paolo Remondelli, my supervisor and ideator of the present project. I appreciate all his contributions of time, ideas, and funding to make my PhD experience productive and stimulating.

Prof. Stefano Bonatti who gave me the opportunity to join his group and to develop part of this project working in his lab at the Department of Biochemistry and Medical Biotechnologies (DBBM) at the University of Napoli "Federico II" (Napoli, IT).

I want to thank all our collaborators: Dr. Simona Palladino for the scientific support during my first steps in confocal microscopy, Prof. Carlo Tacchetti and Dr. Consuelo Venturi for performing Immuno-electro-microscopy, Prof. Agostino Casapullo and Dr. Luigi Margarucci for the proteomic identification of Sec23a Gly-Gly modified peptides. I also want to thank Prof. Massimo Mallardo for the helpful discussion regarding the microRNA analysis, Prof. Nicola Zambrano for performing the 2D-DIGE. The SLO-assay for Sec31 protein and FRAP experiments were performed in collaboration with Dr. Rossella Venditti in the laboratory of Dr. Antonella De Matteis at the Telethon Institute of Genetics and Medicine (TIGEM) of Napoli.

I want to acknowledge Dr. Ornella Moltedo, Dr. Gabriella Caporaso, Dr. Giuseppe Fiume, Dr. Silvia Franceschelli and the PhD students, Massimo D'Agostino and Valentina Lemma, for their friendship and helpful collaboration.

Finally, to my family and Nicola go all my loving thanks.

*Giuseppina Amodio
University of Salerno
December 2011*

References

- Anelli, T., S. Ceppi, L. Bergamelli, M. Cortini, S. Masciarelli, C. Valetti, and R. Sitia. 2007. Sequential steps and checkpoints in the early exocytic compartment during secretory IgM biogenesis. *EMBO J.* 26:4177-4188.
- Anelli, T., and R. Sitia. 2008. Protein quality control in the early secretory pathway. *EMBO J.* 27:315-327.
- Antonny, B., D. Madden, S. Hamamoto, L. Orci, and R. Schekman. 2001. Dynamics of the COPII coat with GTP and stable analogues. *Nat Cell Biol.* 3:531-537.
- Appenzeller-Herzog, C. 2006. The ER-Golgi intermediate compartment (ERGIC): in search of its identity and function. *Journal of Cell Science.* 119:2173-2183.
- Appenzeller, C., H. Andersson, F. Kappeler, and H.P. Hauri. 1999. The lectin ERGIC-53 is a cargo transport receptor for glycoproteins. *Nat Cell Biol.* 1:330-334.
- Aridor, M., S.I. Bannykh, T. Rowe, and W.E. Balch. 1999. Cargo can modulate COPII vesicle formation from the endoplasmic reticulum. *J Biol Chem.* 274:4389-4399.
- Baines, A.C., and B. Zhang. 2007. Receptor-mediated protein transport in the early secretory pathway. *Trends Biochem Sci.* 32:381-388.
- Barlowe, C. 2003. Signals for COPII-dependent export from the ER: what's the ticket out? *Trends Cell Biol.* 13:295-300.
- Barlowe, C., L. Orci, T. Yeung, M. Hosobuchi, S. Hamamoto, N. Salama, M.F. Rexach, M. Ravazzola, M. Amherdt, and R. Schekman. 1994. COPII: a membrane coat formed by Sec proteins that drive vesicle budding from the endoplasmic reticulum. *Cell.* 77:895-907.
- Barlowe, C., and R. Schekman. 1993. SEC12 encodes a guanine-nucleotide-exchange factor essential for transport vesicle budding from the ER. *Nature.* 365:347-349.
- Barr, F.A., N. Nakamura, and G. Warren. 1998. Mapping the interaction between GRASP65 and GM130, components of a protein complex involved in the stacking of Golgi cisternae. *EMBO J.* 17:3258-3268.
- Bartoszewski, R., J.W. Brewer, A. Rab, D.K. Crossman, S. Bartoszewski, N. Kapoor, C. Fuller, J.F. Collawn, and Z. Bebok. 2011. The Unfolded Protein Response (UPR)-activated Transcription Factor X-box-binding Protein 1 (XBP1) Induces MicroRNA-346 Expression That Targets the Human Antigen Peptide Transporter 1 (TAP1) mRNA and Governs Immune Regulatory Genes. *J Biol Chem.* 286:41862-41870.
- Berezikov, E. 2011. Evolution of microRNA diversity and regulation in animals. *Nat Rev Genet.* 12:846-860.
- Bertolotti, A., Y. Zhang, L.M. Hendershot, H.P. Harding, and D. Ron. 2000. Dynamic interaction of BiP and ER stress transducers in the unfolded-protein response. *Nat Cell Biol.* 2:326-332.
- Bhattacharyya, D., and B.S. Glick. 2007. Two mammalian Sec16 homologues have nonredundant functions in endoplasmic reticulum (ER) export and transitional ER organization. *Mol Biol Cell.* 18:839-849.
- Bi, X., R.A. Corpina, and J. Goldberg. 2002. Structure of the Sec23/24-Sar1 pre-budding complex of the COPII vesicle coat. *Nature.* 419:271-277.
- Bi, X., J.D. Mancias, and J. Goldberg. 2007. Insights into COPII coat nucleation from the structure of Sec23.Sar1 complexed with the active fragment of Sec31. *Dev Cell.* 13:635-645.
- Bielli, A., C.J. Haney, G. Gabreski, S.C. Watkins, S.I. Bannykh, and M. Aridor. 2005. Regulation of Sar1 NH2 terminus by GTP binding and hydrolysis promotes membrane deformation to control COPII vesicle fission. *J Cell Biol.* 171:919-924.
- Blumental-Perry, A., C.J. Haney, K.M. Weixel, S.C. Watkins, O.A. Weisz, and M. Aridor. 2006. Phosphatidylinositol 4-phosphate formation at ER exit sites regulates ER export. *Dev Cell.* 11:671-682.
- Boyadjiev, S.A., J.C. Fromme, J. Ben, S.S. Chong, C. Nauta, D.J. Hur, G. Zhang, S. Hamamoto, R. Schekman, M. Ravazzola, L. Orci, and W. Eyaid. 2006. Cranio-lenticulo-sutural dysplasia is caused by a SEC23A mutation leading to abnormal endoplasmic-reticulum-to-Golgi trafficking. *Nat Genet.* 38:1192-1197.
- Caratu, G., D. Allegra, M. Bimonte, G.G. Schiattarella, C. D'Ambrosio, A. Scaloni, M. Napolitano, T. Russo, and N. Zambrano. 2007. Identification of the ligands of protein interaction domains through a functional approach. *Mol Cell Proteomics.* 6:333-345.
- Chen, Z.J., and L.J. Sun. 2009. Nonproteolytic functions of ubiquitin in cell signaling. *Mol Cell.* 33:275-286.
- Cohen, M., F. Stutz, N. Belgareh, R. Haguenaer-Tsapis, and C. Dargemont. 2003. Ubp3 requires a cofactor, Bre5, to specifically de-ubiquitinate the COPII protein, Sec23. *Nat Cell Biol.* 5:661-667.
- Dancourt, J., and C. Barlowe. 2010. Protein Sorting Receptors in the Early Secretory Pathway. *Annual Review of Biochemistry.* 79:777-802.
- Doms, R.W., D.S. Keller, A. Helenius, and W.E. Balch. 1987. Role for adenosine triphosphate in regulating the assembly and transport of vesicular stomatitis virus G protein trimers. *J Cell Biol.* 105:1957-1969.
- Ellgaard, L., and A. Helenius. 2003. Quality control in the endoplasmic reticulum. *Nat Rev Mol Cell Biol.* 4:181-191.
- Erra, M.C., L. Iodice, L.V. Lotti, and S. Bonatti. 1999. Cell fractionation analysis of human CD8 glycoprotein transport between endoplasmic reticulum, intermediate compartment and Golgi complex in tissue cultured cells. *Cell Biol Int.* 23:571-577.
- Farhan, H., M. Weiss, K. Tani, R.J. Kaufman, and H.P. Hauri. 2008. Adaptation of endoplasmic reticulum exit sites to acute and chronic increases in cargo load. *EMBO J.* 27:2043-2054.

References

- Farhan, H., M.W. Wendeler, S. Mitrovic, E. Fava, Y. Silberberg, R. Sharan, M. Zerial, and H.P. Hauri. 2010. MAPK signaling to the early secretory pathway revealed by kinase/phosphatase functional screening. *J Cell Biol.* 189:997-1011.
- Fath, S., J.D. Mancias, X. Bi, and J. Goldberg. 2007. Structure and organization of coat proteins in the COPII cage. *Cell.* 129:1325-1336.
- Forster, R., M. Weiss, T. Zimmermann, E.G. Reynaud, F. Verissimo, D.J. Stephens, and R. Pepperkok. 2006. Secretory cargo regulates the turnover of COPII subunits at single ER exit sites. *Curr Biol.* 16:173-179.
- Franceschelli, S., O. Moltedo, G. Amodio, G. Tajana, and P. Remondelli. 2011. In the Huh7 Hepatoma Cells Diclofenac and Indomethacin Activate Differently the Unfolded Protein Response and Induce ER Stress Apoptosis. *Open Biochem J.* 5:45-51.
- Gamble, M.J., and R.P. Fisher. 2007. SET and PARP1 remove DEK from chromatin to permit access by the transcription machinery. *Nat Struct Mol Biol.* 14:548-555.
- Halachmi, N., and Z. Lev. 1996. The Sec1 family: a novel family of proteins involved in synaptic transmission and general secretion. *J Neurochem.* 66:889-897.
- Harding, H.P., Y. Zhang, and D. Ron. 1999. Protein translation and folding are coupled by an endoplasmic-reticulum-resident kinase. *Nature.* 397:271-274.
- Harding, H.P., Y. Zhang, H. Zeng, I. Novoa, P.D. Lu, M. Calfon, N. Sadri, C. Yun, B. Popko, R. Paules, D.F. Stojdl, J.C. Bell, T. Hettmann, J.M. Leiden, and D. Ron. 2003. An integrated stress response regulates amino acid metabolism and resistance to oxidative stress. *Mol Cell.* 11:619-633.
- Haze, K., H. Yoshida, H. Yanagi, T. Yura, and K. Mori. 1999. Mammalian transcription factor ATF6 is synthesized as a transmembrane protein and activated by proteolysis in response to endoplasmic reticulum stress. *Mol Biol Cell.* 10:3787-3799.
- Hinnebusch, A.G. 2006. eIF3: a versatile scaffold for translation initiation complexes. *Trends Biochem Sci.* 31:553-562.
- Hollien, J., and J.S. Weissman. 2006. Decay of endoplasmic reticulum-localized mRNAs during the unfolded protein response. *Science.* 313:104-107.
- Honore, B., and H. Vorum. 2000. The CREC family, a novel family of multiple EF-hand, low-affinity Ca(2+)-binding proteins localised to the secretory pathway of mammalian cells. *FEBS Lett.* 466:11-18.
- Hotokezaka, Y., K. van Leyen, E.H. Lo, B. Beatrix, I. Katayama, G. Jin, and T. Nakamura. 2009. alphaNAC depletion as an initiator of ER stress-induced apoptosis in hypoxia. *Cell Death Differ.* 16:1505-1514.
- Hughes, H., A. Budnik, K. Schmidt, K.J. Palmer, J. Mantell, C. Noakes, A. Johnson, D.A. Carter, P. Verkade, P. Watson, and D.J. Stephens. 2009. Organisation of human ER-exit sites: requirements for the localisation of Sec16 to transitional ER. *Journal of Cell Science.* 122:2924-2934.
- Jian, P., Z.W. Li, T.Y. Fang, W. Jian, Z. Zhuan, L.X. Mei, W.S. Yan, and N. Jian. 2011. Retinoic acid induces HL-60 cell differentiation via the upregulation of miR-663. *J Hematol Oncol.* 4:20.
- Jones, B., E.L. Jones, S.A. Bonney, H.N. Patel, A.R. Mensenkamp, S. Eichenbaum-Voline, M. Rudling, U. Myrdal, G. Annesi, S. Naik, N. Meadows, A. Quattrone, S.A. Islam, R.P. Naoumova, B. Angelin, R. Infante, E. Levy, C.C. Roy, P.S. Freemont, J. Scott, and C.C. Shoulders. 2003. Mutations in a Sar1 GTPase of COPII vesicles are associated with lipid absorption disorders. *Nat Genet.* 34:29-31.
- Kim, I., W. Xu, and J.C. Reed. 2008. Cell death and endoplasmic reticulum stress: disease relevance and therapeutic opportunities. *Nat Rev Drug Discov.* 7:1013-1030.
- Kirkpatrick, D.S., S.F. Weldon, G. Tsapralis, D.C. Liebler, and A.J. Gandolfi. 2005. Proteomic identification of ubiquitinated proteins from human cells expressing His-tagged ubiquitin. *Proteomics.* 5:2104-2111.
- Klausner, R.D., J.G. Donaldson, and J. Lippincott-Schwartz. 1992. Brefeldin A: insights into the control of membrane traffic and organelle structure. *J Cell Biol.* 116:1071-1080.
- Lederkremer, G.Z., Y. Cheng, B.M. Petre, E. Vogan, S. Springer, R. Schekman, T. Walz, and T. Kirchhausen. 2001. Structure of the Sec23p/24p and Sec13p/31p complexes of COPII. *Proc Natl Acad Sci U S A.* 98:10704-10709.
- Lee, M.C., L. Orci, S. Hamamoto, E. Futai, M. Ravazzola, and R. Schekman. 2005. Sar1p N-terminal helix initiates membrane curvature and completes the fission of a COPII vesicle. *Cell.* 122:605-617.
- Malkus, P., F. Jiang, and R. Schekman. 2002. Concentrative sorting of secretory cargo proteins into COPII-coated vesicles. *J Cell Biol.* 159:915-921.
- Mauro, C., F. Pacifico, A. Lavorgna, S. Mellone, A. Iannetti, R. Acquaviva, S. Formisano, P. Vito, and A. Leonardi. 2006. ABIN-1 binds to NEMO/IKKgamma and co-operates with A20 in inhibiting NF-kappaB. *J Biol Chem.* 281:18482-18488.
- Merksamer, P.I., and F.R. Papa. 2010. The UPR and cell fate at a glance. *J Cell Sci.* 123:1003-1006.
- Merte, J., D. Jensen, K. Wright, S. Sarsfield, Y. Wang, R. Schekman, and D.D. Ginty. 2010. Sec24b selectively sorts Vangl2 to regulate planar cell polarity during neural tube closure. *Nat Cell Biol.* 12:41-46; sup pp 41-48.
- Meunier, L., Y.K. Usherwood, K.T. Chung, and L.M. Hendershot. 2002. A subset of chaperones and folding enzymes form multiprotein complexes in endoplasmic reticulum to bind nascent proteins. *Mol Biol Cell.* 13:4456-4469.

References

- Mezzacasa, A., and A. Helenius. 2002. The transitional ER defines a boundary for quality control in the secretion of tsO45 VSV glycoprotein. *Traffic*. 3:833-849.
- Miller, E., B. Antonny, S. Hamamoto, and R. Schekman. 2002. Cargo selection into COPII vesicles is driven by the Sec24p subunit. *EMBO J*. 21:6105-6113.
- Mironov, A.A., A.A. Mironov, Jr., G.V. Beznoussenko, A. Trucco, P. Lupetti, J.D. Smith, W.J. Geerts, A.J. Koster, K.N. Burger, M.E. Martone, T.J. Deerinck, M.H. Ellisman, and A. Luini. 2003. ER-to-Golgi carriers arise through direct en bloc protrusion and multistage maturation of specialized ER exit domains. *Dev Cell*. 5:583-594.
- Mukhopadhyay, D., and H. Riezman. 2007. Proteasome-independent functions of ubiquitin in endocytosis and signaling. *Science*. 315:201-205.
- Nadanaka, S., H. Yoshida, F. Kano, M. Murata, and K. Mori. 2004. Activation of mammalian unfolded protein response is compatible with the quality control system operating in the endoplasmic reticulum. *Mol Biol Cell*. 15:2537-2548.
- Ni, C.W., H. Qiu, and H. Jo. 2011. MicroRNA-663 upregulated by oscillatory shear stress plays a role in inflammatory response of endothelial cells. *Am J Physiol Heart Circ Physiol*. 300:H1762-1769.
- Nichols, B.J., A.K. Kenworthy, R.S. Polishchuk, R. Lodge, T.H. Roberts, K. Hirschberg, R.D. Phair, and J. Lippincott-Schwartz. 2001. Rapid cycling of lipid raft markers between the cell surface and Golgi complex. *J Cell Biol*. 153:529-541.
- Nyfelner, B., O. Nufer, T. Matsui, K. Mori, and H.P. Hauri. 2003. The cargo receptor ERGIC-53 is a target of the unfolded protein response. *Biochem Biophys Res Commun*. 304:599-604.
- Nyfelner, B., V. Reiterer, M.W. Wendeler, E. Stefan, B. Zhang, S.W. Michnick, and H.P. Hauri. 2008. Identification of ERGIC-53 as an intracellular transport receptor of alpha-1-antitrypsin. *J Cell Biol*. 180:705-712.
- Odorizzi, G. 2006. The multiple personalities of Alix. *J Cell Sci*. 119:3025-3032.
- Okumoto, K., S. Misono, N. Miyata, Y. Matsumoto, S. Mukai, and Y. Fujiki. 2011. Cysteine ubiquitination of PTS1 receptor Pex5p regulates Pex5p recycling. *Traffic*. 12:1067-1083.
- Orci, L., M. Ravazzola, P. Meda, C. Holcomb, H.P. Moore, L. Hicke, and R. Schekman. 1991. Mammalian Sec23p homologue is restricted to the endoplasmic reticulum transitional cytoplasm. *Proc Natl Acad Sci U S A*. 88:8611-8615.
- Palmer, K.J., J.E. Konkel, and D.J. Stephens. 2005. PCTAIRE protein kinases interact directly with the COPII complex and modulate secretory cargo transport. *J Cell Sci*. 118:3839-3847.
- Peng, J., D. Schwartz, J.E. Elias, C.C. Thoreen, D. Cheng, G. Marsischky, J. Roelofs, D. Finley, and S.P. Gygi. 2003. A proteomics approach to understanding protein ubiquitination. *Nat Biotechnol*. 21:921-926.
- Perkins, D.N., D.J. Pappin, D.M. Creasy, and J.S. Cottrell. 1999. Probability-based protein identification by searching sequence databases using mass spectrometry data. *Electrophoresis*. 20:3551-3567.
- Presley, J.F., N.B. Cole, T.A. Schroer, K. Hirschberg, K.J. Zaal, and J. Lippincott-Schwartz. 1997. ER-to-Golgi transport visualized in living cells. *Nature*. 389:81-85.
- Puthalakath, H., L.A. O'Reilly, P. Gunn, L. Lee, P.N. Kelly, N.D. Huntington, P.D. Hughes, E.M. Michalak, J. McKimm-Breschkin, N. Motoyama, T. Gotoh, S. Akira, P. Bouillet, and A. Strasser. 2007. ER stress triggers apoptosis by activating BH3-only protein Bim. *Cell*. 129:1337-1349.
- Qiang, L., H. Wang, and S.R. Farmer. 2007. Adiponectin secretion is regulated by SIRT1 and the endoplasmic reticulum oxidoreductase Ero1-L alpha. *Mol Cell Biol*. 27:4698-4707.
- Renna, M., M.G. Caporaso, S. Bonatti, R.J. Kaufman, and P. Remondelli. 2007. Regulation of ERGIC-53 gene transcription in response to endoplasmic reticulum stress. *J Biol Chem*. 282:22499-22512.
- Rismanchi, N., R. Puertollano, and C. Blackstone. 2009. STAM adaptor proteins interact with COPII complexes and function in ER-to-Golgi trafficking. *Traffic*. 10:201-217.
- Ron, D., and P. Walter. 2007. Signal integration in the endoplasmic reticulum unfolded protein response. *Nat Rev Mol Cell Biol*. 8:519-529.
- Ronchi, P., S. Colombo, M. Francolini, and N. Borgese. 2008. Transmembrane domain-dependent partitioning of membrane proteins within the endoplasmic reticulum. *J Cell Biol*. 181:105-118.
- Saito, K., M. Chen, F. Bard, S. Chen, H. Zhou, D. Woodley, R. Polishchuk, R. Schekman, and V. Malhotra. 2009. TANGO1 Facilitates Cargo Loading at Endoplasmic Reticulum Exit Sites. *Cell*. 136:891-902.
- Salama, N.R., J.S. Chuang, and R.W. Schekman. 1997. Sec31 encodes an essential component of the COPII coat required for transport vesicle budding from the endoplasmic reticulum. *Mol Biol Cell*. 8:205-217.
- Salo, A.M., H. Cox, P. Farndon, C. Moss, H. Grindulis, M. Risteli, S.P. Robins, and R. Myllyla. 2008. A connective tissue disorder caused by mutations of the lysyl hydroxylase 3 gene. *Am J Hum Genet*. 83:495-503.
- Samanta, A.K., S.N. Chakraborty, Y. Wang, H. Kantarjian, X. Sun, J. Hood, D. Perrotti, and R.B. Arlinghaus. 2009. Jak2 inhibition deactivates Lyn kinase through the SET-PP2A-SHP1 pathway, causing apoptosis in drug-resistant cells from chronic myelogenous leukemia patients. *Oncogene*. 28:1669-1681.
- Sato, K., and A. Nakano. 2005. Dissection of COPII subunit-cargo assembly and disassembly kinetics during Sar1p-GTP hydrolysis. *Nat Struct Mol Biol*. 12:167-174.

References

- Sato, M., K. Sato, and A. Nakano. 2002. Evidence for the intimate relationship between vesicle budding from the ER and the unfolded protein response. *Biochem Biophys Res Commun.* 296:560-567.
- Schwarz, K., A. Iolascon, F. Verissimo, N.S. Trede, W. Horsley, W. Chen, B.H. Paw, K.P. Hopfner, K. Holzmann, R. Russo, M.R. Esposito, D. Spano, L. De Falco, K. Heinrich, B. Joggerst, M.T. Rojewski, S. Perrotta, J. Denecke, U. Pannicke, J. Delaunay, R. Pepperkok, and H. Heimpe. 2009. Mutations affecting the secretory COPII coat component SEC23B cause congenital dyserythropoietic anemia type II. *Nat Genet.* 41:936-940.
- Shaywitz, D.A., P.J. Espenshade, R.E. Gimeno, and C.A. Kaiser. 1997. COPII subunit interactions in the assembly of the vesicle coat. *J Biol Chem.* 272:25413-25416.
- Shen, J., E.L. Snapp, J. Lippincott-Schwartz, and R. Prywes. 2005. Stable binding of ATF6 to BiP in the endoplasmic reticulum stress response. *Mol Cell Biol.* 25:921-932.
- Shibata, H., H. Suzuki, H. Yoshida, and M. Maki. 2007. ALG-2 directly binds Sec31A and localizes at endoplasmic reticulum exit sites in a Ca²⁺-dependent manner. *Biochem Biophys Res Commun.* 353:756-763.
- Shimoi, W., I. Ezawa, K. Nakamoto, S. Uesaki, G. Gabreski, M. Aridor, A. Yamamoto, M. Nagahama, M. Tagaya, and K. Tani. 2005. p125 is localized in endoplasmic reticulum exit sites and involved in their organization. *J Biol Chem.* 280:10141-10148.
- Spatuzza, C., M. Renna, R. Faraonio, G. Cardinali, G. Martire, S. Bonatti, and P. Remondelli. 2004. Heat shock induces preferential translation of ERGIC-53 and affects its recycling pathway. *J Biol Chem.* 279:42535-42544.
- Stagg, S.M., C. Gurkan, D.M. Fowler, P. LaPointe, T.R. Foss, C.S. Potter, B. Carragher, and W.E. Balch. 2006. Structure of the Sec13/31 COPII coat cage. *Nature.* 439:234-238.
- Strappazon, F., S. Torch, C. Chatellard-Causse, A. Petiot, C. Thibert, B. Blot, J.M. Verna, and R. Sadoul. 2010. Alix is involved in caspase 9 activation during calcium-induced apoptosis. *Biochem Biophys Res Commun.* 397:64-69.
- Supek, F., D.T. Madden, S. Hamamoto, L. Orci, and R. Schekman. 2002. Sec16p potentiates the action of COPII proteins to bud transport vesicles. *J Cell Biol.* 158:1029-1038.
- Tabata, K.V., K. Sato, T. Ide, T. Nishizaka, A. Nakano, and H. Noji. 2009. Visualization of cargo concentration by COPII minimal machinery in a planar lipid membrane. *EMBO J.* 28:3279-3289.
- Tang, B.L., Y. Wang, Y.S. Ong, and W. Hong. 2005. COPII and exit from the endoplasmic reticulum. *Biochimica et Biophysica Acta (BBA) - Molecular Cell Research.* 1744:293-303.
- Thor, F., M. Gautschi, R. Geiger, and A. Helenius. 2009. Bulk flow revisited: transport of a soluble protein in the secretory pathway. *Traffic.* 10:1819-1830.
- Tomsig, J.L., and C.E. Creutz. 2002. Copines: a ubiquitous family of Ca(2+)-dependent phospholipid-binding proteins. *Cell Mol Life Sci.* 59:1467-1477.
- Travers, K.J., C.K. Patil, L. Wodicka, D.J. Lockhart, J.S. Weissman, and P. Walter. 2000. Functional and genomic analyses reveal an essential coordination between the unfolded protein response and ER-associated degradation. *Cell.* 101:249-258.
- Urano, F., X. Wang, A. Bertolotti, Y. Zhang, P. Chung, H.P. Harding, and D. Ron. 2000. Coupling of stress in the ER to activation of JNK protein kinases by transmembrane protein kinase IRE1. *Science.* 287:664-666.
- Wadhwa, R., K. Taira, and S.C. Kaul. 2002. An Hsp70 family chaperone, mortalin/mthsp70/PBP74/Grp75: what, when, and where? *Cell Stress Chaperones.* 7:309-316.
- Wang, L., and J.M. Lucocq. 2007. p38 MAPK regulates COPII recruitment. *Biochem Biophys Res Commun.* 363:317-321.
- Wang, X.Z., H.P. Harding, Y. Zhang, E.M. Jolicoeur, M. Kuroda, and D. Ron. 1998. Cloning of mammalian Ire1 reveals diversity in the ER stress responses. *EMBO J.* 17:5708-5717.
- Ward, T.H., R.S. Polishchuk, S. Caplan, K. Hirschberg, and J. Lippincott-Schwartz. 2001. Maintenance of Golgi structure and function depends on the integrity of ER export. *J Cell Biol.* 155:557-570.
- Watson, P., R. Forster, K.J. Palmer, R. Pepperkok, and D.J. Stephens. 2005. Coupling of ER exit to microtubules through direct interaction of COPII with dynactin. *Nat Cell Biol.* 7:48-55.
- Watson, P., A.K. Townley, P. Koka, K.J. Palmer, and D.J. Stephens. 2006. Sec16 defines endoplasmic reticulum exit sites and is required for secretory cargo export in mammalian cells. *Traffic.* 7:1678-1687.
- Wei, N., G. Serino, and X.W. Deng. 2008. The COP9 signalosome: more than a protease. *Trends Biochem Sci.* 33:592-600.
- Wendeler, M.W., J.P. Paccaud, and H.P. Hauri. 2007. Role of Sec24 isoforms in selective export of membrane proteins from the endoplasmic reticulum. *EMBO Rep.* 8:258-264.
- Whittle, J.R., and T.U. Schwartz. 2010. Structure of the Sec13-Sec16 edge element, a template for assembly of the COPII vesicle coat. *J Cell Biol.* 190:347-361.
- Yamamoto, K., T. Sato, T. Matsui, M. Sato, T. Okada, H. Yoshida, A. Harada, and K. Mori. 2007. Transcriptional induction of mammalian ER quality control proteins is mediated by single or combined action of ATF6alpha and XBP1. *Dev Cell.* 13:365-376.

References

- Yang, F., L. Zhang, F. Wang, Y. Wang, X.S. Huo, Y.X. Yin, Y.Q. Wang, and S.H. Sun. 2011a. Modulation of the unfolded protein response is the core of microRNA-122-involved sensitivity to chemotherapy in hepatocellular carcinoma. *Neoplasia*. 13:590-600.
- Yang, J.S., M.D. Phillips, D. Betel, P. Mu, A. Ventura, A.C. Siepel, K.C. Chen, and E.C. Lai. 2011b. Widespread regulatory activity of vertebrate microRNA* species. *RNA*. 17:312-326.
- Yang, Y., L.L. Wang, Y.H. Li, X.N. Gao, and L. Yu. 2011c. [Expression level of miRNA-663 in different leukemic cell lines and its biological function]. *Zhongguo Shi Yan Xue Ye Xue Za Zhi*. 19:279-283.
- Yorimitsu, T., U. Nair, Z. Yang, and D.J. Klionsky. 2006. Endoplasmic reticulum stress triggers autophagy. *J Biol Chem*. 281:30299-30304.
- Yoshida, H., T. Matsui, A. Yamamoto, T. Okada, and K. Mori. 2001. XBP1 mRNA is induced by ATF6 and spliced by IRE1 in response to ER stress to produce a highly active transcription factor. *Cell*. 107:881-891.
- Yoshihisa, T., C. Barlowe, and R. Schekman. 1993. Requirement for a GTPase-activating protein in vesicle budding from the endoplasmic reticulum. *Science*. 259:1466-1468.
- Zacharogianni, M., V. Kondylis, Y. Tang, H. Farhan, D. Xanthakis, F. Fuchs, M. Boutros, and C. Rabouille. 2011. ERK7 is a negative regulator of protein secretion in response to amino-acid starvation by modulating Sec16 membrane association. *EMBO J*. 30:3684-3700.
- Zeuschner, D., W.J. Geerts, E. van Donselaar, B.M. Humbel, J.W. Slot, A.J. Koster, and J. Klumperman. 2006. Immuno-electron tomography of ER exit sites reveals the existence of free COPII-coated transport carriers. *Nat Cell Biol*. 8:377-383.